# Microscale acoustofluidics: Microfluidics driven via acoustics and ultrasonics

James Friend[*]

*MicroNanophysics Research Laboratory, Department of Mechanical and Aerospace Engineering and the Melbourne Centre for Nanofabrication, Clayton, Victoria 3800 Australia*

Leslie Y. Yeo

*MicroNanophysics Research Laboratory, Department of Mechanical and Aerospace Engineering and the Melbourne Centre for Nanofabrication, Clayton, Victoria 3800 Australia*

This article reviews acoustic microfluidics: the use of acoustic fields, principally ultrasonics, for application in microfluidics. Although acoustics is a classical field, its promising, and indeed perplexing, capabilities in powerfully manipulating both fluids and particles within those fluids on the microscale to nanoscale has revived interest in it. The bewildering state of the literature and ample jargon from decades of research is reorganized and presented in the context of models derived from first principles. This hopefully will make the area accessible for researchers with experience in materials science, fluid mechanics, or dynamics. The abundance of interesting phenomena arising from nonlinear interactions in ultrasound that easily appear at these small scales is considered, especially in surface acoustic wave devices that are simple to fabricate with planar lithography techniques common in microfluidics, along with the many applications in microfluidics and nanofluidics that appear through the literature.

## CONTENTS

## I. INTRODUCTION

The propagation of acoustic waves in solids and fluids, a venerable classic, has found new life in modern research in the manipulation of fluids and fluid-borne particles at the microscale to nanoscale:

Little explored thus far in microfluidics, acoustic streaming represents one of very few inertial

[*]jamesfriend@mailaps.org

phenomena that may actually play a significant role in microfluidic devices. As discussed, small feature sizes typically prevent flow velocities from being high enough to yield high (Reynolds) numbers. High-frequency acoustic waves, however, can circumvent such difficulties (Squires and Quake, 2005).

Circumventing the limitations of current microfluidics technology is indeed critical to delivering on its idyllic promises (Ho *et al.*, 2011), from handheld medical diagnostic devices for the rapid detection of single molecules associated with heart disease (Gerszten and Wang, 2008), cancer (Lu *et al.*, 2005), and physiological fluid chemistry (Craighead, 2006), to water purification (Shannon *et al.*, 2008) and polymerase chain reaction on a chip (Huang *et al.*, 2006). Fortunately, acoustic wave technology at the microscale to nanoscale is helping to make these things reality, as will be shown, and furthermore promises to allow researchers to produce and exploit interesting physical phenomena seen at the microscale-to-nanometer scale.

Intriguingly complex with viscous effects, compressibility, the presence of free surfaces, coupling to vibrating piezoelectric solid structures, and acoustic forces directly applied to suspended particles, acoustics at the microscale and below requires the breadth of solid and fluid mechanics analysis techniques to deliver answers to even elementary questions. The literature over the past few decades treats this topic from many different and frankly confusing perspectives. Recent work in applying acoustics to microfluidics demonstrates the promise of the approach, yet the physical phenomena are made even more opaque given the unique circumstances necessary in using acoustic fields at such small scales. In the following, an attempt is made to provide a cogent resource for researchers to enter this burgeoning area.

Acoustic microfluidics spans a number of disciplines in an attempt to address the perceived shortcomings of microfluidics. Many of these fields are mature and all are entirely too broad for a focused review. By itself, microfluidics (Stone *et al.*, 2004) is a flourishing research area that has swiftly emerged from microelectronics over the past 15 years. Delivering technology useful for applications in biochemistry and medicine requires an enormous effort to merge these fields with engineering and physics expertise in the fundamentals and fabrication methods of microfluidics (Beebe *et al.*, 2002; Weibel *et al.*, 2007; Domachuk *et al.*, 2010), an effort that remains essentially incomplete. Furthermore, there are a number of significant physical forces present at these scales relevant to microfluidics, from interatomic to microscale, that are comparatively insignificant at larger scales associated with traditional fluid mechanics (Wautelet, 2001). For these reasons, the broad, conspicuous effort in microfluidics research will surely continue for some time to come. In comparison, both acoustics and ultrasonics, as an extension of the former field, are classical fields of physics; a majority of the underlying physical principles in the propagation of sound at audible to ultrasonic frequencies have been known since at least the early 20th century (Chilowsky and Langevin, 1916; Love, 1944; Rayleigh and Lindsay, 1945), or even the mid-19th century if one includes seismology

(Romanowicz *et al.*, 2009). The classical treatment of these areas, however, has been found to be inadequate to describe acoustic wave behavior in microfluidics, because of the unique combination of microscale hydrodynamics with large-amplitude, high-frequency acoustic waves generated by microfabricated piezoelectric materials. Indeed, some of the tenets of classic acoustics—Faraday waves, for example (Qi *et al.*, 2008; Tan *et al.*, 2010a)—have been brought into question as a consequence of recent work in acoustic microfluidics.

This review begins with some historical background on acoustics, microfluidics, and piezoelectric materials, the latter of which is a necessary part of high-frequency acoustics for a large majority of uses in microfluidics. The section that follows on theoretical developments in acoustic hydrodynamics is a large part of the review. Recognizing that much of what has been published in the past in this area has looked at closely related problems in acoustic streaming and the propagation of acoustic waves through fluids, yet presented in such widely different ways, we believe that reconciling these various contributions with a detailed analysis section can only help clarify the confusing state of the literature. Over the past few years, many applications have been posited in microfluidics for the use of acoustic waves, and we follow the analysis section with an applications section and what we believe to be a few emerging areas that may lead to breakthroughs in the near future. We conclude with a glossary of terms commonly used (and misused) in analysis, in hopes that the reader benefits from clarification of the jargon.

## II. BACKGROUND

### A. Acoustics

The entirety of recorded history is entwined with the study of sound across many ancient cultures. The Babylonians created what is believed to be the earliest known examples of written melodic notation (West, 1994)—the *Hurrian Melodic Texts* from around 1800 BC—with a complexity that remains mostly undeciphered. Chinese stone chimes, *bianqing*, from before 450 BC have been uncovered, played, and used as evidence of the skill with which the ancient Chinese made them (Yoo and Rossing, 2006). Even in South America, Peruvians were found to make whistling bottles as early as 500 BC for what anthropologists believe was communication and perhaps ritual ceremonies (Garrett and Star, 1977). Music as a human interpretation of sound rapidly advanced from Pythagoras' time (Hunt, 1978), and much has been made of the development of sound and acoustics as a scientific endeavor since the 18th century (Rayleigh and Lindsay, 1945; Beyer, 1998), as both ancient phenomena, such as the Chinese spouting bowl (Schufle, 1981) studied by John Tyndall and a crude predecessor of some of the atomizers described later in this review, and contemporary phenomena such as Kundt's tube (Hutchisson and Morgan, 1931) were studied and explained by leading scientists of the time. Many of the known phenomena in acoustics bear their name, with Lord Rayleigh's studies of fluid surface instabilities, human hearing and fluid jets (Nobel Foundation, 1967), Helmholtz's studies of resonant acoustic

cavities, Faraday's observation of vibration-induced surface waves (Faraday, 1831; Miles, 1992), Rayleigh's acoustic streaming (Rayleigh, 1884), and the study of wave propagation in solids by Adams and Soh (2010) are five examples. Unfortunately, acoustics also has a history of attracting eccentrics and outright frauds from Tyndall's time to today, as humorously described by Wright (2006), for example, "in a recent web page claiming extraordinary benefits of acoustics in health treatment: '...introducing a person to the frequency formula for niacin...can cause skin flushing, the same as if the person actually ingested the nutrient' ." Still, the applications of genuine, modern acoustics span a diverse range of disciplines, as illustrated from the following list:

    (1) underwater acoustics (Lurton and Jackson, 2004), oceanography (Medwin *et al.*, 1999), and sound navigation and ranging (SONAR);

    (2) architectural (Long, 2006) and musical acoustics (Hall, 2002);

    (3) psychological and physiological acoustics and communication (Gelfand, 1998);

    (4) noise and its control (Kuo and Morgan, 1999);

    (5) medical ultrasonics (Hill *et al.*, 2004);

    (6) physical acoustics (Blackstock, 2000): phononics, actuation, levitation, and other physical phenomena; and

    (7) acoustic holography and imaging (Maynard *et al.*, 1985), and sensing (Länge *et al.*, 2008).

The texts by Shutilov (1988) and Blackstock (2000) are together an excellent introduction to the field of acoustics.

The useful frequency range of scientifically based acoustics spans 15 orders of magnitude, as shown in Fig. 1. Natural phenomena appear in the *infrasound* range below the limits of human hearing ($10^{-2}$–10 Hz), but the most prominent man-made applications of acoustics make use of frequencies well into the ultrasonic range (20 kHz to 10 GHz). The far more narrow range of 20 kHz to 10 MHz is used for medical purposes; drug delivery, imaging, and nerve and bone repair are all aided by devices in this frequency range (Mitragotri, 2005), as shown in Fig. 2. However, recent work discussed in Sec. IV has shown that the range above 10 MHz should also prove useful in drug delivery and tissue engineering.

In a similar fashion, the amplitude of scientifically relevant acoustic waves spans at least 10 orders of magnitude. An average young human can perceive sound at 1 kHz with an amplitude of only 7.8 nm, while some of the most intense acoustic waves generated in air at ultrasonic frequencies are at least 200 dB, generating waves with amplitudes of 1.5 mm at 50 kHz. Because of this, it is in part perhaps no surprise that the human cochlea has an extraordinarily non-linear response to sound (Eguíluz *et al.*, 2000), as do many biological structures tasked with the generation (Hughes *et al.*, 2009) and detection of acoustic waves, not to mention microphones and other man-made technology. Further, the behavior of the acoustic wave and the fluid that carries it are strongly influenced by the amplitude of the wave, to the extent that shock waves and *fast acoustic streaming* formed as a nonlinear response to high intensity acoustic (finite-amplitude) waves exhibit different physical characteristics and uses compared to their small-amplitude (infinitesimal) wave counterparts (see Table I). This area has been extensively studied in the former Soviet Union, as reviewed by Naugolnykh (2009).

The traditional overlap of acoustics and microstructures has principally been in sensor technologies, particularly
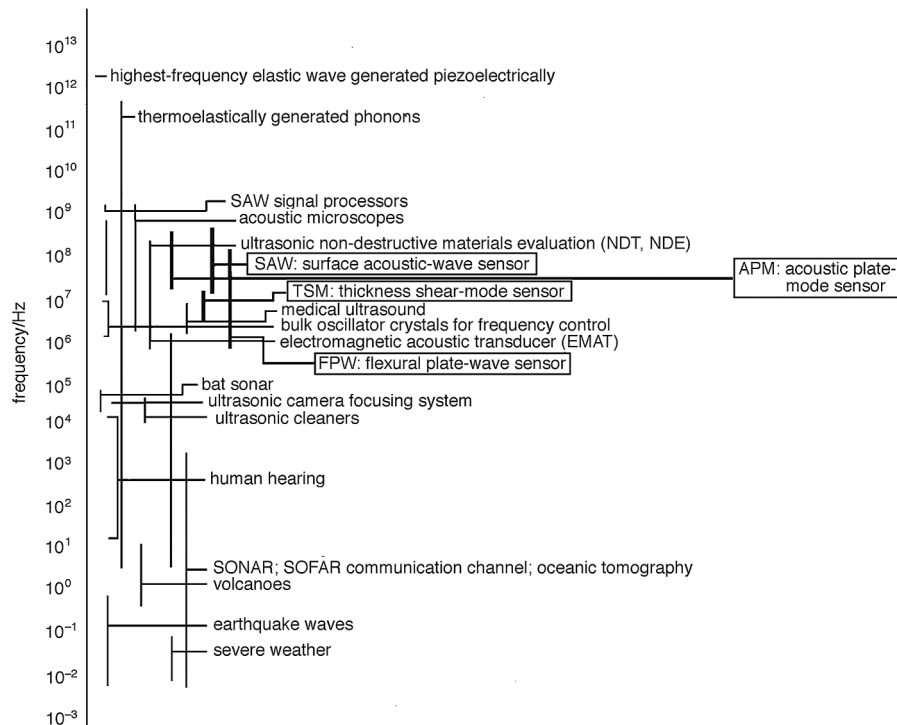


FIG. 1. The range of acoustic wave excitation at the close of the 20th century. The upper limit of this range, a few THz, has drawn the interest of many researchers in the past decade. The generation, analysis (Reed *et al.*, 2008), and creative use (Armstrong *et al.*, 2009) of THz-order acoustic waves has become almost routine since this figure was originally published. From White, 1997.
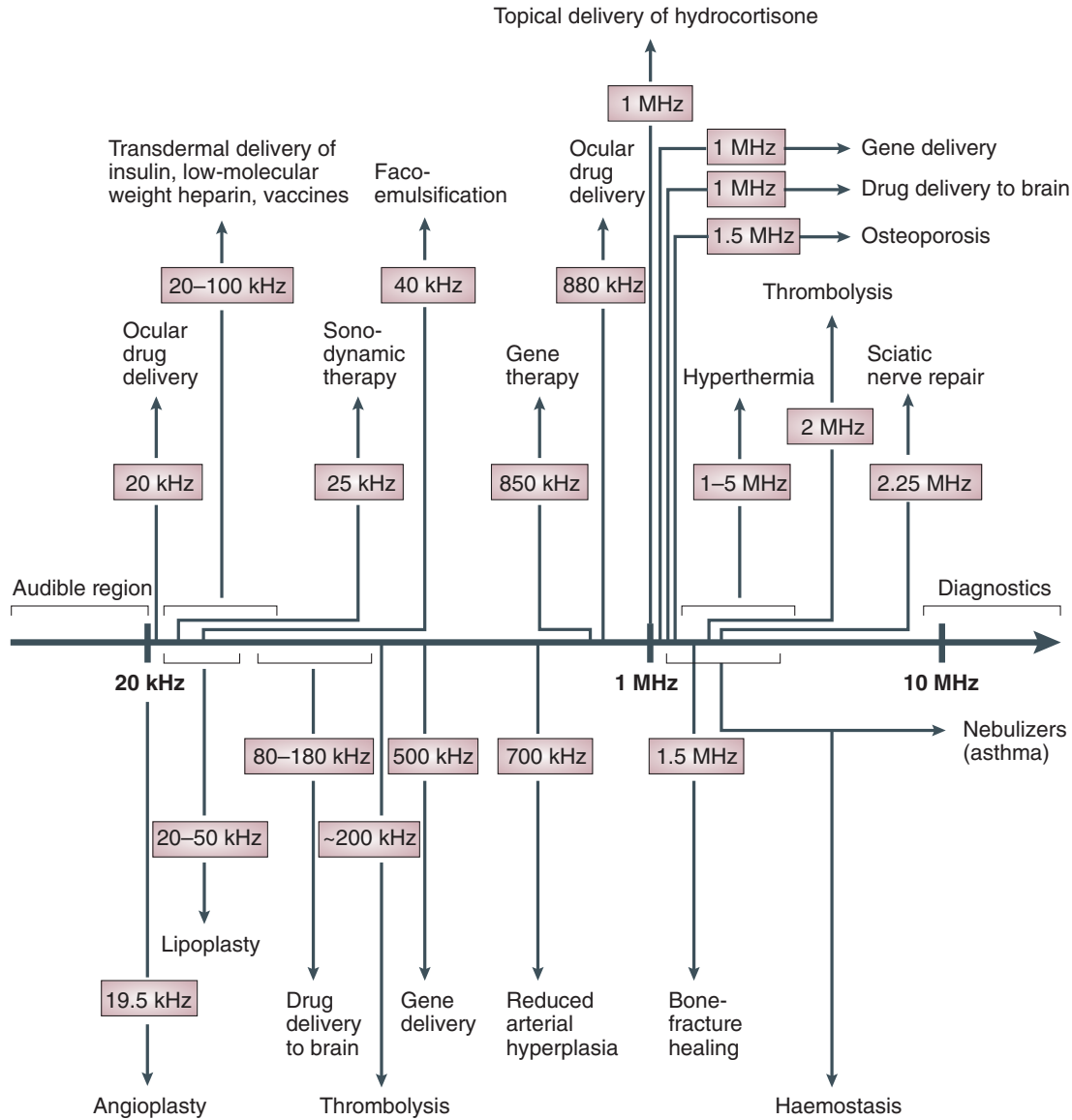
FIG. 2 (color online).   Medical treatments and research in medical ultrasound span the 20 kHz–10 MHz range. The range of treatments encompasses both the destructive capabilities of high-power ultrasound in lithotripsy, thrombolysis, and drug delivery, and the sensitivity of ultrasound transduction in imaging. From Mitragotri, 2005.

surface acoustic wave sensors, cantilevers, and quartz crystal microbalances that are useful for characterizing fluid viscosity and density, and detecting the presence of monolayers due to binding or growth, biopolymers or biomolecules, or even entire cells and tissue. A comprehensive review of the area requires an entirely separate effort, and in light of the reviews by Grate   et al. (1993), Marx (2003), and Lucklum and Hauptmann (2006), the other areas of sensor development for microfluidics, using optics, for example, as reported by Monat   et al. (2007), not to mention the work by McHale et al. (2003) on Love wave and shear-horizontal wave sensors, the review of work on biosensors by Länge  et al. (2008) and biomolecular binding in acoustic sensing by Cavić  et al. (1999), the article by Ellis   et al. (2003) on predicting the effects of slip at the interface, and even the use of tailored electrode configurations such as the ones reported by Kondoh et al. (2007), we focus upon actuation in lieu of sensing in

most of what follows, because the recent developments in the application of acoustics at the microscale and beyond appear to principally be on actuation.

**B. Piezoelectric materials**

Although many associate the discovery of the piezoelectric phenomenon with Jacques and Pierre Curie (Curie and Curie, 1880), the human use of piezoelectric materials together with triboluminescence is associated with the earliest archaeologically significant practices known. White quartz pebbles, rocks, and stones are found at a number of prehistorical sites worldwide, and the ethnographic interpretation of this behavior is the ancient peoples' belief that the materials contained supernatural power with their emission of bright flashes of light upon fracture or impact (Whitley   et al., 1999). Theophrastus noted in 314 BC that after heating

TABLE I.  Forms of streaming relevant to microfluidics and the underlying assumptions, characteristics, and notable references for each.

| Streaming | Assumptions | Characteristics | References | Notes |
|---|---|---|---|---|
| Slow | $U_0 \ll u_1 \equiv \mathrm{Re} \ll 1$ | $U_0 \propto u_1^2$. Streaming flow (Ramos *et al.*, 2001). With plane traveling wave, the acoustic force on the fluid $F \propto \alpha u_1^2$. Convective acceleration $(\mathbf{u} \cdot \boldsymbol{\nabla})\mathbf{u} \approx \mathbf{0}$. | Rayleigh (1884); Westervelt (1953a); Nyborg (1965); Lighthill (1978); Bradley (1996) | Successive approximation-perturbation method valid. Also called "creeping motion" by some (Lighthill, 1978; Tjøtta and Tjøtta, 1994). |
| Fast | $U_0 \gtrsim u_1 \equiv \mathrm{Re} \gtrsim 1$ | For coarse-grained streaming, $U_0 \propto u_1^{2+n}$, where $n$ is some value depending upon the non-linearity of the acoustic wave ($n = 1$ for a sawtooth wave). Convective acceleration $(\mathbf{u} \cdot \boldsymbol{\nabla})\mathbf{u}$ is significant. | Stuart (1963); Zarembo (1971); Rudenko and Soluîan (1977); Lighthill (1978); Qi (1993) | Zarembo's averaging method appropriate for analysis; successive approximation method not appropriate. Related to Stuart streaming as coined by Lighthill; see the Glossary. Finite-amplitude effects, similar to shocks, may be important to consider; check $\mathrm{Re}_{ac}$. |
| Coarse-grained (multidimensional) Eckart | Traveling acoustic wave from single source along an axis, with characteristic length scale $\mathcal{L} \gg \lambda$. | Streaming away from sound source into viscous fluid. The Reynolds number $\mathrm{Re}_{\mathcal{L}} = \rho_f U_0 \mathcal{L}/\mu$ determines whether the streaming is fast or slow. | Zarembo (1971); Nachef *et al.* (1995); Tan, Friend *et al.* (2010) | Eckart streaming, but without one-dimensional assumption. Convective acceleration $(\mathbf{u} \cdot \boldsymbol{\nabla})\mathbf{u}$ is potentially significant (compared to one-dimensional Eckart streaming). Starritt *et al.* (1991) showed that even when controlling for acoustic intensity, nonlinear distortion in the acoustic wave can cause far larger acoustic streaming amplitudes, about a 1 order of magnitude increase due to the presence of harmonics and their consequent attenuation in the fluid. |
| One-dimensional Eckart | The quantity $(\mathbf{u} \cdot \boldsymbol{\nabla})\mathbf{u} = 0$ by definition, and, therefore, momentum equation for flow is linear. Traveling acoustic wave from single, planar source with characteristic length scale of wave propagation $\mathcal{L} \gg \lambda$. Viscous fluid and divergenceless (solenoidal) flow. | Streaming away from sound source into unbounded fluid. The Reynolds number $\mathrm{Re}_{\mathcal{L}} = \rho_f U_0 \mathcal{L}/\mu$ determines whether the streaming is fast or slow. | Eckart (1948); Markham (1952); Tjøtta and Tjøtta (1994); Bradley (1996); | Unbounded at one end of sound propagation path: traveling-wave propagation. Viscous attenuation length scale $\ll$ acoustic wave attenuation length scale. A model derived by Eckart (1948) to describe quartz wind as a one-dimensional solution including only the solenoidal (divergenceless) component of the streaming; he showed that the forces generating the streaming were dependent upon the shear and bulk viscosities, while the dissipative forces depend only on the shear viscosity. Lighthill (1978) showed that other forms of dissipation are important as well, and so the situation is usually more complex. Bradley (1996) illustrated the importance of retaining the curl term in the second-order streaming solution for cases where the acoustic radiator is moving with a spatiotemporal phase shift across its surface, e.g., Rayleigh SAW. Corresponds to Poiseuille flow in standard fluid dynamics. |

James Friend and Leslie Y. Yeo: Microscale acoustofluidics: Microfluidics …

TABLE I.   (*Continued*)

| Streaming | Assumptions | Characteristics | References | Notes |
|---|---|---|---|---|
| Medium-grained (Rayleigh) | Acoustic wave bounded along sound propagation path: standing acoustic wave. Incompressible everywhere and inviscid in bulk of fluid (classical assumptions). | The Reynolds number $\mathrm{Re}_\lambda = \rho_f U_0 \lambda / \mu$ determines whether the streaming is fast or slow. For slow streaming, $U_0 \propto u_1^2$. Vortex flow; the scale of the vortices is approximately the same as the acoustic wavelength. Analysis valid only outside viscous (Stokesian) boundary layers. | Rayleigh (1884); Lighthill (1978); Riley (2001); Hamilton *et al.* (2003) | Streaming outside the viscous boundary layer due to *Rayleigh's law*: the matching of the vortical flow in the fluid bulk to the vortices in the Stokes boundary layer (Riley, 2001). Rayleigh streaming is sometimes (and arguably incorrectly) called *microstreaming* (Spengler *et al.*, 2003) in recognition of the smaller length scale at which it appears compared to coarse-grained streaming; microstreaming is usually used to describe fine-grained streaming. For cases where either both walls are oscillating or where the system is axisymmetric with an oscillating boundary; see Secomb (1978). |
| Fine-grained (Schlichting) | Acoustic wave bounded along sound propagation path: standing acoustic wave. Classical assumptions: incompressible (see text) everywhere and inviscid in bulk of fluid. | The Reynolds number $\mathrm{Re}_\delta = \rho_f U_0 \delta / \mu$ determines whether the streaming is fast or slow. Bounded along sound propagation path: standing wave. $U_0 \propto u_1^2$. Vortex flow; the scale of the vortices is approximately the same as the acoustic wavelength. | Schlichting (1932); Jackson and Nyborg (1958); Nyborg (1965); Bradley (1996); Ramos *et al.* (2001) | Streaming in the viscous boundary layer, sometimes called microstreaming (Jackson and Nyborg, 1958; Rife *et al.*, 2000; Doinikov and Bouakaz, 2010). Qi (1993) showed that compressibility in gases is important to properly determine the acoustic streaming near rigid boundaries. Bradley (1996) showed that the curl term in the second-order streaming solution cannot be neglected for cases where the acoustic radiator moves with a spatio-temporal phase shift across its surface, e.g., Rayleigh-Lamb waves. For cases where either both walls are oscillating or where the system is axisymmetric with an oscillating boundary, see Secomb (1978). Boundary-layer thickness is traditionally defined to be approximately $1.9\delta = 1.9\sqrt{\mu/\pi f \rho}$ where $\delta$ represents the viscous boundary-layer thickness; in water at 1 MHz, $\delta = 120$ nm. |

Streaming velocity $\sim U_0$; acoustic particle velocity $\sim u_1$. Generally, $\mathrm{Re}_\mathcal{L} \gg \mathrm{Re}_\lambda \gg \mathrm{Re}_\delta$; compare to other Reynolds numbers in Glossary.

(piezoelectric) tourmaline, small pieces of straw and wood were attracted to it; understanding that an electrostatic field in the material was causing the attraction had to wait until the 19th century, along with a name provided by Brewster in 1824: *pyroelectricity*. All pyroelectric materials are also piezoelectric, and the study of the latter (Chilowsky and Langevin, 1916) provided transducers for SONAR for detecting submarines near the end of the first World War. This success provided much of the impetus for research on these materials throughout the remainder of the 20th century.

Although a detailed description of piezoelectric material properties, modeling, and usage is provided by Friend and Yeo (2008a), a summary is supplied here for completeness. All piezoelectric materials are also anisotropic, and there are examples of piezoelectric materials that are single crystals (Berlincourt *et al.*, 1964), polycrystalline ceramics (Park *et al.*, 2004), and polymers (C. Li *et al.*, 2007). Many of the known piezoelectric materials have at one time or another been used in microfluidics, for which their rapid response and large force transmission have been beneficial, although researchers have had to learn to overcome small strains, thermal losses, aging, and fabrication difficulties.

These materials are able to transform energy between mechanical and electrical forms; a given material is said to be piezoelectric if either an applied stress generates an electric field within or vice versa, with a linear relationship (as opposed to *electrostrictive* materials that exhibit a quadratic relationship). In current applications, they are used to generate static and dynamic mechanical motion at frequencies up to a few tens of gigahertz, depending on the motion to be induced, the scale of the device, and the material used. Compared to other methods of power transduction, piezoelectric transduction provides large forces at small strain rates (usually less than 1% strain) from electrical energy input via the *inverse piezoelectric* effect, and relatively large voltages and small currents from mechanical energy input as described by Umeda *et al.* (1996) via the *direct piezoelectric* effect. Piezoelectricity is usually treated as a linear interaction between mechanical and electrical phenomena, although this assumption is generally invalid for high-power applications or in materials either possessing large hysteresis losses or undergoing large deformations (Hall, 2001).

All polarized piezoelectric materials are also pyroelectric, and changing the temperature of such materials with remnant polarization may cause large electric fields to form within (Smith and Welsh, 1971). Static voltages of 1 kV order are not unheard of in polycrystalline lead zirconium titanate (PZT) after a temperature change of 50 °C, warranting due care in handling, especially in photolithography (Bordui *et al.*, 1999). A piezoelectric material will also lose its polarization if its temperature is raised above the Curie temperature, near the temperature of maximum dielectric constant, the Curie-Weiss temperature. The polarization loss will be permanent in both polycrystalline materials such as PZT and piezoelectric polymers (at least until they are *repolarized*).

Since the mechanical and electrical behaviors are coupled in these materials, a change in boundary conditions in one domain will change the behavior of the material in the other domain. By leaving a polarized piezoelectric element open circuited, the mechanical stiffness of the material will be higher, known as *stress stiffening*. Similarly, mechanically clamping a piezoelectric element will tend to increase its impedance.

Microfabrication is an essential part of the research effort in acoustic microfluidics because of the obstacles present in integration of piezoelectric materials into devices for generating the acoustic waves. Piezoelectric materials have a wide range of applications by themselves, from actuators and motors (Ueha *et al.*, 1993; Hemsel and Wallaschek, 2000; Watson *et al.*, 2009), control of structural dynamics (Irschik, 2002), memory (Alexe *et al.*, 2001) (see Fig. 3), SONAR (Gallego-Juarez, 1989), and quantum computing (Ahlers *et al.*, 2004; König *et al.*, 2005) to sensors and power generation (Sodano *et al.*, 2004; Priya, 2007), even using radioisotopes (Lal *et al.*, 2005).

Fabrication of these materials typically takes one of five routes (Polla and Francis, 1998):

(1) Traditional solid-state chemistry in sintering powdered oxides to form a polycrystalline ceramic from a green state, itself formed by pressing the mixed oxide powders into a semicompact form as a pellet, especially common using PZT and its doped variants (Randall *et al.*, 1998).
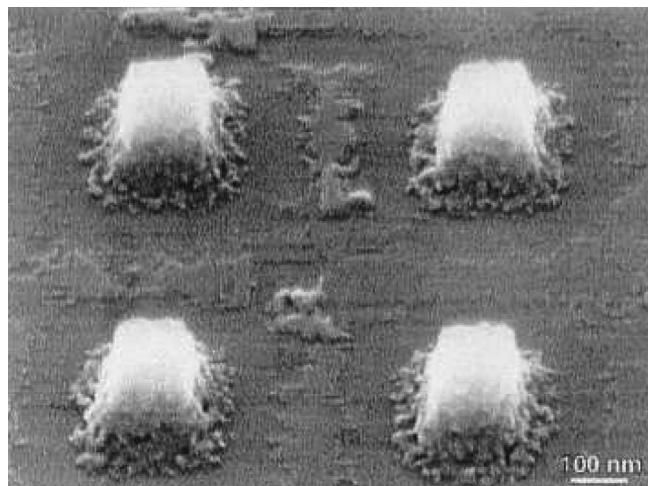


FIG. 3.   Piezoelectric memory: PZT polycrystalline nanostructures annealed for 1 h at 650 °C. From Alexe *et al.*, 2001.

(2) Polymer-assisted techniques (Jia *et al.*, 2004) such as screen printing (Yao *et al.*, 2005), the hydrothermal technique (Kutty and Balachandran, 1984; Ohba *et al.*, 1994; Deng *et al.*, 2003), or tape casting (Schwarzer and Roosen, 1999).

(3) The Czochralski process to form single-crystal materials, especially for lithium niobate and lithium tantalate (Nassau *et al.*, 1966).

(4) Physical vapor deposition techniques including sputtering (Watanabe *et al.*, 1995; Yoshino *et al.*, 2000) and pulsed-laser deposition (Ryu *et al.*, 2000), which is particularly amenable to complex chemistries (Wang *et al.*, 2008).

(5) Chemical vapor deposition (CVD) techniques, particularly metalorganic CVD (Kim and Lee, 2007; Takeuchi *et al.*, 2007), that are well suited to single-crystal fabrication.

These methods together offer a great deal of flexibility in using piezoelectric materials in microfluidics, much of which remains unexplored.

Although some of these methods have been around for years, the deposition of piezoelectric materials onto surfaces both suitable for actuation and compatible with microelectronics and microfluidics—silicon, for example—has only been possible in the past decade (Muralt, 2000; Wang *et al.*, 2002). Traditionally, the choices of piezoelectric material for mechanical energy output was limited to Rochelle salt, tourmaline, quartz, lithium niobate (Weis and Gaylord, 1985), zinc oxide, and the inherently polycrystalline PZT. Of these choices, PZT offered the most powerful mechanical output and came to dominate most ultrasonic transducer applications. Given the importance of biomedical applications for microfluidics, the use of lead-containing piezoelectric materials such as PZT, with typically over 60% lead by weight and much of it trapped in the grain interstices in solid solution, is precluded. Worse, one must tolerate lead contamination of fabrication equipment, an unrealistic situation for most microfabrication facilities. Fortunately, recent developments in high-performance, lead-free piezoelectric materials (Saito *et al.*, 2004) may solve this problem. Other lead-free piezoelectric materials such as lithium niobate, lithium tantalate, zinc oxide (Fu *et al.*, 2010), polypyrrole (Y. Wu *et al.*, 2005), and polyvinylidene fluoride (C. Li *et al.*, 2007) are already being used as piezoelectric materials in microfluidics, and their use will surely expand as the fabrication processes for these materials are improved (Jia *et al.*, 2004) and tailored to accommodate the special requirements of fluid handling at small scales.

The issues in controlling and exploiting scale in microfluidics take on additional complexity with the use of piezoelectric materials, particularly polycrystalline polarized media such as zinc oxide and PZT that have specific grain sizes and their own scaling rules as a consequence (Setter *et al.*, 2006; Setter, 2008). In addition, these materials exhibit reduced performance in thin-film form, and one cannot forget the additional difficulty of incorporating electrodes and circuitry to provide electrical energy to these piezoelectric materials for transduction to mechanical output in actuation or vice versa in sensing. The number of new piezoelectric materials and ways in which they may be deposited and used is proliferating as scientists deal with these problems (Wilson *et al.*, 2007; Hodgson *et al.*, 2009).

## C. Ultrasonic devices

In combining the ability for piezoelectric materials to efficiently generate vibration in solid materials with the use of those vibrations for productive purposes, ultrasonic devices span many applications from medical to industrial. While a complete review of the devices would be overwhelming, we highlight a few interesting uses of this technology in an admittedly incomplete fashion.

The generation of acoustic waves even in piezoelectric materials is a challenge defined by the ability to pattern electrodes on or in the material that will form an appropriate electric field for forming the acoustic wave. One may choose from configurations as simple as a pair of planar electrodes covering a majority of the exposed faces of a piezoelectric material, as is typical in ultrasonic cleaner applications (Kobayashi *et al.*, 2008), for example, to arrangements with complex electrode configurations to drive and pick up surface acoustic waves with very narrow bandwidth (Jung, 2005). Surface acoustic waves, in particular, are useful for a broad range of applications and so the literature covering methods and materials for their generation is vast; Kadota (2005) provided an erudite review of the area. The simple electrode configurations permit the generation of thickness and planar vibrations with good efficiency, and for specific cuts of quartz, they can be used for shear mode vibrations in quartz crystal microbalances (Marx, 2003). Indeed, with some creative machining, it is possible to generate torsional vibration (Friend *et al.*, 2004; Liu *et al.*, 2008; Watson *et al.*, 2010) and to tailor the vibration response of the material to suppress spurious modes, for example, the suppression of transverse vibration in ultrasonic transducers to produce a purely longitudinal acoustic pulse for medical imaging (Marx, 2003).

By stacking many layers of piezoelectric material with interspersed electrodes to form a *multilayer piezoelectric actuator* (MLPA), largely invented by Furuta and Uchino (1993), one can increase the overall displacement amplitude of the material while avoiding large voltages. These actuators required years of development and are now common in static displacement applications of a few micrometers, although more recently the availability of so-called hard PZT (Jullian *et al.*, 2004) in their manufacture makes it possible to use such MLPAs for ultrasonic actuation up to a few MHz.

Patterning those electrodes on surfaces can lead to complex electric fields within the piezoelectric material appropriate for generating other kinds of waves. Although there are numerous examples, from traveling-wave motors (Watson *et al.*, 2009) to atomic force microscopy actuators (Fantner *et al.*, 2006), the most relevant form of electrode patterning was originally developed four decades ago in a desire to generate acoustic waves on the planar surface of a piezoelectric substrate (White and Voltmer, 1965). This achievement in part resulted in a broad development of ultrasonic devices for communication applications that continues today (Hashimoto, 2000). Because microfluidics is also based on
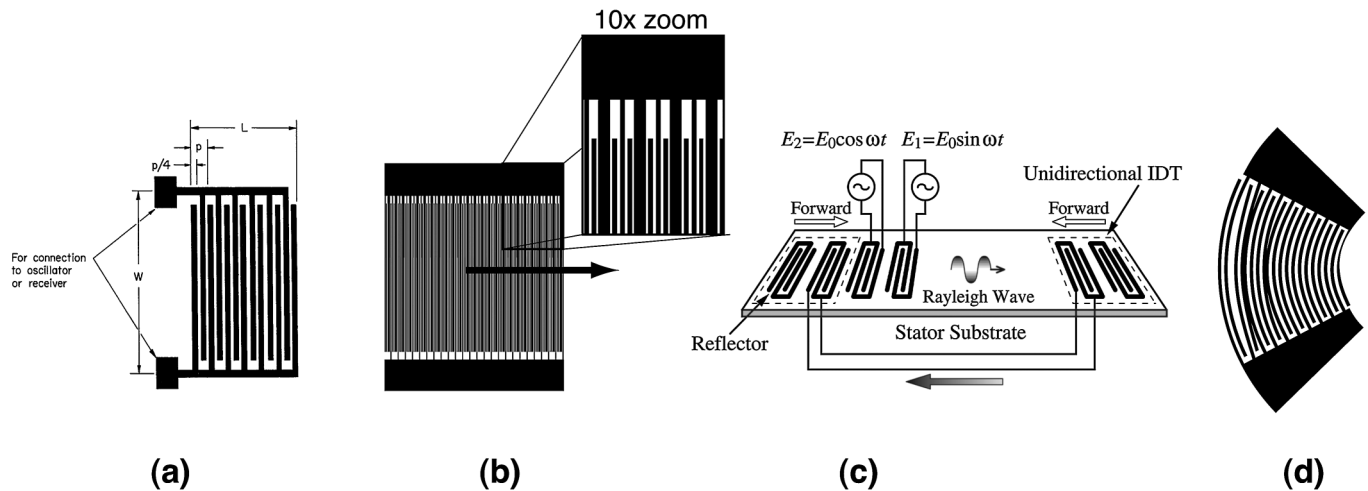
FIG. 4. The simplicity of (a) the first interdigital electrode (from White and Voltmer, 1965) remains attractive for many applications despite the usefulness of more complex designs such as (b) the SPUDT which directs most of the acoustic wave energy in a single direction. (c) Circulation structure used to return acoustic energy back to the supply transducer (from Asai *et al.*, 2004). (d) Tapered designs for focusing acoustic energy.

planar fabrication techniques, this technology is a natural fit. Among the many designs available for consideration, the use of unidirectional electrodes, circulation techniques, and tapered structures are, for the moment, among the most useful adaptations of that original structure for microfluidics applications.

Proposed many years ago (Hanma and Hunsinger, 1976; Hartmann and Abbott, 1989), the single phase unidirectional transducer [SPUDT; see Fig. 4(b)] only came into popular usage in telecommunications about a decade ago (Hode *et al.*, 1995), probably due to the challenges of properly analyzing the electrical and acoustic fields present in the piezoelectric substrate (Chen *et al.*, 1992). By providing internally placed electrodes to reflect the electroacoustic wave and induce constructive interference, nearly all of the acoustic energy generated via transduction by the SPUDT propagates out from the electrode in a single direction. Because of the complexity of the electromechanical coupling, new electrode designs continue to be devised which are easier to fabricate and offer better performance (Martin *et al.*, 2004). Even so, the current designs are useful for microfluidics as will be discussed.

Although the SPUDT design prevents loss of the acoustic energy by directing it in the desired direction from the transducer, it is likely that some of the energy will not be used up in the application and will propagate to the boundary of the device and reflect back, causing interference. While introducing an absorber to eliminate the reflection problem is simple, it also reduces the overall efficiency of the device. For some applications in microfluidics, this is unacceptable, and other techniques to recapture that energy are appropriate. Perhaps the most interesting approach is the power circulation technique described by Kurosawa's group (Asai *et al.*, 1999), which can be designed to be entirely contained on the substrate surface as an integrated structure. In their extremely high-power application (with input powers of over 10 W at 10 MHz), the efficiency was increased by a factor of 7.

Another approach to improving the utility of the acoustic energy generated on a planar surface is to focus the energy

using a tapered design [see Fig. 4(d)] (T. Wu *et al.*, 2005). Such designs are deceptively simple in that they appear to function much like lens elements in optics, but are complicated by the presence of anisotropy in the substrate material, particularly in cuts typically used to obtain large mechanical displacements in the substrate, such as the 127.68° *Y* axis rotated about the *X* axis, and the *X*-propagating (128YX LN) cut of lithium niobate. There are a variety of focusing designs, including elliptical and circular structures, that give different focal patterns of acoustic waves, which in itself can be useful (Shilton *et al.*, 2008). Additionally, Laude *et al.* (2008), using interdigital electrodes that are designed from the *slowness curves* of the piezoelectric substrate (Auld, 1973), showing an ability to increase the fidelity of the mechanism to focus the acoustic energy to subwavelength scales.

### D. Microfluidics

The discipline of microfluidics relies upon the ubiquity of fluids in performing tasks in chemistry, biology, and materials science. Working at a scale where the fluid physics is dominated by surface tension and viscosity, *surface* forces in lieu of *body* forces such as gravity, where the flows are nearly universally laminar, and where mixing is solely defined by diffusion, scientists have been seeking to provide nearly all of the functionality of a modern research laboratory on a single chip, the *lab-on-a-chip* concept. Besides the features of speed and small sample sizes that are a consequence of the small scale, the massively parallel manufacturing techniques offered from integrated circuit *photolithography* methods, MEMS or microelectromechanical systems, promise to greatly reduce the cost of medical diagnostics, drug delivery systems, and materials fabrication, among other areas upon application into microfluidics. Because of its importance, the area has been reviewed by many over the 20 years since the area was founded by Manz *et al.* (1990) who described a new method for liquid chromatography, and so we only briefly comment on a few review articles here.

Whitesides (2006) described in his overview how the field began and provided an accessible introduction to the field. Stone *et al.* (2004) provided a comprehensive review of microfluidics up to about 2003, especially focusing on the use of electric fields to manipulate fluids. A recent text by one of us (Chang and Yeo, 2010) reviews the same field more comprehensively. Stone and his colleagues' work also considered ways in which to manipulate dispersion and mixing within the fluids propagating through the microfluidics device, mainly to enhance mixing, which has long been an important prerequisite of the practical use of microfluidics. Because the flow is laminar and thus the mixing predominantly relies on diffusion, chemical reactions upon which most practical applications rely proceed very slowly even though the diffusion distances are smaller than for benchtop-sized reaction vessels. The methods available to mix fluids chaotically at the microscale are typically grouped into passive and active mixer groups. Passive mixers, where the mixing action is simply a consequence of the fluid passing through the device, are ostensibly attractive because they do not require a separate power source and perhaps complexity in design to incorporate some unique electromechanical component. However, they can be difficult to fabricate at small scales because of the intricate design usually required to achieve effective performance while avoiding unacceptably high losses. Active mixers, on the other hand, usually move the requisite complexity from the structure to the materials; later we show very effective mixing devices that make use of piezoelectric materials that generate acoustic waves and in turn act to improve the mixing.

Squires and Quake (2005) provided a broader review that considered the underlying physical phenomena seen in a series of practical microfluidics devices from the perspective of typical nondimensional quantities such as the Reynolds, Péclet, Grashof, and Knudsen numbers, among others, that may be used to characterize the fluid behavior. They curiously note the emergence of acoustic streaming as a means to manipulate fluids in microdevices, briefly covering the same area we aim to discuss in detail in this review. Craighead (2006) focused upon the application of microfluidics in an integrated, lab-on-a-chip approach to find and characterize individual biomolecules of particular importance to the future of acoustic microfluidics in Sec. V. Ohno *et al.* (2008) presented a review of microfluidics as applied to analytical chemistry and biochemistry, and Salieb-Beugelaar *et al.* (2010) provided a recent review of microfluidics applied to cellular biology, both from the same group that established microfluidics thinking in this same area some 10 years prior; Meyvantsson and Beebe (2008) provided a thorough review on the application of microfluidics to cell culture. Ho *et al.* (2011) provided a comprehensive and broad review of laboratory and consumer biotechnological applications emerging from the past decade of microfluidics. Teh *et al.* (2008) covered a particularly interesting aspect of microfluidics in association with acoustics: *drop* microfluidics. Notwithstanding the problems caused by evaporation, surface tension and contact line pinning that interfere with the accurate manipulation of drops at small scales, they described a variety of effective methods of working with multiphase flows in closed and open systems. The formation and ma-

nipulation of drops is a key application of standing and traveling acoustic waves, and much remains to be considered in how the acoustic waves can be used in practical ways for this application as discussed later.

## III. WAVE GENERATION AND PROPAGATION IN SOLIDS AND FLUIDS

In this section the sole aim is to introduce the reader to techniques for analysis of acoustic wave propagation in solids and fluids, particularly ones appropriate for working at small scales. We hope to provide just enough coverage of the relevant mathematics so that one can interpret the many mathematical models describing the physical phenomena of acoustic wave propagation. A complete coverage of the topic would easily overwhelm the scope of this review, and so several key references to more in-depth works are provided for those wishing to learn more.

A significant reason for the confusion in applying acoustics to microfluidics and nanofluidics as expressed in the literature is the use of implicit assumptions that give rise to different equations modeling the acoustic phenomena. The tendency to laconically discard and include terms in the modeling of fluid dynamics based on an apparent physical intuition, especially in the classic literature (King, 1934; Eckart, 1948; Westervelt, 1953a), makes reconciling the analysis to an appropriate model for modern use arduous. By presenting an abbreviated derivation of the physical model as applied to surface acoustic wave devices, a popular means to generate acoustic streaming for microfluidics, we hope to couch these various assumptions and terms—Rayleigh, Schlichting, Stuart, and Eckart streaming; incompressible or inviscid fluids; Stokes, viscous, and acoustic boundary layers; infinitesimal acoustic waves; and inertia-free flow, for example—in a cogent, consistent way to weave together the various threads of effort past workers have made to understand these phenomena. We also aim to make acoustic microfluidics accessible to readers with experience limited to either piezoelectric materials, microfabrication, microfluidics, or acoustics. Although some sections may be elementary to the reader, we hope that the others are beneficial.

In what follows, the acoustic wave is presumed to be formed in a piezoelectric material and then transmitted into a fluid. We begin, closely following the approach by Tan (2010) and the approaches used by past workers (Auld, 1973; Campbell, 1998; Royer and Dieulesaint, 2000), by reviewing the equations that describe the propagation of acoustic waves in nonpiezoelectric and piezoelectric solids. Electric field propagation, including the quasistatic approximation for electromagnetic fields, is discussed soon after. Section III.D is focused on the characteristics of $X$-axis surface acoustic wave (SAW) propagation on the especially useful 128YX LN, incorporating anisotropy and piezoelectricity. This specific example was chosen as a brief representation of an approach one can use in analyzing these phenomena. Subsequently, the equations of fluid dynamics are reworked to apply them to infinitesimal acoustic wave propagation and the associated slow second-order acoustic streaming. An extension to acoustic wave propagation in fluids with sufficient amplitude to drive convective acceleration and the

concomitant nonlinear effects giving rise to fast streaming are then covered to complete this section. Readers are advised to consult the Glossary in Sec. VI for definition of some of the terms.

## A. Acoustic waves in solids

An orthogonal Cartesian coordinate system is henceforth used where $i$, $j$, $k$, $l \in \{1, 2, 3\}$, and the Einstein summation convention over repeated subscripts is assumed. The usual assumption of coordinate directions such that $x \equiv 1$, $y \equiv 2$, and $z \equiv 3$ is also used, with $z \equiv 3$ representing the polarization direction in piezoceramics such as PZT. A more comprehensive presentation is provided elsewhere (Pipkin and Rivlin, 1959). Using form-invariance relations and noting the choice of a single orthogonal coordinate system for both the covariant and contravariant representation of the tensors, the second-order strain and stress tensors are symmetric and thus each have only six independent coefficients. The strain may be represented in matrix form as

$$\mathbf{S} = \begin{bmatrix} S_{xx} & S_{xy} & S_{xz} \\ S_{yx} & S_{yy} & S_{yz} \\ S_{zx} & S_{zy} & S_{zz} \end{bmatrix} = \begin{bmatrix} S_1 & \frac{1}{2}S_6 & \frac{1}{2}S_5 \\ \frac{1}{2}S_6 & S_2 & \frac{1}{2}S_4 \\ \frac{1}{2}S_5 & \frac{1}{2}S_4 & S_3 \end{bmatrix} \quad (1)$$

by abbreviating subscripts (Friend and Yeo, 2008a) using the definition $p = \frac{1}{2}(i + j)[1 - |\mathrm{sgn}(i - j)|] + (-i - j + 9) \times |\mathrm{sgn}(i - j)|$, where $i$ and $j$ are subscripts that are combined to give a single subscript $p \in \{1, 6\}$, $1 \leftrightarrow xx = (11)$, $2 \leftrightarrow yy = (22)$, $3 \leftrightarrow zz = (33)$, $4 \leftrightarrow yz = zy = (23) = (32)$, $5 \leftrightarrow xz = zx = (31) = (13)$, and $6 \leftrightarrow xy = yx = (12) = (21)$; the one-half terms are eliminated by definition where present. The relationship between the strain and displacement is then simplified (using notation by Auld, 1973) to

$$\mathbf{S} = \tfrac{1}{2}(\nabla \boldsymbol{\xi} + \widetilde{\nabla \boldsymbol{\xi}}) = \nabla_s \xi_i, \quad (2)$$

where the (˜) tilde designates a transpose of the inner term (·), and $\boldsymbol{\xi}$ is the particle displacement. By using Eqs. (1) and (2), an abbreviated form of the strain and particle displacement relationship may be written as

$$\begin{bmatrix} S_1 \\ S_2 \\ S_3 \\ S_4 \\ S_5 \\ S_6 \end{bmatrix} = \nabla_s \xi_i = \begin{bmatrix} \frac{\partial \xi_x}{\partial x} \\ \frac{\partial \xi_y}{\partial y} \\ \frac{\partial \xi_z}{\partial z} \\ \frac{\partial \xi_y}{\partial z} + \frac{\partial \xi_z}{\partial y} \\ \frac{\partial \xi_x}{\partial z} + \frac{\partial \xi_z}{\partial x} \\ \frac{\partial \xi_x}{\partial y} + \frac{\partial \xi_y}{\partial x} \end{bmatrix}. \quad (3)$$

Given the matrix representation of the stress tensor,

$$\mathbf{T} = \begin{bmatrix} T_{xx} & T_{xy} & T_{xz} \\ T_{yx} & T_{yy} & T_{yz} \\ T_{zx} & T_{zy} & T_{zz} \end{bmatrix} = \begin{bmatrix} T_1 & T_6 & T_5 \\ T_6 & T_2 & T_4 \\ T_5 & T_4 & T_3 \end{bmatrix}, \quad (4)$$

Hooke's law,

$$T_{ij} = c_{ijkl} S_{kl}, \quad (5)$$

$$\begin{bmatrix} T_1 \\ T_2 \\ T_3 \\ T_4 \\ T_5 \\ T_6 \end{bmatrix} = \begin{bmatrix} c_{11} & c_{12} & c_{13} & c_{14} & c_{15} & c_{16} \\ c_{12} & c_{22} & c_{23} & c_{24} & c_{25} & c_{26} \\ c_{13} & c_{23} & c_{33} & c_{34} & c_{35} & c_{36} \\ c_{14} & c_{24} & c_{34} & c_{44} & c_{45} & c_{46} \\ c_{15} & c_{25} & c_{35} & c_{45} & c_{55} & c_{56} \\ c_{16} & c_{26} & c_{36} & c_{46} & c_{56} & c_{66} \end{bmatrix} \begin{bmatrix} S_1 \\ S_2 \\ S_3 \\ S_4 \\ S_5 \\ S_6 \end{bmatrix}, \quad (6)$$

provided the constitutive relationship between stress and strain in the solid. Because of symmetry, the first two and last two indices of the stress and strain tensors are interchangeable, i.e., $c_{ijkl} = c_{jikl}$ and $c_{ijkl} = c_{ijlk}$, and so the fourth-order elastic stiffness tensor may be represented by a $6 \times 6$ matrix by simplifying the notation using abbreviated subscripts. Inverting the elastic stiffness $[c]$ gives a matrix representation for the elastic compliance $[s]$ with constants $s_{ijkl}$: $S_{ij} = s_{ijkl} T_{kl}$. The relationship for stress to particle displacement (as the infinitesimal and strong form of Newton's second law) is governed by the equation of motion

$$\nabla \cdot \mathbf{T} = \rho_s \frac{\partial^2 \xi}{\partial t^2}, \quad (7)$$

where $\rho_s$ is the material's mass density and $t$ is time. The last constitutive relationship in the material was between the electric displacement ($\mathbf{D}$, a second rank tensor) and the electric field $\mathbf{E}$ with component representation

$$D_i = \epsilon_{ik} E_k, \quad (8)$$

where $\epsilon_{ik}$ is the dielectric constant and $E_k$ is the electric field. Equation (3) relating strain and mechanical displacement, Eq. (5) relating stress and strain, Eq. (7) relating stress and the mechanical displacement, and Eq. (8) relating electric displacement and the electric field together form the fundamental relationships between the variables. A thorough derivation of this relationship is provided by Singh and Pipkin (1966).

## B. Acoustic wave propagation in nonpiezoelectric solids

To estimate the speed of acoustic wave propagation in crystalline materials, the equation of motion (7) and the strain-displacement relation (5) are used as follows [where the double-dot notation refers to a double-dot product as in Auld (1973)]:

$$\nabla \cdot \mathbf{T} = \rho_s \frac{\partial \mathbf{u}}{\partial t}, \quad (9)$$

$$\frac{\partial \mathbf{T}}{\partial t} = \mathbf{c} : \frac{\partial \mathbf{S}}{\partial t} \Rightarrow \frac{\partial \mathbf{T}}{\partial t} = \mathbf{c} : \nabla_s \mathbf{u}, \quad (10)$$

where $\mathbf{u}$ is the particle velocity and $\rho_s$ is the solid media's density. For acoustic wave propagation along the $x$ direction ($\partial / \partial y = 0$ and $\partial / \partial z = 0$), and using the material properties of single-crystal LN (trigonal, class $3m$) (Auld, 1973), we find that $c_{15} = c_{16} = c_{25} = c_{26} = c_{35} = c_{36} = c_{45} = c_{46} = 0$ for 128YX LN. Expanding and simplifying Eq. (10) then gives
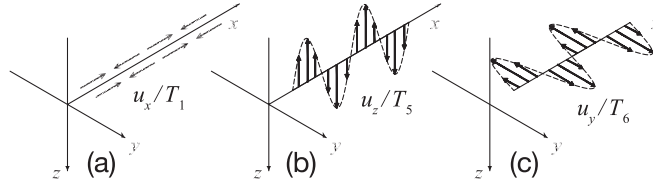
FIG. 5. Wave solutions representing (a) longitudinal, (b) quasitransverse, $z$-polarized shear, and (c) quasitransverse, $y$-polarized shear acoustic wave propagation along the positive $x$ direction, without coupling to the electric field. Most surface waves are a combination of these motions; for example, Rayleigh and Sezawa waves combine (a) longitudinal and (b) transverse, $z$-polarized shear motion, while Love and SH-SAW waves combine (a) longitudinal and (c) transverse, $y$-polarized shear motion.

$$\frac{\partial T_1}{\partial t} = c_{11}\frac{\partial u_x}{\partial x}, \tag{11a}$$

$$\frac{\partial T_2}{\partial t} = c_{12}\frac{\partial u_x}{\partial x}, \tag{11b}$$

$$\frac{\partial T_3}{\partial t} = c_{13}\frac{\partial u_x}{\partial x}, \tag{11c}$$

$$\frac{\partial T_4}{\partial t} = c_{14}\frac{\partial u_x}{\partial x}, \tag{11d}$$

$$\frac{\partial T_5}{\partial t} = c_{55}\frac{\partial u_z}{\partial x} + c_{56}\frac{\partial u_y}{\partial x}, \tag{11e}$$

$$\frac{\partial T_6}{\partial t} = c_{65}\frac{\partial u_z}{\partial x} + c_{66}\frac{\partial u_y}{\partial x}. \tag{11f}$$

By expanding Eq. (10) in a similar way and differentiating and combining the $x$ axis propagating Eq. (11a) and its counterpart from Eq. (10), we get

$$\frac{\partial^2 T_1}{\partial x \partial t} = \rho_s \frac{\partial^2 u_x}{\partial t^2} \quad \text{and} \quad \frac{\partial^2 T_1}{\partial t \partial x} = c_{11}\frac{\partial^2 u_x}{\partial x^2}, \tag{12}$$

that, through elimination of the stress flux term, results in

$$\frac{\partial^2 u_x}{\partial t^2} = \frac{c_{11}}{\rho_s}\frac{\partial^2 u_x}{\partial x^2}, \tag{13}$$

and leads to the well-known one-dimensional wave equation, with a general solution of

$$u_x = f_1\left(t - \frac{x}{U_a}\right) + f_2\left(t + \frac{x}{U_a}\right), \tag{14}$$

where $U_a = \sqrt{c_{11}/\rho_s}$. The function $f_1$ is a wave traveling with phase velocity $U_a$ in the $+x$ direction and the function $f_2$ is a wave traveling with phase velocity $U_a$ in the $-x$ direction, representing a pure longitudinal or compressional wave with phase velocity $U_a$ and its polarization vector [and therefore the Poynting vector as shown by Nelson (1996)] parallel to the direction of propagation [Fig. 5(a)].

Examining Eqs. (11e), (11f), and (12), we may eliminate $T_6$ and $T_5$ to obtain two wave equations:

$$\rho_s \frac{\partial^2 u_y}{\partial t^2} = c_{65}\frac{\partial^2 u_z}{\partial x^2} + c_{66}\frac{\partial^2 u_y}{\partial x^2}, \tag{15a}$$

$$\rho_s \frac{\partial^2 u_z}{\partial t^2} = c_{55}\frac{\partial^2 u_z}{\partial x^2} + c_{56}\frac{\partial^2 u_y}{\partial x^2}. \tag{15b}$$

Assuming the wave is a harmonic, two-dimensional traveling wave defined by $e^{(i\omega t - ikx - iky)}$, where $k = \omega/U_a$ is the wave number and $\omega \equiv 2\pi f$ is the angular frequency if $f$ is the frequency of the wave, Eqs. (15a) and (15b) give, via substitution and rearrangement,

$$(c_{66} - U_a^2\rho_s)u_y + c_{65}u_z = 0, \tag{16a}$$

$$c_{56}u_y + (c_{55} - U_a^2\rho_s)u_z = 0. \tag{16b}$$

Recognizing Eqs. (16a) and (16b) form an eigenvalue problem in $U_a$ and solving, two solutions may be found:

$$(U_a^2)_{\text{I,II}} = \frac{c_{66} + c_{55} \pm \sqrt{(c_{66} + c_{55})^2 - 4(c_{66}c_{55} - c_{65}c_{56})}}{2\rho_s}. \tag{17}$$

These particle velocity solutions possess both $y$ and $z$ components and therefore do not describe a wave moving purely aligned along a particular direction. Solutions $(U_a^2)_{\text{I}}$ and $(U_a^2)_{\text{II}}$ are called either the *quasitransverse* or *quasishear* wave solutions with polarizations transverse to the direction of propagation. Figure 5 shows the computed velocity fields for three kinds of acoustic uniform plane waves propagating along the $x$ direction in a 128YX LN substrate without piezoelectricity. There is one pure compressional wave and two quasitransverse waves.

### C. Acoustic wave propagation in piezoelectric materials

The modeling of wave propagation in piezoelectric materials is complicated by the presence of the electromechanical coupling, naturally, but their anisotropy also makes the analysis difficult. Most useful piezoelectric materials exhibit strong anisotropy in both mechanical and electrical properties, requiring care in the proper utilization of these materials to generate the desired electroacoustic fields. The lengths one must go to to obtain a suitable substrate to propagate acoustic waves can be daunting; effectively generating a simple Rayleigh wave in single-crystal LN demands the use of a 128YX LN substrate as illustrated by Campbell and Jones (1968) in a thorough analysis of the material, upon which only the X axis is really suitable for Rayleigh wave propagation with this cut. An introduction to piezoelectric materials (Friend and Yeo, 2008a) is provided elsewhere, and certainly there are some exemplary reference works in this area (Auld, 1973; Milsom *et al.*, 1977; Hashimoto, 2000; Royer and Dieulesaint, 2000; Xiao and Bhattacharya, 2008) for learning more about modeling acoustic wave propagation in solid piezoelectric media. A challenging aspect of proper analysis is the possibility of a variety of wave types appearing in a piezoelectric material from one form of excitation, or as a consequence of the presence of a fluid on the piezoelectric substrate (Maezawa *et al.*, 2008). Although we focus upon Rayleigh waves here in the analysis, shear-horizontal surface

Rayleigh wave: longitudinal + transverse to interface

Love wave: longitudinal + parallel (shear) to interface

Bleustein–Gulyaev wave: only in piezoelectric substrates

Solid–Vacuum

Scholte wave (or Scholte–Stoneley) wave

Leaky Rayleigh wave

Solid–Fluid

Solid–Solid (Stoneley wave)

Capillary wave

Gravity–capillary wave

Cnoidal wave

Tollmien–Schlichting wave

Faraday wave

Fluid–Fluid

Interface

Sezawa wave (piezoelectric thin film on nonpiezoelectric substrate)

Lamb wave (nonpiezoelectric thin film on substrate)

Generalized Lamb wave (thin film on substrate)

Thin–Film/Pseudo–SAW

**Waves**

Longitudinal wave

Thickness–shear waves (i.e., for quartz crystal microbalances)

Rotary shear wave

Longitudinally–propagating, transverse shear wave

Shear wave

Bulk

Flexural wave: Kirchhoff–Love theory (wavelength/cross–section ratio large)

Flexural wave: Mindlin–Reissner theory (wavelength/cross–section ratio not large)

Lamb wave (nonpiezoelectric without substrate)

Membrane wave (without bending stiffness)

Plate/Shell/2–D Structure

Axial or Longitudinal: Pochhammer–Chree Wave

Torsional wave

Flexural wave (wavelength/cross–section ratio large): Euler–Bernoulli beam

Flexural wave (wavelength/cross–section ratio not large): Timoshenko beam

Rod/1–D Structure

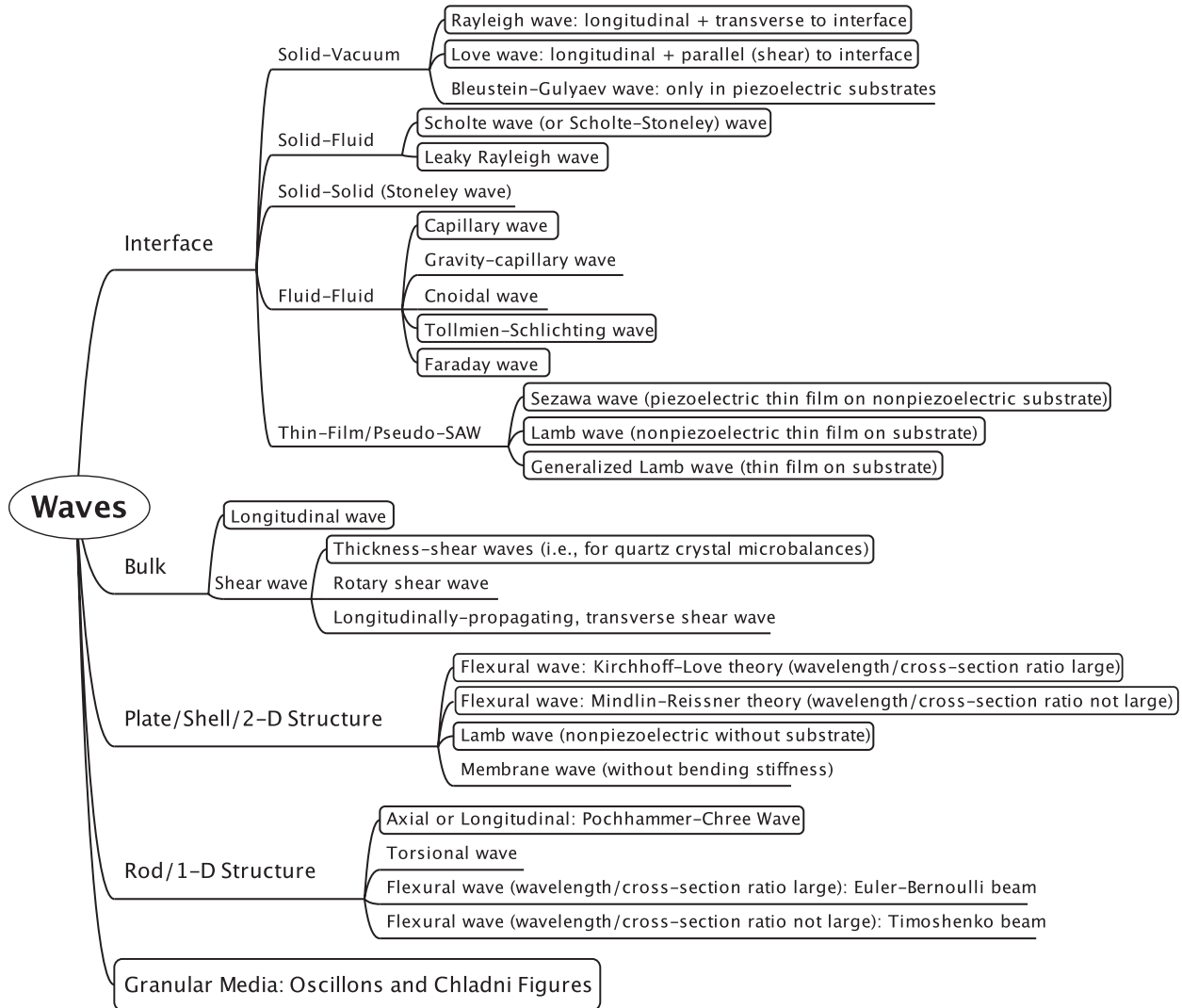Granular Media: Oscillons and Chladni Figures

FIG. 6.    The many forms of acoustic wave transmission as indicated in an incomplete hierarchical list. Among those shown, the boxed items are most likely to appear in acoustic microfluidics.

acoustic waves [SH-SAW (Hashimoto and Yamaguchi, 2001)], surface-skimming bulk waves [SSBW, (Lewis, 1977)], leaky SAW and Scholte waves, by Schröder and Scott, Jr. (2001) and Zarembo and Krasil'nikov (1960), Sezawa waves (Kushibiki *et al.*, 1990), pseudo-SAW (Adler, 1994), and many others may appear and indeed may be used in applications in lieu of the Rayleigh wave. The variety of wave types and names used in describing them reflects the complexity of wave motion that arises from combining materials together that have different sound speeds and impedances (not to mention geometries), as shown in Fig. 6. In many cases, several of the wave types will exist in the same system, SSBW and SAW, for example, and can lead to confusing results if care is not taken to ensure the desired wave type is the only one being generated.

A set of constitutive equations governing the piezoelectric motion written in terms of the components is (Tiersten, 1963; Auld, 1973)

$$D_i = e_{ikl}S_{kl} + \epsilon_{ik}^S E_k, \tag{18a}$$

$$T_{ij} = c_{ijkl}^E S_{kl} - e_{kij}E_k, \tag{18b}$$

where $e_{ikl}$ are the components of the (third rank tensor) piezoelectric stress tensor, $\epsilon_{ik}^S$ are the dielectric constants at constant strain (second rank tensor), and $c_{ijkl}^E$ are the elastic stiffness constants at a constant electric field (fourth rank tensor).[1] Note that the first term of the electric field displacement equation (18a) arises from the relation between electric displacement and electric field [Eq. (8)], while the first term of the stress equation (18b) arises from Hooke's law [Eq. (5)]. Equations (18) take into account the piezoelectric, electromechanical coupling through the piezoelectric stress tensor $e_{ikl}$. Because of the particular coordinate systems used here, the tensor $e_{ikl}$ is symmetric with respect to the last two indices $k$ and $l$, i.e., $e_{ikl} = e_{ilk}$, because of the symmetry in the

---

[1]Figures 1 and 2 in the chapter by Friend and Yeo (2008a) illustrate the meaning of the symbols, superscripts, and subscripts typically appearing in the analysis of piezoelectric materials; there are a much larger set of symbols and three other sets of constitutive equations that are commonly used to represent linear piezoelectric phenomena.

strain tensor, $S_{kl} = S_{lk}$, and so only 18 piezoelectric stress coefficients are required in a matrix representation

$$[e] = \begin{bmatrix} e_{11} & e_{12} & e_{13} & e_{14} & e_{15} & e_{16} \\ e_{21} & e_{22} & e_{23} & e_{24} & e_{25} & e_{26} \\ e_{31} & e_{32} & e_{33} & e_{34} & e_{35} & e_{36} \end{bmatrix}. \tag{19}$$

A set of time-domain piezoelectric constitutive relations and an infinitesimal strain-displacement relationship suitable for use in computational analysis may be derived by taking the time derivative of Eqs. (2) and (18) resulting in, respectively (Auld, 1973; Chagla and Smith, 2006; Tan, 2010),

$$\frac{\partial D_i}{\partial t} = e_{ikl} \frac{\partial S_{kl}}{\partial t} + \epsilon_{ik}^S \frac{\partial E_k}{\partial t}, \tag{20a}$$

$$\frac{\partial T_{ij}}{\partial t} = c_{ijkl}^E \frac{\partial S_{kl}}{\partial t} - e_{kij} \frac{\partial E_k}{\partial t}. \tag{20b}$$

$$\frac{\partial S_{kl}}{\partial t} = \frac{1}{2} \left( \frac{\partial^2 \xi_k}{\partial x_l \partial t} + \frac{\partial^2 \xi_l}{\partial x_k \partial t} \right). \tag{20c}$$

In a piezoelectric substrate the elastic field, described by Eqs. (18), and the electromagnetic field, as Maxwell's equations, are coupled. Although one can solve the coupled equations simultaneously, the velocity of the electromagnetic wave is 5 orders of magnitude faster than the elastic wave. Therefore, the mechanical dynamics, and its effect on the electromagnetic field generated through the piezoelectric coupling, are far slower then the electromagnetic radiation, so much so that we can treat them as quasistatic. This allows us to simplify Eq. (18a) based on the quasistatic assumption represented by

$$\frac{\partial \mathbf{D}}{\partial t} = \mathbf{\nabla} \times \mathbf{H} = 0. \tag{21}$$

Equations (2), (7), (18a), (18b), and (21) form a complete set for analysis of acoustic wave propagation in piezoelectric solids. One can use finite difference techniques (our approach as shown later in this section), finite element analysis (Gantner *et al.*, 2007), lattice Boltzmann methods (Haydock and Yeomans, 2003), and in a few rare cases, closed-form analysis by directly solving the equations. We have also on occasion adopted hybrid techniques, combining closed-form and numerical techniques to avoid the computational costs of numerical methods to handle the wildly different length and time scales in high-frequency acoustic wave propagation for microfluidics (Tan *et al.*, 2007a).

In the next section, we focus upon the propagation of surface acoustic waves on the 128YX LN substrate and into fluids atop the substrate, and provide numerical results in Sec. IV illustrating the use of the derivations of the previous sections in determining the behavior of acoustic wave propagation and the consequent fluid flow in microfluidics devices.

## D. Transmission of acoustic waves and acoustic streaming

In this section, we introduce the governing equations for fluid motion. First we consider the effects of weak, infinitesimally small-amplitude acoustic waves where one can safely assume that the acoustic wave propagates in a linear elastic medium (Zarembo and Krasil'nikov, 1959, 1960; Nyborg,

1965; Morse and Ingard, 1968).[2] For many practical situations, however, the wave amplitude is sufficient to cause distortion of the wave as it propagates (Zarembo and Krasil'nikov, 1959, 1960; Rozenberg, 1971; Rudenko and Soluîan, 1977), requiring more complex analysis of the finite-amplitude acoustic wave propagation.

In microfluidics, understanding how the scale of the experiment affects the phenomena under study is paramount. One of the few investigators to consider the consequences of acoustic streaming at small scales, Frampton *et al.* (2003) illustrated with classical scaling analysis that acoustic streaming is an attractive means to overcome viscous losses and their concomitant resistance to fluid flow in microfluidic channels, because the generation of streaming is itself a direct consequence of the viscous attenuation of the acoustic energy. But Frampton's analysis restricts itself to the perturbation formulation by Nyborg (1965), provided later in Eqs. (30), and omits the fluid inertia in the calculation of the "second-order" acoustic streaming phenomena appearing from the time-averaged product of the first-order density and flow acceleration as does Nyborg, as described by Lighthill (1978) [whereas we include the inertial effects, even for slow streaming, i.e., Eq. (49)], limiting the applicability of his results to slow streaming, rare in acoustic microfluidics devices as explained later. Even with these limitations, Frampton considered the dimensions of the channels in microfluidics devices in comparison to the size of the acoustic boundary layer (defined later), and studied cases where the latter was significant compared to the former. This complicated Frampton's analysis over earlier work by Rife *et al.* (2000), but was necessary due to the importance of viscosity in microfluidics and the large acoustic boundary layers within which the viscous attenuation of the acoustic energy dominates. Other important factors absent in Frampton's analysis were the possible presence of other boundary layers (Stuart, 1963) and additional forms of streaming, to be covered in subsequent portions of this review.

The widely separated time scales of the hydrodynamic and acoustic phenomena are as important as the effects of the physical scale in microfluidics. For acoustic fields, fluid motion occurs on a time scale of $\mathcal{T}_A \sim \mathcal{O}(f^{-1})$ s, while for acoustic streaming, fluid motion occurs in a typical hydrodynamic time scale of $\mathcal{T}_s \sim \mathcal{O}((\alpha u_1)^{-1})$ s, where $\alpha$ is the small-amplitude acoustic absorption coefficient and $u_1$ is the acoustic particle velocity, the amplitude of the velocity fluctuations produced by the passage of an acoustic wave. For example, in many of our own experiments using high intensity surface acoustic waves, the frequency $f$ ranges from $10^6$ to $10^7$ Hz; therefore $\mathcal{T}_A \sim \mathcal{O}(10^{-7})$–$\mathcal{O}(10^{-8})$ s, while $\alpha \sim 5 \times 10^2$ m$^{-1}$ and $u_1 \sim 10$ m/s, and so $\mathcal{T}_s \sim \mathcal{O}(10^{-4})$ s. The 3 to 4 orders of magnitude difference in period between the two phenomena brings its own challenges in analysis and in forming extraordinary nonlinear phenomena.

Over the years, investigators devised a variety of models to try to accurately model acoustic streaming. After providing a derivation from first principles of the governing equations in the following section, we start by taking into account only

---

[2]Note that Fig. 5 in Zarembo, 1959 is upside down (Zarembo and Krasil'nikov, 1959, 1960).

simple forms of streaming and then follow with consideration of fast streaming and nonlinear waves. In considering what follows, it is important to keep in mind the variety of conflicting and overlapping ways solid and fluid dynamics is treated in the literature, and the potential for misunderstanding depending on the reader's background. A Glossary is provided in Sec. VI to especially help the reader with acoustic streaming terminology.

## E. Equations for fluid motion

### 1. The governing equations

In the fluid medium, using conservation of mass, momentum, and energy in the typical way [via Batchelor (1967), for example] results in a set of governing equations appropriate for analysis (Nyborg, 1965; Morse and Ingard, 1968; Bradley, 1996; Doinikov, 1996; Howe, 2007):

$$\frac{\partial \rho_f}{\partial t} + \boldsymbol{\nabla} \cdot (\rho_f \mathbf{u}) = 0, \tag{22}$$

$$\rho_f \frac{\partial \mathbf{u}}{\partial t} + \rho_f (\mathbf{u} \cdot \boldsymbol{\nabla}) \mathbf{u} = -\boldsymbol{\nabla} p + \mu \boldsymbol{\nabla}^2 \mathbf{u}$$
$$+ \left( \mu_B + \frac{\mu}{3} \right) \boldsymbol{\nabla} \boldsymbol{\nabla} \cdot \mathbf{u}, \tag{23}$$

$$\rho_f T \left[ \frac{\partial s}{\partial t} + (\mathbf{u} \cdot \boldsymbol{\nabla}) s \right] = \mu \left( \frac{\partial u_i}{\partial x_k} + \frac{\partial u_k}{\partial x_i} - \frac{2}{3} \frac{\partial u_j}{\partial x_j} \delta_{ik} \right) \frac{\partial u_i}{\partial x_k}$$
$$+ \mu_B (\boldsymbol{\nabla} \cdot \mathbf{u})^2 + \kappa^t \boldsymbol{\nabla}^2 T, \tag{24}$$

where $\rho_f$ is the fluid density, $\mu_B$ is the bulk or dilatational viscosity, $\mu$ is the shear viscosity, $p$ is the pressure, $\mathbf{u}$ is the fluid velocity, $T$ is the temperature, $s$ is the energy, $\kappa^t$ is the thermal conductivity, and $\delta_{ik}$ is the Kronecker delta. The second term in Eq. (23) is associated with *Reynolds stress* and is part of the acoustic streaming to be discussed in Sec. III.F. Reynolds stress is conventionally defined as the stress tensor in a fluid due to the random turbulent fluctuations in the fluid momentum. Lighthill (1952) was best known for his rewriting of the Navier-Stokes equation as Lighthill's aeroacoustic analogy, an inhomogeneous wave equation with the turbulence represented by Reynolds stress as a significant contributor to acoustic noise and consequent structural vibration. But Lighthill (1978) also recognized the converse situation could occur: Passing sound—even noise—through a fluid could generate bulk flow, flow that could become turbulent, and again Reynolds stress was a key contributor to the interaction, and one must take care to recognize this to avoid confusion in terminology. Perhaps it is best noted here that the acoustic wave itself does not have a momentum. Mcintyre (1981) explained in detail how easily one can be led down the path of believing otherwise, particularly in acoustics where even Rayleigh, in a rare mistake, came to believe in 1905 that acoustic forces on objects were induced by a change in the wave's momentum. Even though the waves do not possess momentum, they do transmit momentum flux, and this is the source of the eventual acoustic forces on objects exposed to the waves.

The first and second terms on the right-hand side of the energy equation (24) are together the rate of

heat production by frictional dissipation, while $\kappa^t \boldsymbol{\nabla}^2 T$ is conduction (Howe, 2007). A thermodynamic relation $p = p(\rho, s)$ is used to close the set of equations for a fluid medium (Zarembo and Krasil'nikov, 1959; Zarembo, 1971; Beyer, 1997):

$$p - p_0 = A \left( \frac{\rho_f - \rho_{f0}}{\rho_{f0}} \right) + \frac{B}{2} \left( \frac{\rho_f - \rho_{f0}}{\rho_{f0}} \right)^2 + \cdots. \tag{25}$$

The subscript 0 denotes the fluid properties at equilibrium, and the coefficients $A$ and $B$ represent the adiabatic bulk modulus of elasticity and the so-called nonlinear modulus, respectively (Shutilov, 1988),

$$A \equiv \rho_{f0} \left( \frac{\partial c_0^2}{\partial \rho_f} \right) \bigg|_{s, \rho_f = \rho_{f0}}, \tag{26a}$$

$$B \equiv \rho_{f0}^2 \left( \frac{\partial c_0^2}{\partial \rho_f} \right)^2 \bigg|_{s, \rho_f = \rho_{f0}}, \tag{26b}$$

where $c_0$ is the isentropic, small-signal acoustic wave speed and the $s$ subscript indicates the process occurs with constant entropy. The unitless ratio $B/A$ is common in the literature than $B$ or $A$ by themselves, a consequence of the monumental effort by Beyer (1960) in measuring and describing it. The ratio simply adjusts the sound speed as a linear function of the acoustic wave's vibration velocity amplitude $u_1 = |\mathbf{u}_1|$: $c = c_0 + (B/A)u_1$. The coefficient of nonlinearity is defined as $\beta \equiv 1 + B/(2A)$ (Beyer, 1997), often appearing in nonlinear acoustics analyses. For acoustic wave propagation in a gaseous medium, the following two thermodynamic equations may be used (Doinikov, 1996):

$$d\rho_f = \frac{\gamma}{c_0^2} dp - \alpha_V \rho_f dT, \tag{27}$$

$$ds = \frac{c_p}{T} dT - \frac{\alpha_V}{\rho_f} dP, \tag{28}$$

where $\gamma$, $c_p$, and $\alpha_V$ are the specific heat ratio, specific heat at constant pressure, and the coefficient of volumetric thermal expansion, respectively. For an ideal gas one can connect the nonlinearity parameter $B/A$ to the ratio of specific heats through $B/A = \gamma - 1$.

### 2. Westervelt's paradox: The difference between Lagrangian and Eulerian means is Stokes's drift

A significant contribution to the confusion in acoustic streaming analyses has been the mixing of Lagrangian and Eulerian means to describe a fluid's characteristics. Chu and Apfel (1982) described Westervelt's paradox, where the Eulerian mean of the velocity flow field is constant and oriented toward the source of acoustic radiation. Yet the mean mass flux for this same system, a vibrating piston at one end of a tube that is open at the opposite end transmitting planar acoustic waves down its length, is zero. The paradox is between the mean velocity of the flow and absence of mass flow. However, the Eulerian mean of the flow at a given location along the tube is not the mean velocity of a fluid particle in the tube. The Lagrangian mean *is*; the Lagrangian mean of the velocity of the fluid in the tube is *also* everywhere zero. Further, the density of the fluid is

varying as the wave passes such that $(\rho_f - \rho_{f0})/\rho_{f0} = u_1/c_0$, where $\rho$ and $\rho_{f0}$ are the time-varying and quiescent values, respectively. When the fluid is moving away from the piston as the wave passes, it has a greater density than when it is moving toward the piston. The velocity of the less-dense fluid toward the piston is greater to compensate such that mass conservation holds: There is no mass flow. The term Stokes' drift is sometimes used to describe the difference between the two velocities (Bertelsen *et al.*, 1973; Vega *et al.*, 2004).

### 3. Hydrodynamic and acoustic Reynolds numbers, among others

In microfluidic systems that incorporate acoustic waves, there are at least two important Reynolds numbers that help to characterize the system. In ordinary fluid dynamics problems, the hydrodynamic Reynolds number $\mathrm{Re}_{\mathrm{hydro}} \equiv \rho_f u_0^2/\omega\mu$ defines whether or not the convective acceleration term in the momentum equation, the second term in Eq. (31b), is significant. If $\mathrm{Re}_{\mathrm{hydro}} \gg 1$, the convective acceleration is indeed necessary and the flow will be nonlinear as a consequence. The laminar to turbulent flow transition is known to occur as $\mathrm{Re}_{\mathrm{hydro}}$ grows beyond $\sim 10^2$–$10^6$ depending on the configuration. However, as acoustic waves propagate through a fluid, whether in a microfluidics device or not, the appropriate velocity to consider in the Reynolds number is not simply the apparent velocity of the fluid [the Eulerian fluid velocity or streaming velocity (Westervelt, 1953a)], as traditionally used for the Reynolds number. The Lagrangian fluid velocity should be used in the Reynolds number instead, incorporating both the Eulerian fluid velocity and the particle velocity of the fluid due to the acoustic energy propagating through it. We write this Reynolds number simply as Re because it is ubiquitous in fluid dynamics problems that have significant acoustic fields in them, and we call it the streaming Reynolds number to make it clear it incorporates the Lagrangian fluid velocity, distinctly different from the hydrodynamic Reynolds number that uses the Eulerian fluid velocity. This usage is common in the acoustic streaming literature (Riley, 2001), although the specific definitions widely vary. A system designed to be a microfluidic system can actually have a hydrodynamic $\mathrm{Re}_{\mathrm{hydro}} \ll 1$ that is the same as the streaming Reynolds number, yet upon the application of acoustic irradiation the streaming Reynolds number can drastically increase to $\mathrm{Re} \gg 1$, while the hydrodynamic Reynolds number remains unchanged.

Presuming we know a characteristic Lagrangian fluid velocity $U_0$, we can use this to determine when the flow is *slow* or only encounters resistance from viscosity and exhibits linear behavior, or *fast*, with convective acceleration also present (Rudenko and Soluîan, 1977) by defining $\mathrm{Re} \equiv \rho_f U_0 \mathcal{L}/\mu$, where $\mathcal{L}$ is a characteristic length and $U_0 \equiv |\mathbf{U}|$ is the characteristic flow velocity incorporating both the velocity of the fluid itself $\mathbf{u}_0$ and the effect of the acoustic wave propagation $\mathbf{U} \equiv \mathbf{u}_0 + \langle \mathbf{I} \rangle/\rho_{f0}c_0^2 = \mathbf{u}_0 + \langle \rho_{f1}\mathbf{u}_1 \rangle/\rho_{f0}$, where $\mathbf{I}$ is the acoustic intensity, the flow of acoustic energy per unit cross-sectional area. A transition to nonlinear flow where the convective acceleration is relevant can occur in stages because of the appearance of different forms of streaming in a given system, from Schlichting (micro) streaming to Rayleigh and (non-one-dimensional) Eckart streaming; in other words, fine-grained, medium-grained, and coarse-grained streaming (Zarembo, 1971). The Reynolds number for each form uses a different length scale: $\mathcal{L} = \delta_v$, $\mathcal{L} = \lambda$, and $\mathcal{L} = L$, respectively, where $\delta_v = \sqrt{2\mu/\rho_{f0}\omega}$ is the Stokesian viscous boundary-layer thickness, and $L$ is a characteristic scale of the system that is presumed to be much larger than the acoustic wavelength $\lambda$.

Acoustic wave propagation in fluids can further be characterized by several different acoustic Reynolds numbers. One of the most useful is presented by Naugolnykh and Ostrovsky (1998):

$$\mathrm{Re}_{\mathrm{ac}} = \frac{\beta}{\alpha} \frac{u_1 \omega}{c_0^2}. \tag{29}$$

If $\mathrm{Re}_{\mathrm{ac}} \ll 1$, the wave propagates linearly, because either its amplitude is small (infinitesimal) or the dissipation within the fluid is sufficiently strong to attenuate the wave before its nonlinear, compressibility effects cause it to "overturn" and form a shock. If $\mathrm{Re}_{\mathrm{ac}} \gg 1$, the (finite-amplitude) wave will propagate nonlinearly and will require treatment with either Burgers' equation or the Korteveg–de Vries–Burgers equation and can be expected to exhibit a transition to a sawtooth waveform at a characteristic distance away from the acoustic source, as explained by Tjøtta and Tjøtta (1994) for simple, finite-amplitude waves. With finite-amplitude acoustic wave propagation, portions of the compressible wave traveling through higher pressure regions do so at a higher speed, causing the formation of shocks. This process is countered by viscous and thermal dissipation and dispersion in the propagation speed. The acoustic Reynolds number describes only the propagation behavior of the acoustic wave, and therefore has nothing to do with the convective acceleration term in the momentum equation and its significance as determined by the streaming Reynolds number Re (or the hydrodynamic Reynolds number $\mathrm{Re}_{\mathrm{hydro}}$ for fluid dynamics problems absent acoustic waves).

The peculiar nature of acoustic wave modeling in fluids does not end at the Reynolds number. In standard fluid dynamics problems, the hydrodynamic Mach number $\varepsilon_{\mathrm{hydro}} \equiv u_0/c_0$ must be above about 0.3 to expect compressibility effects in the flow. However, a small acoustic Mach number (Shutilov, 1988), $\varepsilon \equiv u_1/c_0$, does not indicate that the wave can be appropriately treated with an incompressible analysis (Naugolnykh and Ostrovsky, 1998). In water ($c_0 = 1500$ m/s and $\beta = 4$), transmitting an acoustic wave at $f = 10$ MHz with a vibration (particle) velocity of $u_1 = 1.5$ m/s gives an acoustic Mach number of $\varepsilon = 0.001$, although if the wave is sinusoidal and planar, the shock will appear at $\mathcal{L}_N = c_0\lambda/(2\pi\beta v_0) = 40\lambda = 6$ mm from the sound source.

### 4. Acoustic radiation pressure and the radiation stress tensor

Some investigators, Hasegawa *et al.* (2000), for example, inaccurately describe the linear and nonlinear components of acoustic radiation pressures [i.e., the tractions (stresses) that would appear on a surface exposed to an acoustic wave] as

Langevin and Rayleigh radiation pressures, respectively. The linear Langevin component is said to be $\Pi_L \equiv \frac{1}{2}\rho_{f0}u_1^2$, while the nonlinear Rayleigh component is said to be $\Pi_R \equiv \frac{1}{4}(\gamma + 1)\rho_{f0}u_1^2$ for an ideal gas and is related to the nonlinear parameter in a nonelementary way for fluids (Shutilov, 1988). The actual situation for these two radiation pressures is far more complex, explained by Chu and Apfel (1982) and reviewed by Borgnis (1953). The Rayleigh radiation pressure does not necessarily depend on the nonlinear properties of the medium, rather it can depend upon the nonlinear response of a surface that the acoustic wave interacts with. Further, the Rayleigh radiation pressure is not always simply dependent upon the mean energy density of the acoustic field, implying the equation for $\Pi_R$ above is not always correct. Regardless of which radiation pressure is used, the steady-state, acoustic-wave-absent condition must be specified to eliminate the possibility of large errors in the radiation pressure prediction. These two radiation pressures are classically described from a practical perspective as, respectively, the difference between the time averages of the pressure at any point of a fluid traversed by a compressional wave and the pressure of that fluid at rest, and the difference between the pressure of the fluid adjacent to a wall as a compressional acoustic wave is incident and the pressure of that fluid at rest. In a perfectly linear elastic fluid, the acoustic radiation pressure upon either a perfectly reflecting or a perfectly absorbing surface generates no Rayleigh pressure but does generate a Langevin radiation pressure, giving rise to the flawed idea that Rayleigh radiation pressure is associated with the nonlinear component of the acoustic radiation. Wang and Lee (1998) noted that, for fully three-dimensional acoustic radiation propagation problems, the concept of acoustic radiation pressure of whatever sort is inappropriate and best replaced by the consideration of the acoustic radiation stress tensor. Confusing, certainly, and as stated by Beyer (1978) (and quoted by Chu and Apfel) on the long, difficult history of radiation pressure,

It might be said that radiation pressure is a phenomenon that the observer thinks he understands—for short intervals, and only every now and then.

### F. Infinitesimally small-amplitude waves and slow streaming

Presuming infinitesimally small-amplitude waves, the method of successive approximations can be used to linearize the equations, a method popularized for acoustic streaming by Nyborg (1965). We begin by examining the dependent variables for the fluid. The perturbation expansion in the Mach number $\varepsilon = u_1/c_0$ of the fluid velocity, pressure, and density field is, respectively (Hunt, 1955; Nyborg, 1965; Morse and Ingard, 1968; Bradley, 1996; Doinikov, 1996)

$$\mathbf{u} = \mathbf{u}_0 + \varepsilon\mathbf{u}_1 + \varepsilon^2\mathbf{u}_2 + \mathcal{O}(\varepsilon^3) + \cdots, \tag{30a}$$

$$p = p_0 + \varepsilon p_1 + \varepsilon^2 p_2 + \mathcal{O}(\varepsilon^3) + \cdots, \tag{30b}$$

$$\rho_f = \rho_{f0} + \varepsilon\rho_{f1} + \varepsilon^2\rho_{f2} + \mathcal{O}(\varepsilon^3) + \cdots, \tag{30c}$$

$$T = T_0 + \varepsilon\theta_1^T + \varepsilon^2\theta_2^T + \mathcal{O}(\varepsilon^3) + \cdots, \tag{30d}$$

where the subscript 0 refers to the ambient environment, 1 refers to the first-order correction, and the subscript 2 refers to the second-order correction in the expansion in representing the actual value on the left side of the equation; $\theta_1^T$ and $\theta_2^T$ refer to fluctuations of the temperature in the first- and second-order systems, respectively. Note that since subscript 0 refers to equilibrium, then $\mathbf{u}_0 = 0$ m/s, $p_0 =$ atmospheric pressure, $\rho_{f0} = 1.21$ kg/m$^3$ (air), $\rho_{f0} =$ 998 kg/m$^3$ (water), and $T_0 = 300$ K under typical conditions. The fluid velocity field $\mathbf{u}$ can be used to determine the acoustic field's intensity $\mathbf{I}$, and this in turn indicates the power of the acoustic wave by multiplying through by the cross-sectional area. Because this derivation uses the method of successive approximations, the terms in Eqs. (30) are supposed to become progressively smaller. This is not always true, a problem explored later in Sec. III.G.

Expansions (30) may then be substituted into Eqs. (23) and (24); by grouping in terms of $\varepsilon$, one can then form the expressions for the zeroth-, first-, and second-order components of the acoustic field. The usual analysis approach for infinitesimally small-amplitude wave propagation is then to examine the behavior of the system in terms of the first-order acoustic field, followed by a time average of the second-order equations to give the acoustic streaming.

### 1. First-order acoustic field: Linear acoustic waves

The first-order approximations to the conservation of mass, momentum, and energy equations, presuming the zeroth-order velocity $u_0 = 0$, are (Nyborg, 1965; Morse and Ingard, 1968; Bradley, 1996)

$$\frac{\partial\rho_{f1}}{\partial t} + \rho_{f0}(\boldsymbol{\nabla}\cdot\mathbf{u}_1) = 0, \tag{31a}$$

$$\rho_{f0}\frac{\partial\mathbf{u}_1}{\partial t} = -\boldsymbol{\nabla}p_1 + \mu\boldsymbol{\nabla}^2\mathbf{u}_1$$
$$+ \left(\mu_B + \frac{\mu}{3}\right)\boldsymbol{\nabla}\boldsymbol{\nabla}\cdot\mathbf{u}_1, \tag{31b}$$

$$\text{and } \left[\rho_{f0}T_0\frac{\partial s_1}{\partial t}\right]_{s_1=s_0} = 0, \tag{31c}$$

$$\text{or } \rho_{f0}T_0\frac{\partial s_1}{\partial t} = \kappa^t\boldsymbol{\nabla}^2\theta_1^T, \tag{31d}$$

respectively. The first-order momentum equation is linear and therefore applicable only when the inertia is insignificant [Re $\ll 1$, Zarembo (1971)]. Equations (31c) and (31d) are for steady or unsteady heat conduction, depending on the arrangement of the system.

Using the equation of state (25) for an adiabatic process ($s = s_0$) with $A = \rho_{f0}c_0^2$ gives (Morse and Ingard, 1968)

$$p_1 = c_0^2\rho_{f1}. \tag{32}$$

Equation (32) shows that the acoustic wave pressure is independent of the first-order fluid temperature for adiabatic sound wave propagation; any change in density is entirely due to a change in pressure. As such, no first-order temperature calculation is required and Eq. (31c) is applicable under this condition. However, if the nonadiabatic process is significant, such as if the acoustic waves propagate within a gaseous medium, Eq. (31d) should be used in order to take

into account the effect of temperature variations. In this case, the first-order version of Eqs. (27) and (28),

$$\frac{\partial \rho_{f1}}{\partial t} = \frac{\gamma}{c_0^2}\frac{\partial p_1}{\partial t} - \alpha_V \rho_{f0}\frac{\partial \theta_1^T}{\partial t}, \tag{33a}$$

$$\frac{\partial s_1}{\partial t} = \frac{c_p}{T_0}\frac{\partial \theta_1^T}{\partial t} - \frac{\alpha_V}{\rho_{f0}}\frac{\partial p_1}{\partial t}, \tag{33b}$$

completes the set of equations needed to analytically represent the fluid motion.

Equation (31b) can be uniquely decomposed into dilatory and shear components as a consequence of its linearity; the longitudinal velocity, defined such that $\nabla \times \mathbf{u}_l = 0$, gives

$$\rho_{f0}\frac{\partial \mathbf{u}_l}{\partial t} = -\nabla p_1 + \left(\mu_B + \frac{4\mu}{3}\right)\nabla\nabla \cdot \mathbf{u}_l, \tag{34}$$

describing the acoustic propagation in the bulk of the fluid. We note that, in substituting in the particle displacement $\xi_f$ for the fluid velocity $\mathbf{u}_1$, we may write $\nabla \cdot \mathbf{u}_1 \equiv \nabla \cdot \partial \xi_f/\partial t \equiv (\partial/\partial t)\nabla \cdot \xi_f$ by exchanging the order of the derivatives. The $\nabla \cdot \xi_f$ term is essentially the *dilation* of the medium at a point. Therefore, a solution to Eq. (34) involves no shearing of the fluid element, only dilation. These waves are called longitudinal or compressional waves. The transverse velocity (shear wave mode) is given by the remaining component

$$\rho_{f0}\frac{\partial \mathbf{u}_t}{\partial t} = -\mu\nabla \times \nabla \times \mathbf{u}_t, \tag{35}$$

which describes a shear wave that has no dilation and satisfies the criteria $\nabla \cdot \mathbf{u}_t = 0$. This transverse motion in the viscous boundary layer is nonpropagating, and its amplitude decreases exponentially to zero from a maximum at the solid-fluid boundary as we move to the edge of the Stokesian viscous boundary layer with a thickness of $\delta_v$ and is completely absent beyond the layer. If vorticity is defined as $\mathbf{\Omega} = \frac{1}{2}\nabla \times \mathbf{u}_t$ (Morse and Ingard, 1968; Howe, 2007), Eq. (35) can be written as

$$\rho_{f0}\frac{\partial \mathbf{u}_t}{\partial t} = -2\mu\nabla \times \mathbf{\Omega}, \tag{36}$$

implying that the viscosity causes vorticity to diffuse away. The first-order expression of the fluid velocity field is then the sum of these two acoustic fields, $\mathbf{u}_1 = \mathbf{u}_l + \mathbf{u}_t$. The two parts of the velocity solution, $\mathbf{u}_l$ and $\mathbf{u}_t$, can be solved separately and need not be combined until we need them, together, to satisfy the boundary conditions.

## 2. The Stokesian boundary-layer thickness $\delta_v$ and the transverse fluid velocity $\mathbf{u}_t$

For a solid surface vibrating in two dimensions ($x$ and $y$ directions), conservation of mass gives (Morse and Ingard, 1968)

$$\nabla \cdot \mathbf{u}_t = \frac{\partial u_{tx}}{\partial x} + \frac{\partial u_{ty}}{\partial y} = 0 \tag{37}$$

in which the possible solutions are (Morse and Ingard, 1968)

$$u_{tx} = A_x e^{(ik_t x + ik_v y - i\omega t)}, \tag{38a}$$

$$u_{ty} = A_y \frac{k_t}{k_v} e^{(ik_t x + ik_v y - i\omega t)}, \tag{38b}$$

where $k_t$ and $k_v$ are the wave numbers in the boundary layer. Substituting Eqs. (38) into Eq. (35) we find

$$\rho_{f0}(-i\omega)A_x e^{(ik_t x + ik_v y - i\omega t)}$$
$$= -A_x(k_t^2 + k_v^2)e^{(ik_t x + ik_v y - i\omega t)}, \tag{39}$$

where $k_v^2 = -i\omega\rho_{f0}/\mu - k_t^2 \approx -i\omega\rho_{f0}/\mu$ for $\lambda_f \gg l_v$, resulting in

$$k_v = \sqrt{\frac{\rho_{f0}\omega}{2\mu}}(1 + i), \tag{40}$$

using $l_v \equiv \mu/\rho_{f0}c_0$ as the characteristic length (Morse and Ingard, 1968). Using this result in the original solutions, Eq. (38), then gives

$$u_{tx} = A_x e^{[ik_t x + (y/\delta_v)(i-1) - i\omega t]}, \tag{41a}$$

$$u_{ty} = A_y k_t \frac{\delta_v}{2}(1 - i)e^{[ik_t x + (y/\delta_v)(i-1) - i\omega t]}, \tag{41b}$$

where $\delta_v = \sqrt{2\mu/\omega\rho_{f0}}$.

By assuming the two-dimensional solutions of the acoustic pressure and velocity are harmonic,

$$p_1 = Pe^{(ik_t x + ik_v y - i\omega t)}, \tag{42a}$$

$$u_{tx} = \frac{Pk_t}{\rho_f \omega}e^{(ik_t x + ik_v y - i\omega t)}, \tag{42b}$$

$$u_{ty} = \frac{Pk_v}{\rho_f \omega}e^{(ik_t x + ik_v y - i\omega t)}, \tag{42c}$$

where $P$ is the amplitude of the acoustic (over)pressure, and substituting into the first-order momentum equation gives

$$\rho_{f0}\frac{\partial \mathbf{u}_1}{\partial t} = -\nabla p_1 + (\mu_B + 4\mu/3)$$
$$\times \nabla\nabla \cdot \mathbf{u}_1 - \mu\nabla \times \nabla \times \mathbf{u}_1. \tag{43}$$

The substitution for each of these terms can be considered in turn as follows, noting $\nabla \cdot \mathbf{u}_1 = -(\partial p_1)/(c_0^2 \rho_{f0}\partial t)$ and $k = \omega/c_0$:

$$\rho_{f0}\frac{\partial \mathbf{u}_1}{\partial t} = -i\omega\rho_{f0}(u_{tx}\mathbf{i} + u_{ty}\mathbf{j})$$
$$\times e^{(ik_t x + ik_v y - i\omega t)}, \tag{44a}$$

$$\boldsymbol{\nabla} - p_1 = (ik_t\mathbf{i} + ik_v\mathbf{j})Pe^{(ik_t x + ik_v y - i\omega t)}, \tag{44b}$$

$$\boldsymbol{\nabla}\boldsymbol{\nabla}\cdot\mathbf{u}_1 = \frac{k}{c_0\rho_{f0}}P\{k_t\mathbf{i} + k_v\mathbf{j}\}$$
$$\times e^{(ik_t x + ik_v y - i\omega t)}, \tag{44c}$$

$$\mu\boldsymbol{\nabla}\times\boldsymbol{\nabla}\times\mathbf{u}_1 = \mu\{(k_v^2 u_x - k_t k_v u_y)\mathbf{i}$$
$$+ (k_t^2 u_y - k_t k_v u_x)\mathbf{j}\}$$
$$\times e^{(ik_t x + ik_v y - i\omega t)}. \tag{44d}$$

Substituting Eqs. (44) into Eq. (43) and eliminating the common exponential term, we find

$$-i\omega\rho_{f0}u_{tx} = ik_t P + (\mu_B + 4\mu/3)\frac{kk_t}{c_0\rho_{f0}}P$$
$$+ \mu k_v^2 u_{tx} - \mu k_t k_v u_{ty}, \tag{45a}$$

$$-i\omega\rho_{f0}u_{ty} = ik_v P + (\mu_B + 4\mu/3)\frac{kk_v}{c_0\rho_{f0}}P$$
$$+ \mu k_t^2 u_{ty} - \mu k_t k_v u_{tx}. \tag{45b}$$

For MHz-order acoustic waves propagating in water, $\rho_{f0} \sim \mathcal{O}(10^3)$, $\omega \sim \mathcal{O}(10^7)$, $c_0 \sim \mathcal{O}(10^3)$, and $b \sim \mathcal{O}(10^{-3})$. Since $k_t \leq k$, we assume $k_t \approx k \sim \mathcal{O}(10^4)$, and $k_v \sim \sqrt{\rho_{f0}\omega/\mu} \sim \mathcal{O}(10^7)$. From our numerical results for this system, the ratio between the acoustic pressure $P$ and $\mathbf{u}_1$ can be estimated as $P \approx 10^6 u_{tx} \approx 10^6 u_{ty}$. Therefore, the magnitudes of each term in the $x$ and $y$ components of the momentum in the boundary layer are

$$\mathcal{O}(10^{10})u_t \sim \mathcal{O}(10^{10})u_t + \mathcal{O}(10^5)u_t + \mathcal{O}(10^{11})u_t, \tag{46a}$$
$$\mathcal{O}(10^{10})u_t \sim \mathcal{O}(10^{13})u_t + \mathcal{O}(10^8)u_t - \mathcal{O}(10^8)u_t. \tag{46b}$$

The above suggests that the compressive stresses [the third term in Eq. (46a) which gives rise to the transverse motion of the fluid] are insignificant inside the boundary layer of thickness $\delta_v$. The coefficients for the first and second terms are imaginary [Eqs. (45)]: The fluid inertia and pressure are not dissipative. These terms within the boundary layer ensure continuity of the fluid media as the acoustic wave propagates from the boundary layer into the rest of the fluid, which some call Rayleigh's law of streaming (Lighthill, 1978; Riley, 2001). The boundary layer acts as a persistent region that absorbs a portion of the acoustic energy as it passes into the bulk of the fluid. The third and fourth terms in Eqs. (46) represent this absorption of energy, dissipated by the fluid to drive streaming.

The definition of a viscous boundary layer depends entirely on the presumed flow field. For many cases in acoustic field propagation, where a boundary is present, the viscous boundary layer is said to be a Stokes boundary layer generated by fluid motion above a flat plate oscillating back and forth in its

own plane (Wang, 1991). The boundary layer was assumed above [following Morse and Ingard (1968)] to have a thickness of $\delta_v \approx \sqrt{2\mu/\rho_{f0}\omega}$, yet for steady flow over a flat plate, for example, the boundary-layer thickness is $\delta_{\mathrm{Blasius}} \sim \sqrt{\mu x/U}$, where $U$ is the flow velocity in the bulk and $x$ is the distance down the plate from the leading edge (Bertolotti et al., 1992). Indeed one may have several different boundary layers as Stuart (1966) found for large hydrodynamic Reynolds number flows around oscillating cylinders. One may compare the Stokes boundary layer with the acoustic wavelength in the fluid $\lambda_f \sim c_0/f$ as noted by Bradley (1996). The acoustic wave can be expected to travel a few acoustic wavelengths into the fluid, unless the fluid is extremely viscous (and therefore attenuates the wave over a distance less than the acoustic wavelength, a most unusual situation), allowing us to use $\lambda_f$ as a characteristic parameter for this phenomena. Equating the acoustic wavelength and the Stokes boundary-layer thickness terms gives a critical frequency $f_{\mathrm{crit}} = \rho_{f0}c_0^2/8\pi^2\mu$. If $f < f_{\mathrm{crit}}$, the acoustic wave can be expected to propagate well outside the boundary layer, while for $f > f_{\mathrm{crit}}$ the acoustic wave will be attenuated within the boundary layer. For water at room temperature, this critical frequency is about 27.8 MHz, interestingly relevant in SAW microfluidics.

Another problem in microfluidics is the nature of the acoustic wave itself, rarely a simple rectilinear motion; with Rayleigh SAW, for example, the surface oscillates perpendicular to its plane causing a planar acoustic wave to propagate into the fluid. This acoustic wave does not attenuate over the length scale defined by the Stokesian boundary layer, but is still dissipated via viscosity [and other effects as noted by Lighthill (1978)]. Thus, there is potential for confusion between the propagation distances of these various forms of acoustic energy induced near a moving surface due to the use of classical terminology. Bradley (1996) noted the appearance of a curl term in the second-order streaming solution; he used the successive approximations technique in his solution that is important for correctly modeling the flow near the acoustic radiator when it is moving with a spatiotemporal phase difference, e.g., Rayleigh or Sezawa SAWs and Lamb waves. This term accounts for the extraordinary difference in the flow field generated by either a simple rectilinear motion of the solid boundary and the *elliptical* motion of the solid boundary that is typical of cases where a Rayleigh, Lamb, or Love wave is propagating in the solid media. In addition, Bertoni and Tamir (1973) showed a lateral shift of the wave propagating into the fluid from the beginning of the fluid-solid edge, the Schoch distance, and phase reversals near the edge of the propagating sound wave, a phenomenon beyond simple scattering. The possibility of other wave types also complicates the problem, and although most researchers make use of only simple pistonlike reciprocal motion or Rayleigh waves, Scholte waves, as reported by Glorieux et al. (2002), are also useful. Attenuation in their system shows a strong leakage of energy to form bulk waves in the fluid through nonlinear mixing between the different wave modes and dispersion and viscosity-induced turbulence, a chaotic phenomena also discussed in the formation of capillary waves in Sec. IV.

### 3. Second-order slow streaming

At second order, the fluid motion consists of a superposition of the steady-state and harmonic flows. The second-order components of the continuity equation (22), the momentum equation (23), and the energy equation (24) are, respectively (Nyborg, 1965; Bradley, 1996),

$$\frac{\partial \rho_{f2}}{\partial t} + \boldsymbol{\nabla} \cdot (\rho_{f0}\mathbf{u}_2) + \boldsymbol{\nabla} \cdot (\rho_{f1}\mathbf{u}_1) = 0, \tag{47a}$$

$$\rho_{f0}\frac{\partial \mathbf{u}_2}{\partial t} + \rho_{f1}\frac{\partial \mathbf{u}_1}{\partial t} + \rho_{f0}(\mathbf{u}_1 \cdot \boldsymbol{\nabla})\mathbf{u}_1 = -\boldsymbol{\nabla}p_2 + \mu\nabla^2\mathbf{u}_2 + \left(\mu_B + \frac{\mu}{3}\right)\boldsymbol{\nabla}\boldsymbol{\nabla} \cdot \mathbf{u}_2, \tag{47b}$$

$$(\rho_{f0}\theta_1^T + \rho_{f1}T_0)\frac{\partial s_1}{\partial t} + \rho_{f0}T_0(\mathbf{u}_1 \cdot \boldsymbol{\nabla})s_1 = \mu_B(\boldsymbol{\nabla} \cdot \mathbf{u}_1)^2 + \mu\left(\frac{\partial u_{1i}}{\partial x_k} + \frac{\partial u_{1k}}{\partial x_i} - \frac{2}{3}\frac{\partial u_{1j}}{\partial x_j}\delta_{ik}\right)\frac{\partial u_{1i}}{\partial x_k}. \tag{47c}$$

Since the second-order component of the heat equation (47c) is not related to either the momentum equation (47b) or continuity equation (47a), the second-order (streaming) fluid velocities are independent of the second-order heat distribution in the fluid, for both liquids and gases, and hence we may omit Eq. (47c) in the subsequent analysis.

The second-order approximation of the equation of state (25) gives

$$p_2 = A\left[\frac{\rho_2}{\rho_{f0}} + \frac{1}{2}\frac{B}{A}\left(\frac{\rho_{f1}}{\rho_{f0}}\right)^2\right]$$
$$= \frac{c_0^2}{\rho_{f0}}\left[\frac{1}{2}\frac{B}{A}\rho_{f1}^2 + \rho_{f0}\rho_2\right]. \tag{48}$$

By time averaging all the terms in Eqs. (47a), (47b), and (48), one can obtain

$$\left\langle\rho_{f1}\frac{\partial \mathbf{u}_1}{\partial t}\right\rangle + \rho_{f0}\langle(\mathbf{u}_1 \cdot \boldsymbol{\nabla})\mathbf{u}_1\rangle = -\boldsymbol{\nabla}p_{\rm dc} + \mu\nabla^2\mathbf{u}_{\rm dc} + \left(\mu_B + \frac{\mu}{3}\right)\boldsymbol{\nabla}\boldsymbol{\nabla} \cdot \mathbf{u}_{\rm dc}, \tag{49a}$$

$$\rho_{f0}(\boldsymbol{\nabla} \cdot \mathbf{u}_{\rm dc}) + \boldsymbol{\nabla} \cdot \langle\rho_{f1}\mathbf{u}_1\rangle = 0, \tag{49b}$$

$$p_{\rm dc} = \frac{1}{2}\frac{c_0^2}{\rho_{f0}}\left[\frac{B}{A}\langle\rho_{f1}^2\rangle + 2\rho_{f0}\rho_{f,\rm dc}\right], \tag{49c}$$

where $\langle a\rangle \equiv 1/T\int_0^T a(t)dt$. The subscript "dc" refers to the steady-state value of the associated second-order component, which also refers to the entire steady-state value of the component if we add to it the zero-order values, for example, $p_{\rm dc} + p_0$. By combining Eqs. (49a) and (49b), grouping first-order terms into one equation, placing the remaining terms into the second equation, and using Eq. (32), we find

$$\mathbf{F}_{\rm dc} \sim \boldsymbol{\nabla}p_{\rm dc} - \mu\nabla^2\mathbf{u}_{\rm dc}, \tag{50}$$

where the body force density $\mathbf{F}_{\rm dc}$ is given by

$$\mathbf{F}_{\rm dc} = -\frac{1}{c_0^2}\left\langle p_1\frac{\partial \mathbf{u}_1}{\partial t}\right\rangle - \rho_{f0}\langle(\mathbf{u}_1 \cdot \boldsymbol{\nabla})\mathbf{u}_1\rangle$$
$$- \frac{1}{c_0^2\rho_{f0}}\left(\mu_B + \frac{\mu}{3}\right)\boldsymbol{\nabla}\boldsymbol{\nabla} \cdot \langle p_1\mathbf{u}_1\rangle. \tag{51}$$

Since Eq. (51) involves only first-order quantities, we can estimate the order of magnitude for each individual term. Assuming the wave function for the first-order pressure and velocity is $ikx + iky - i\omega t$, we then have the following:

$$-\frac{1}{c_0^2}\left\langle p_1\frac{\partial \mathbf{u}_1}{\partial t}\right\rangle = -\frac{\omega}{c_0^2}i\langle p_1\mathbf{u}_1\rangle,$$

$$-\rho_{f0}\langle(\mathbf{u}_1 \cdot \boldsymbol{\nabla})\mathbf{u}_1\rangle = -k\rho_{f0}i\langle\mathbf{u}_1^2\rangle,$$

$$-\frac{1}{c_0^2\rho_{f0}}\left(\mu_B + \frac{\mu}{3}\right)\boldsymbol{\nabla}\boldsymbol{\nabla}\langle p_1\mathbf{u}_1\rangle = \frac{k^2}{c_0^2\rho_{f0}}\left(\mu_B + \frac{\mu}{3}\right)\langle p_1\mathbf{u}_1\rangle. \tag{52}$$

Substituting these back into Eq. (51), we obtain

$$\mathbf{F}_{\rm dc} = \frac{i\omega}{c_0^2}\langle p_1\mathbf{u}_1\rangle - ik\rho_{f0}\langle\mathbf{u}_1^2\rangle$$
$$+ \frac{k^2}{c_0^2\rho_{f0}}\left(\mu_B + \frac{\mu}{3}\right)\langle i^2 p_1\mathbf{u}_1\rangle. \tag{53}$$

Again, for MHz-order acoustic waves propagating in water, $\rho_{f0} \sim \mathcal{O}(10^3)$, $\omega \sim \mathcal{O}(10^7)$, $c_0 \sim \mathcal{O}(10^3)$, $\mu \sim \mathcal{O}(10^{-3})$, $\mu_B \approx 2.4\mu$, $k = \omega/c_0 \sim \mathcal{O}(10^4)$, and $p_1 \approx 10^6\mathbf{u}_1$. Substituting these into Eq. (53), we find

$$\mathbf{F}_{\rm dc} = \mathcal{O}(10^7)i\langle\mathbf{u}_1^2\rangle - \mathcal{O}(10^7)i\langle\mathbf{u}_1^2\rangle + \mathcal{O}(10^2)\langle\mathbf{u}_1^2\rangle.$$

In this case, the assumption of incompressible flow at this order ($\boldsymbol{\nabla} \cdot \mathbf{u}_1 = 0$) is valid since the third term, representing the compressive stresses, has a small order of magnitude compared to the first and second terms. The streaming force then becomes

$$\mathbf{F}_{dc} = -\frac{1}{c_0^2}\left\langle p_1 \frac{\partial \mathbf{u}_1}{\partial t}\right\rangle - \rho_{f0}\langle(\mathbf{u}_1 \cdot \boldsymbol{\nabla})\mathbf{u}_1\rangle, \qquad (54)$$

with $\boldsymbol{\Omega} = \frac{1}{2}\boldsymbol{\nabla} \times \mathbf{u}_1$, Eq. (54) may then be written as

$$\mathbf{F}_{dc} = -\frac{1}{c_0^2}\left\langle p_1 \frac{\partial \mathbf{u}_1}{\partial t}\right\rangle - \frac{\rho_f}{2}\langle\boldsymbol{\nabla}(\mathbf{u}_1 \cdot \mathbf{u}_1)\rangle$$
$$+ 2\rho_f\langle\mathbf{u}_1 \times \boldsymbol{\Omega}\rangle, \qquad (55)$$

where the last term represents the vorticity. As discussed, the vorticity is sustainable only at regions close to the boundary layer or possessing large shear. Bradley (1996) described the importance of this term to correctly model the flow near the acoustic radiator when it is moving with a spatiotemporal phase difference, giving rise to elliptical motion of points at the surface of the radiator. It helps to account for the potentially enormous difference in the flow field generated by such motion compared to a simple rectilinear motion of the solid boundary and can predict the very large streaming flows parallel to and near the radiator surface.

Some works omit this term, including Eckart (1948), Westervelt (1953a), and Nyborg (1965), and Bradley goes to great lengths to explain how the vorticity arises and propagates within the fluid. Bradley also noted the physical meaning of the first two terms in Eq. (55) for the body force $\mathbf{F}_{dc}$ as a time average of the fluid density multiplied against the fluid's acceleration $\mathbf{a}$, the latter represented by

$$\mathbf{a} = \frac{\partial \mathbf{u}_1}{\partial t} + (\mathbf{u} \cdot \boldsymbol{\nabla})\mathbf{u}. \qquad (56)$$

If the density and acceleration at a point in the fluid oscillate with a phase difference other than $\pm\pi/2$, the density of the fluid will be different when the acceleration is "forward" than when the acceleration is "backward." This results in a momentum flux being carried by the acoustic wave as it propagates through the fluid, in turn generating flow. Such phenomena can even be used to examine the singularities of phase possible in acoustic wave interaction as they propagate through a fluid, as described by Marchiano and Thomas (2008).

The first-order fluid velocity field $\mathbf{u}_1$ is substituted into Eq. (55) to obtain the body force distribution. The streaming velocity $\mathbf{u}_{dc}$ is then obtained by solving Eqs. (49c) and (50). Again, Bradley (1996) made an interesting contribution by showing how the irrotational, solenoidal, and vortical components[3] of the acoustic streaming phenomena contribute to this velocity. Certain parallels with the terms in Bradley's representation and the classical solutions of acoustic streaming problems may be made, especially between Eckart (1948) streaming and the solenoidal component of the acoustic streaming velocity: Eckart streaming assumes only the solenoidal component is relevant. Schlichting (1932) streaming is also reliant on the solenoidal component, but the vortical term absent in Schlichting's original derivation and mentioned previously can be a significant contributor to the flow field in the boundary layer. Rayleigh (1884) and Stuart (1966)

---

[3]Irrotational and solenoidal vector fields give a value of zero everywhere for the curl and divergence of the vector, respectively.

streaming rely on all the terms. The situation is summarized in Table I.

Owing to the constraints inherent in using the method of successive approximations (in other words, the perturbation method), the so-called slow acoustic streaming (second-order) velocities $\mathbf{u}_{dc}$ must be much smaller than the (first-order) acoustic particle velocities $\mathbf{u}_1$, i.e., $\mathbf{u}_{dc} \ll \mathbf{u}_1$: each of the successive approximations made in improving the estimate of the true value of some physical quantity must become progressively smaller (Dyke, 1975). Because of this requirement, the possibility of fluid acceleration in response to acoustic forces must be small and Re $\ll$ 1. In many cases where one would use acoustic streaming in microfluidics, however, the acoustic streaming velocities are at least comparable to the acoustic particle velocities, requiring another approach as presented next.

### G. Finite-amplitude acoustic waves and fast streaming

In this section, we recast the derivation of the acoustic streaming equations to accommodate fast streaming (Re $\geq$ 1) and finite-amplitude, nonlinear acoustic waves (Re$_{ac}$ $\geq$ 1) in a nonheat conducting medium, none of which is treated by the classical analysis methods presented to this point, although we avoid the treatment of shocks, presuming the scale of the microfluidics device is smaller than the propagation distance from the acoustic sound source to the appearance of shock waves $\mathcal{L}_N$. Here we retain terms up to second order in deriving these equations.

#### 1. Finite-amplitude acoustic waves: Nonlinear acoustics

The second-order approximation to the continuity equation (22) is

$$\frac{\partial \rho_{f1}}{\partial t} + (\rho_{f0} + \rho_{f1})\boldsymbol{\nabla} \cdot \mathbf{u}_1 + \mathbf{u}_1 \cdot \boldsymbol{\nabla}\rho_{f1} = 0. \qquad (57)$$

Placing the first- $[\mathcal{O}(\varepsilon)]$ and second- $[\mathcal{O}(\varepsilon^2)]$ order terms on the left and right hands of the equation, respectively,

$$\frac{\partial \rho_{f1}}{\partial t} + \rho_{f0}\boldsymbol{\nabla} \cdot \mathbf{u}_1 = -\rho_{f1}\boldsymbol{\nabla} \cdot \mathbf{u}_1 - \mathbf{u}_1 \cdot \boldsymbol{\nabla}\rho_{f1}. \qquad (58)$$

Substituting the first-order $\mathcal{O}(\varepsilon)$ relations into the second-order $\mathcal{O}(\varepsilon^2)$ terms, we obtain more useful equations; for example, substituting $p_1 = c_0^2\rho_{f1}$ and $\boldsymbol{\nabla} \cdot \mathbf{u}_1 = -(1/c_0^2\rho_{f0})\partial p_1/\partial t$ into the third term in Eq. (58) gives

$$-\rho_{f1}(\boldsymbol{\nabla} \cdot \mathbf{u}_1) = -\left(\frac{p_1}{c_0^2}\right)\left(-\frac{1}{c_0^2\rho_{f0}}\frac{\partial p_1}{\partial t}\right) = \frac{1}{2\rho_{f0}c_0^4}\frac{\partial p_1^2}{\partial t}, \qquad (59)$$

and for the fourth term in Eq. (58) we find

$$-(\mathbf{u}_1 \cdot \boldsymbol{\nabla})\rho_{f1} = \frac{1}{c_0^2}(\boldsymbol{\nabla}p_1) \cdot \mathbf{u}_1 - \frac{1}{c_0^2}\{(\boldsymbol{\nabla}p_1) \cdot \mathbf{u}_1$$
$$+ p_1(\boldsymbol{\nabla} \cdot \mathbf{u}_1)\}$$
$$= \frac{1}{2\rho_{f0}c_0^4}\frac{\partial p_1^2}{\partial t}. \qquad (60)$$

Substituting these terms back into Eq. (58), we obtain for the second-order component of the continuity equation

$$\frac{\partial \rho_{f1}}{\partial t} + \rho_{f0}\mathbf{\nabla} \cdot \mathbf{u}_1 = \frac{1}{\rho_{f0}c_0^4}\frac{\partial p_1^2}{\partial t}. \tag{61}$$

Expanding the variables of the momentum equation (23) into first- and second-order terms, we find

$$\rho_{f0}\frac{\partial \mathbf{u}_1}{\partial t} + \rho_{f1}\frac{\partial \mathbf{u}_1}{\partial t} + \frac{\rho_{f0}}{2}\mathbf{\nabla}\mathbf{u}_1 \cdot \mathbf{u}_1 - \rho_{f0}\mathbf{u}_1 \times \mathbf{\nabla} \times \mathbf{u}_1$$
$$= -\mathbf{\nabla}p_1 + \left(\mu_B + \frac{\mu}{3}\right)\mathbf{\nabla}^2\mathbf{u}_1 + \left(\mu_B + \frac{\mu}{3}\right)\mathbf{\nabla} \times \mathbf{\nabla} \times \mathbf{u}_1. \tag{62}$$

Using the first-order $\mathcal{O}(\varepsilon)$ relations and substituting into all the $\mathcal{O}(\varepsilon^2)$ terms, we obtain for the second-order component of the continuity equation the following:

$$\rho_{f0}\frac{\partial \mathbf{u}_1}{\partial t} = -\mathbf{\nabla}p_1 - \frac{1}{2}\mathbf{\nabla}\mathcal{L} + \rho_{f0}\mathbf{u}_1 \times \mathbf{\nabla} \times \mathbf{u}_1$$
$$- \frac{1}{\rho_{f0}c_0^2}\left(\mu_B + \frac{\mu}{3}\right)\mathbf{\nabla}\frac{\partial p_1}{\partial t} - \mu\mathbf{\nabla} \times \mathbf{\nabla} \times \mathbf{u}_1, \tag{63}$$

where $\mathcal{L} \equiv \rho_{f0}(\mathbf{u}_1 \cdot \mathbf{u}_1) - p_1^2/(\rho_{f0}c_0^2)$ is the second-order Lagrangian density (Hamilton and Morfey, 1998). For plane progressive waves, $\mathcal{L} = 0$ since the first-order pressure $p_1 \approx \rho_{f0}c_0\mathbf{u}_1$.

Two different kinds of nonlinear effects may arise, defined by Hamilton and Morfey (1998) as cumulative and local. Convection and nonlinearity of the pressure-density relation are each classified as a cumulative nonlinear effect because they each cause waveform steepening, an effect over longer length scales that grows with propagation distance, into the far field of the acoustic radiation, that is, beyond a distance of about $\delta_\nu$. Local distortion of the acoustic wave is typical near the source, in the near field (within the Stokesian boundary layer), where cumulative distortion is still very small (Hamilton and Morfey, 1998), and so for this region the local nonlinear effects dominate. As noted previously for infinitesimal acoustic waves and slow streaming (see Sec. III.F), the curl terms are associated with the boundary-layer effects. Because the cumulative nonlinear effects, such as the waveform distortion, dominate in far-field regions away from the source, we can drop the curl terms just as we dropped the Lagrangian density for these regions. Thus, Eq. (63) reduces to

$$\rho_{f0}\frac{\partial \mathbf{u}_1}{\partial t} = -\mathbf{\nabla}p_1 - \frac{1}{\rho_{f0}c_0^2}\left(\mu_B + \frac{4\mu}{3}\right)\mathbf{\nabla}\frac{\partial p_1}{\partial t}. \tag{64}$$

We have made three assumptions to obtain Eq. (64) for the second-order component of the continuity:

(1) The waves are not "excessively strong," specifically, $|U_0| \ll c_0$ or $\varepsilon \ll 1$.
(2) The distortion is dominated by cumulative effects, implying that we are concerned with the fluid behavior in regions away from the source.
(3) The wave propagation is an isentropic process ($s_1 = 0$).

The justification for omitting the Lagrangian density is based on the dominance of cumulative over local nonlinear effects;

as a consequence, such a distinction between these nonlinear effects greatly simplifies the analysis. For progressively propagating acoustic waves, cumulative effects generally dominate. One must carefully consider whether making this assumption is appropriate in other cases. In microfluidics and nanofluidics, whether the ability to separate these effects into such distinct regions is valid or not is an open question. In another work, Hamilton *et al.* (1985) studied how nonlinear phenomena propagate out from the near field to the far field, terms that are familiar to scientists working with acoustics, and found that the nonlinear effects can be strong well out into the far field if the attenuation is weak. Therefore, while the cumulative versus local effects may be distinguished between the two regions, the nonlinear effects cannot. Blackstock (1966) related the two regions in terms of the Fubini (near-field) and Fay (far-field) solutions for the acoustic wave's propagation behavior with an analysis that bridges the two regions and in a manner that may be familiar to some readers.

The energy equation remains unchanged as Eqs. (31c) and (31d) from its presentation in the derivation of the infinitesimal acoustic wave equations. The second-order approximation to the equation of state (25) does change, however, and is given by

$$p_1 = c_0^2\rho_{f1} + \frac{c_0^2}{\rho_{f0}}\frac{B}{2A}\rho_{f1}^2 + \left(\frac{\partial p}{\partial s}\right)_{\rho,0}s_1. \tag{65}$$

Note the appearance of the two additional terms in this relation, compared to Eq. (32), that take the nonlinear behavior into account. The quantity $B/A \approx 5$ for distilled water at room temperature (Beyer, 1997). For non-heat-conducting fluids ($s_1 = 0$), Eq. (65) becomes

$$p_1 = c_0^2\rho_{f1} + \frac{c_0^2}{\rho_{f0}}\frac{B}{2A}\rho_{f1}^2. \tag{66}$$

Substituting the first-order relation in Eq. (32) into the second-order term of Eq. (66), and rearranging a bit,

$$\rho_{f1} = \frac{p_1}{c_0^2} - \frac{1}{\rho_{f0}c_0^4}\frac{B}{2A}p_1^2. \tag{67}$$

Substituting Eq. (67) into Eq. (61) gives, after some algebra,

$$\frac{\partial p_1}{\partial t} = -\frac{\rho_{f0}^2c_0^4}{\rho_{f0}c_0^2 - p_1\beta}\mathbf{\nabla} \cdot \mathbf{u}_1. \tag{68}$$

Equations (64) and (68) may be used to describe the propagation of nonlinear ($\mathrm{Re_{Ac}} \geq 1$) acoustic waves. We next see how these nonlinear waves induce acoustic streaming.

### 2. Fast streaming

Following Zarembo (1971), the dependent variables for the fluid can then be decomposed into the time-averaged streaming flow component, denoted by the subscript dc, and the instantaneous first-order acoustic forcing component, denoted by the subscript 1:

$$\mathbf{u} = \mathbf{u}_{dc}(x, y, z) + \mathbf{u}_1(x, y, z, t), \tag{69a}$$
$$p = p_{dc}(x, y, z) + p_1(x, y, z, t), \tag{69b}$$
$$\rho_f = \rho_{f,dc}(x, y, z) + \rho_{f1}(x, y, z, t). \tag{69c}$$

Because the steady-state components are entirely captured in the dc terms, the instantaneous first-order terms all have a zero time-average value; $\langle \mathbf{u}_1 \rangle = 0$, $\langle p_1 \rangle = 0$, and $\langle \rho_{f1} \rangle = 0$, where $T = nf^{-1}$ in which $n = 1, 2, 3, \ldots$. In contrast to the successive approximations (or perturbation) approach used in the derivation of Eqs. (47) for the infinitesimal acoustic wave propagation in Sec. III.F, which is valid only for slow streaming (Re $\ll$ 1) (Nyborg, 1965; Bradley, 1996; Riley, 2001), the decomposition given by Eqs. (69) permits the acoustic streaming velocities to be larger than the particle velocities, $\mathbf{u}_{\mathrm{dc}} > \mathbf{u}_1$.

Substituting Eqs. (69a)–(69c) into Eq. (23), taking the time average, and assuming $\rho_{f1} \ll \rho_{f,\mathrm{dc}}$, we obtain for the momentum equation

$$\frac{\partial \mathbf{u}_{\mathrm{dc}}}{\partial t} + (\mathbf{u}_{\mathrm{dc}} \cdot \boldsymbol{\nabla})\mathbf{u}_{\mathrm{dc}} - \frac{\mu}{\rho_{f,\mathrm{dc}}}\boldsymbol{\nabla}^2 \mathbf{u}_{\mathrm{dc}}$$
$$- \frac{1}{\rho_{f,\mathrm{dc}}}\left(\mu_B + \frac{\mu}{3}\right)\boldsymbol{\nabla}\boldsymbol{\nabla} \cdot \mathbf{u}_{\mathrm{dc}} = -\frac{1}{\rho_{f,\mathrm{dc}}}\boldsymbol{\nabla}p_{\mathrm{dc}} + \mathbf{F}_{\mathrm{dc}},$$

$$(70)$$

where

$$\mathbf{F}_{\mathrm{dc}} = -\langle (\mathbf{u}_1 \cdot \boldsymbol{\nabla})\mathbf{u}_1 \rangle + \frac{1}{\rho_{f,\mathrm{dc}}^2}\bigg[ \langle \rho_{f1}\boldsymbol{\nabla}p_1 \rangle - \mu \langle \rho_{f1}\boldsymbol{\nabla}^2 \mathbf{u}_1 \rangle$$
$$- \left(\mu_B + \frac{\mu}{3}\right)\langle \rho_{f1}\boldsymbol{\nabla}\boldsymbol{\nabla} \cdot \mathbf{u}_1 \rangle \bigg].$$

$$(71)$$

Following Zarembo (1971), the steady-state density $\rho_{f,\mathrm{dc}}$ need not be equal to the density of the fluid in the unperturbed medium $\rho_{f0}$. However, if $\varepsilon_{\mathrm{dc}} \ll 1$, where $\varepsilon_{\mathrm{dc}} \equiv u_{\mathrm{dc}}/c_0$ is the Mach number for fast streaming, it is nevertheless reasonable to presume that $\rho_{f,\mathrm{dc}} \approx \rho_{f0}$. Therefore, our earlier assumption $\rho_{f1} \ll \rho_{f,\mathrm{dc}}$ requires the condition $\varepsilon_{\mathrm{dc}} \ll 1$. Invoking this, it follows that

$$\frac{1}{\rho} = \frac{1}{\rho_{f,\mathrm{dc}} + \rho_{f1}}\frac{\rho_{f,\mathrm{dc}} + \rho_{f1}}{\rho_{f,\mathrm{dc}} + \rho_{f1}} \approx \frac{\rho_{f,\mathrm{dc}} + \rho_{f1}}{\rho_{f,\mathrm{dc}}^2}.$$

$$(72)$$

The streaming force in Eq. (71) can then be further simplified to become $\mathbf{F}_{\mathrm{dc}} \approx -\langle (\mathbf{u}_1 \cdot \boldsymbol{\nabla})\mathbf{u}_1 \rangle$ if $\rho_{f1} \ll \rho_{f,\mathrm{dc}}$. The first-order fluid velocity field $\mathbf{u}_1$ can be substituted into this result to obtain the body force distribution. The streaming velocity $\mathbf{u}_{\mathrm{dc}}$ can then be calculated by solving Eq. (70). The many forms of streaming are presented in Table I for comparison, and readers are advised to consult the glossary in Sec. VI.

Underlying these analysis methods is a presumption: Separation of acoustic and hydrodynamic phenomena based on widely different time scales is justifiable. For weakly nonlinear phenomena, there is no particular problem and indeed analyses using these sort of techniques have been successful in describing a broad variety of such phenomena (Cross and Hohenberg, 1993). But when the nonlinearities become stronger, indeed sufficient to drive coupling across many orders of magnitude in time via dispersion and diffusion, as with atomization and capillary wave generation as will be shown later, such separation approaches could become difficult to justify. However, there are currently few alternative approaches in the literature, and strongly nonlinear acoustic phenomena at small scales remain a largely unexplored area. We leave this topic at this point, and with the

phenomena of piezoelectrically driven acoustic streaming appropriate for microfluidics now covered in some detail, we look across the literature at the many applications of these phenomena that scientists and engineers are beginning to exploit. The next section covers the many areas in which acoustics are finding use in microfluidics, organized by the way the acoustic energy is used.

## IV. APPLICATIONS

### A. Map

In most cases, the analysis of acoustic microfluidics is driven by a need to understand the phenomenon and make use of it in fulfilling a particular application. This section examines the many applications appearing in recent years and the ways the technology is being used to address them. A map of the current activity is provided in Table II as an attempt to organize the disparate activities in the field into a coherent structure, a structure that is loosely followed over the rest of this section.

### B. Fluid manipulation

#### 1. Oscillation and transport of sessile drops

We begin with an area that predates most other activities in acoustic microfluidics, yet turns out to be one of the most challenging due to the presence of evaporation, free surfaces, pinned drop edges, and varying surface conditions in microfluidics devices. McHale *et al.* (1999) considered the interaction of SAW with very viscous (100 000 cS polydimethylsiloxane oil) sessile drops to try to determine whether the system would be a suitable alternative to quartz crystal microbalances in sensing reactions, the presence of microparticles, and so forth within the drops. What they found instead was a drop that, when exposed to Rayleigh SAW or SH-SAW, exhibited resonances and consequent variation in energy absorption. This was due to the propagation of a component of the acoustic wave into the fluid that was subsequently reflected from its free surface and directed back into the substrate, a phenomenon especially strong in very viscous fluids. Their modeling of the fluid as a Maxwell viscoelastic fluid was useful in forming a theoretical model of the phenomena, although it did not include compressibility. Because the fluid tended to spread upon exposure to the SAW, Ellis *et al.* (2003) sought to model the slip induced by the acoustic wave at the solid-fluid interface, recasting the Blake-Tolstoi theory of molecular and hydrodynamic slip (Blake, 1990) for this purpose. Notwithstanding the many limitations of these theories, they found that as the fluid's contact angle increases (associated with a decrease in disjoining pressure), the magnitude of the resonant frequency shift decreases due to the reduction in the negative disjoining pressure. The frequency shift from this was found to be a more sensitive indicator of surface coupling than a change in the dissipation itself. Alzuaga *et al.* (2005) reported a method for transporting drops by driving them to nodes of a flexurally vibrating beam. As different modes of vibration were chosen by changing the frequency of excitation, the drop could be made to move in either direction among the nodes, although the vibration

TABLE II. A guide to the published applications of acoustic microfluidics.

| Category | Phenomenon | Vibration | Investigators |
|---|---|---|---|
| Droplet or film | Vibration | Thickness | Noblin *et al.* (2004); Vukasinovic *et al.* (2007a, 2007b) |
| | | SAW | McHale *et al.* (1999); Newton *et al.* (1999); Ellis *et al.* (2003); Brunet *et al.* (2010); Tan, Friend *et al.* (2010) |
| | | SH-SAW | Ellis *et al.* (2003) |
| | | Beam | Alzuaga *et al.* (2005) |
| | Translation | Vibration | Brunet *et al.* (2007) |
| | | SAW | Wixforth (2003); Tan *et al.* (2007b); Hodgson *et al.* (2009); Bourquin *et al.* (2010); Brunet *et al.* (2010) |
| | Levitation | Pistonlike | Yarin *et al.* (1998); Santesson and Nilsson (2004); Wood *et al.* (2005) |
| | Jetting and drops | Orifice | Maehara *et al.* (1986); Lee and Lal (2004); Demirci (2005); Meacham *et al.* (2005) |
| | | SAW | Elrod *et al.* (1989); Shiokawa *et al.* (1990); Tan, Friend, and Yeo (2009); Bhattacharjee *et al.* (2010) |
| | Pumping | Thickness | Hasegawa *et al.* (2005); Ma *et al.* (2006); Huang *et al.* (2008); Langelier *et al.* (2009) |
| | | FPW | Moroney *et al.* (1991); Nguyen and White (2000) |
| | | SAW | Li *et al.* (2007b); Cecchini *et al.* (2008); Girardo *et al.* (2008); Bok *et al.* (2009); Tan, Yeo, and Friend (2009); Masini *et al.* (2010) |
| | Internal flow | SAW | Guttenberg *et al.* (2004); Wixforth *et al.* (2004); Jang *et al.* (2005); Dong *et al.* (2006); Schindler *et al.* (2006); Köster (2007); Sankaranarayanan *et al.* (2008); Tan, Yeo, and Friend (2009); Fu *et al.* (2010); Raghavan *et al.* (2010) |
| | Patterning | SAW | Alvarez, Yeo, and Friend (2008) |
| | | Thickness | Keisuke *et al.* (2004); Issenmann *et al.* (2008) |
| | Atomization | Thickness | Lang (1962); Mir (1980); Jin *et al.* (2000); Barreras *et al.* (2002); Felder *et al.* (2003); James *et al.* (2003); Donnelly *et al.* (2004); Forde *et al.* (2006); Vukasinovic *et al.* (2007b) |
| | | Droplet ejection | Elrod *et al.* (1989); Kripfgans *et al.* (2004); Demirci (2005) |
| | | SAW | Kurosawa *et al.* (1995); Kurosawa *et al.* (1997); Chono *et al.* (2004); Kim *et al.* (2005); Alvarez, Yeo, and Friend (2008), Friend *et al.* (2008); Qi *et al.* (2008); Alvarez *et al.* (2009); Heron *et al.* (2010); Qi *et al.* (2010); Ho *et al.* (2011) |
| Particle and bubble suspensions | Manipulation | Membrane | Chladni (1787); Faraday (1831) |
| | | Flexural beam | Dorrestijn *et al.* (2007) |
| | | Thickness | Thomas and Squires (1998); Kaajakari *et al.* (2001) |
| | | SAW | Tan *et al.* (2007b) |
| | | Stoneley wave | Yantchev *et al.* (2010) |
| | | Fluid standing wave | Hutchisson and Morgan (1931); King (1934); Yosioka and Kawasima (1955); Gor'kov (1961); Doinikov (1996); Vainshtein *et al.* (1996); Spengler *et al.* (2000); Haake and Dual (2002); Mitri (2005); Whitehill *et al.* (2010) |
| | | Fluid traveling wave | King (1934); Doinikov (1996) |
| | | Surface tension | Falkovich *et al.* (2005), with SAW: Li *et al.* (2008) |
| | | Bubbles | Doinikov (1999); Rensen *et al.* (2001); Doinikov and Dayton (2006) |
| | Separation | General review | Qi and Brereton (1995) |
| | | Thickness | Woodside *et al.* (1997); Yasuda *et al.* (1997); Spengler *et al.* (2000); Kapishnikov *et al.* (2006) |
| | Mixing | Thickness | Kaajakari *et al.* (2001); Yaralioglu *et al.* (2004); Araz and Lal (2010) |
| | | SAW | Wixforth *et al.* (2004); Sritharan *et al.* (2006); Frommelt *et al.* (2008); Shilton *et al.* (2008); Tan, Yeo, and Friend (2009); Bourquin *et al.* (2010) |
| | | Bubbles | Liu *et al.* (2003); Garstecki *et al.* (2006); Wang *et al.* (2009) |

TABLE II. (*Continued*)

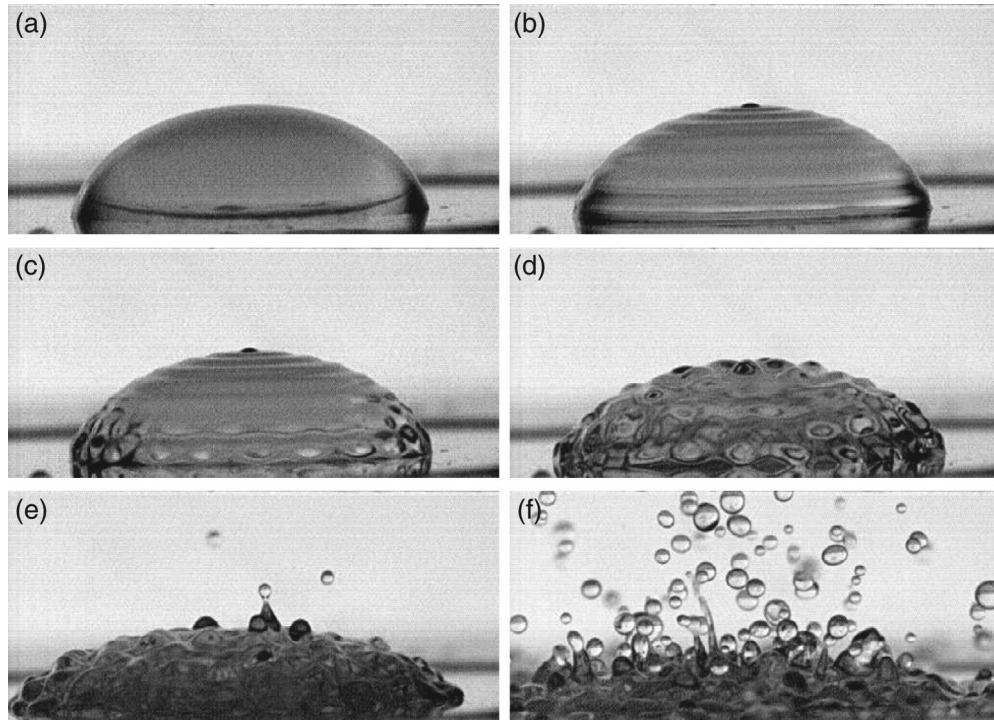| Category | Phenomenon | Vibration | Investigators |
|---|---|---|---|
| | Pointwise concentration | SAW | Li *et al.* (2007a); Shilton *et al.* (2008); Li *et al.* (2008); Shi *et al.* (2009); Wood *et al.* (2009); Bourquin *et al.* (2010); Raghavan *et al.* (2010) |
| | | Thickness | Hertz (1995); Sobanski *et al.* (2000); Wiklund and Hertz (2006); Lee *et al.* (2009); Araz and Lal (2010) |
| | Linewise concentration | Thickness | Vainshtein *et al.* (1996); Goddard and Kaduchak (2005); Kapishnikov *et al.* (2006); Neild *et al.* (2006); Goddard *et al.* (2007); Manneberg *et al.* (2009); Oberti, Neild *et al.* (2009) |
| | | SAW | Takeuchi and Yamanouchi (1994); Shi *et al.* (2008); Wood *et al.* (2008) |
| | Single particle manipulation | Thickness | Hu *et al.* (2004); Neild *et al.* (2006); Lee *et al.* (2009); Oberti, Moller *et al.* (2009) |
| | Dispersion | SAW | Li *et al.* (2007a) |
| | Pumping | SAW | Li *et al.* (2007b); Bok *et al.* (2009); Li *et al.* (2009) |
| | Cavitation and microstreaming | Thickness | Miller *et al.* (2002); Liu *et al.* (2003); Marmottant and Hilgenfeldt (2004); Lauterborn *et al.* (2007); Coussios and Roy (2008); Suslick and Flannigan (2008); Doinikov and Bouakaz (2010); Lee *et al.* (2010) |
| | Alignment | SAW | Smorodin *et al.* (2005); Kong *et al.* (2010) |
| | | Fluid traveling wave | Lopatnikov *et al.* (2009) |
| | Stretching | SAW | Schneider *et al.* (2008) |
| | | Thickness | Dukhin and Goetz (2001); Wiklund and Hertz (2006); Versluis *et al.* (2010) |
| | Characterization | | |
| Microchannel flow | Pumping | Thickness | Kaajakari *et al.* (2001); Araz and Lal (2010); Tan, Yeo, and Friend (2010) |
| | Mixing | SAW | Tseng, *et al.* (2006); Tan, Yeo, and Friend (2009), Tan, Yeo, and Friend (2010) |
| | Separation | SAW | Kumar *et al.* (2005); Kapishnikov *et al.* (2006); Shi *et al.* (2008); Tan, Tjeung *et al.* (2009); Franke *et al.* (2010) |
| | | Stoneley wave | Yantchev *et al.* (2010) |
| Chemistry | Reaction enhancement | SAW | Tseng *et al.* (2006); Kulkarni *et al.* (2009), Kulkarni *et al.* (2010) |
| | Cavitation (sonochemistry) | Thickness | Suslick and Price (1999); Brenner *et al.* (2002); Shchukin *et al.* (2010) |

FIG. 7.   (a) A 100 $\mu\ell$ water drop exhibits (b) axisymmetric waves followed by a breakage of azimuthal symmetry and the formation of (c)–(e) azimuthal-radial waves that eventually result in (e) drop ejection and (f) complete drop breakup as the amplitude of vibration is increased. From Vukasinovic *et al.*, 2007a.

amplitude required for this to work was near the transition to atomization.

By vibrating a sessile drop purely in a direction transverse to the solid surface, Vukasinovic *et al.* (2007a) were able to study the onset and frequency distribution of the consequent capillary wave and followed this phenomena through to bursting and atomization of the drop as the amplitude of the vibration was increased as shown in Fig. 7, a topic covered in more detail below in relation to atomization.

At times the vibration of a sessile drop leads to surprises, as Brunet *et al.* (2007) found. Although a sessile drop will typically move downward on an inclined slope once it reaches a critical angle, they found vertical oscillation of that slope can actually cause the drop to travel *upward*, due to the nonintuitive interaction of the contact line hysteresis and the rectilinear, pistonlike vibration. Noblin *et al.* (2004) examined similar drops placed on a horizontal surface and determined the effects of contact hysteresis on the spreading of the drop and the appearance of specific resonances of the capillary wave in a manner akin to the work mentioned previously by McHale *et al.* (1999). Noblin *et al.* also reported transitions in the drop's free surface shape similar to Vukasinovic *et al.* (2007a) a few years later, but only for axisymmetric capillary waves. They uniquely described conditions of contact line pinning tied to specific resonance frequencies of the drop and most importantly provided a simple model for the release of those contact lines when $a/g > H/(1 - \cos\theta_E) \approx 0.26$ and $\ddot{\xi}/g > 4H/\pi(1 - \cos\theta_E) \approx 0.32$ for complete slippage of the contact line using water and polystyrene; $\ddot{\xi}$ and $g$ are the vibration acceleration and gravitational acceleration, respectively, $H \equiv \cos\theta_r - \cos\theta_a$ is the hysteresis angle between the receding ($\theta_r$) and

approaching contact angles ($\theta_a$) of the pinned edge of the drop, and $\theta_E \equiv \frac{1}{2}(\theta_r + \theta_a)$ is the equilibrium contact angle.

Wixforth (2003) found, using Rayleigh SAW, that sessile drops could be moved at will and with control across the surface of lithium niobate for polymerase chain reactions. Bourquin *et al.* (2010) presented a specially tapered interdigital electrode (IDT) structure designed to achieve many of the same things. Because of the contact line hysteresis, the acoustic streaming induced within the drop from the SAW, and creative modification of the wettability of the substrate, they showed that drops can be moved rapidly across the substrate without risk of spreading the drop into a thin film or bursting at input powers of just a few milliwatts. Indeed, Tan *et al.* (2007b) found a sessile drop could be moved across a surface contaminated with particles, such as pollen, and could actually be used to collect these particles, as shown in Fig. 8. Combined with separate work in concentration (Li *et al.*, 2007a; Shilton *et al.*, 2008; Raghavan *et al.*, 2010) as described in Sec. IV.C.1, a method was made possible for rapidly concentrating dust and surface contaminants to a small location, *microcentrifugation,* perhaps over a sensor. Because the particles collected in Fig. 8 are spherical and have a smooth morphology, pollen was also studied and found to collect in the drop with better performance (about 30%) than the hydrophilic melamine particles (almost all pollens are hydrophilic and have a very rough morphology).

Unfortunately, these devices all require that microfluidic operations be conducted directly on the piezoelectric substrate itself, with at most a thin surface layer separating the fluid from it. Because most microfluidics applications require sterility, low cost, and biocompatibility, only a few materials have found their way into common use: glass, silicon, paper
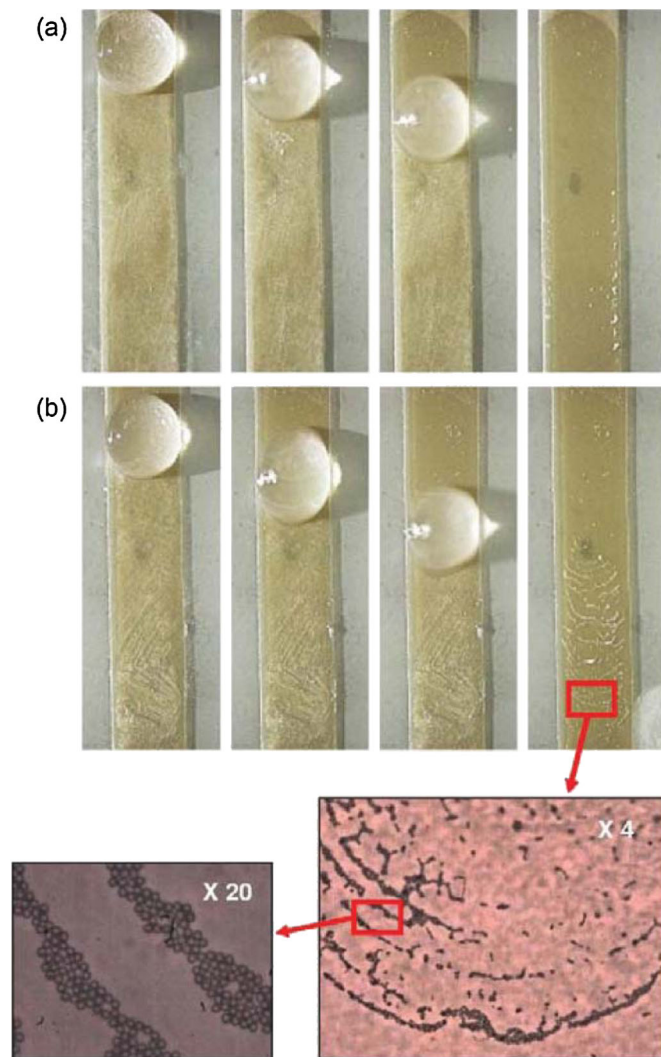
FIG. 8 (color online). Collection of (a) melamine (hydrophilic) and (b) polystyrene (hydrophobic) particles. Some of the melamine particles were left alongside the drop track, while some of the polystyrene particles were dropped out across the width of the drop in a regimented monolayer ring formation. From Tan *et al.*, 2007b.

(Martinez *et al.*, 2007), and polydimethylsiloxane [PDMS, Friend and Yeo (2010a)]. Piezoelectric materials are certainly not among these choices, despite most being inexpensive (ZnO, PZT) and biocompatible (ZnO, LN). For this reason the ability to couple acoustic energy from the piezoelectric material into a "superstrate" on which microfluidic operations can be performed, as reported by Hodgson *et al.* (2009), with about 50% efficiency using a fluid couplant as an attractive compromise between the need to reduce the cost of the microfluidics device itself while addressing the requirement of fluid motion, mixing, particle separation, or the like using acoustic energy. By placing a sessile water drop on the glass superstrate with water as the fluid couplant to a SAW device using LN, they found the speed of the drop was directly proportional to the fourth power of the electrical input power put into the SAW device, and that the wave being formed in the superstrate was at the same frequency as the Rayleigh SAW in the LN substrate, although it was instead a Lamb wave with a similar wavelength to the SAW.

### 2. Patterning and wettability manipulation

Acoustic waves can be used to move more than sessile drops. By ejecting picoliter-sized drops from an orifice as an ultrasonic ink-jet printer, Demirci (2005) illustrated a means to achieve spinless drop-by-drop photoresist deposition and flattening as a suitable alternative to the wasteful process of spin coating typical of the photolithography process. The time required to deposit the drops is perhaps an issue with this approach, but the approach adopted a few years prior by Keisuke *et al.* (2004), with an acoustic "doctor blade" (Williams, 1976) that acts to level sprayed photoresist is a high-speed alternative. An interesting variation on this idea is presented by Issenmann *et al.* (2008), who showed the transverse deformation of a chloroform-water interface to be well predicted by the theory of Langevin acoustic radiation pressure mentioned in the previous section, although it appears to miss the localized deformation of the interface that occurs with a length scale corresponding to the wavelength of sound in the fluid containing the source of the acoustic energy as seen by Keisuke *et al.* (2004). Naturally, the ability to generate consistently uniform layers of materials such as photoresist is attractive, but equally attractive is the ability to concurrently pattern these layers without requiring the use of physical or chemical templating. Alvarez, Friend, and Yeo (2008) showed that by using Rayleigh SAW to drive a suitably viscous drop across a substrate, a thin film of the fluid could be left behind over centimeter length scales. With control of the boundary conditions of the substrate that contains the SAW, a portion of the SAW's energy was allowed to reflect back toward the original source of SAW on the substrate causing the formation of a weak standing wave. After the thin film had been formed by the swept drop, this standing wave interacted with the thin film to pattern it into regularly spaced drops in a face-centered cubic configuration, separated by a few tens to a few hundred micrometers depending solely on the frequency of the SAW. With a polymer or protein dissolved in the fluid, upon evaporation this material appears as regularly spaced dots on the surface as shown in Fig. 9. Whether this can be extended to the nanoscale for use in fabrication of novel structures at those scales, as Barth *et al.* (2005) reported via other techniques, is a topic left unexplored.

### 3. Pumping

A vital part of any fluid system is a means to controllably pump fluids through the system against the resistance posed by both the connecting pipes and channels and the mixing, sensing, and filtering components that collectively accomplish the goals of the system. Laser and Santiago (2004) presented a review of micropumping technology, including the use of acoustic waves both with and without integrated valves. Some crude attempts were made using high-power ultrasonic transducers with decent results, as reported by Hasegawa *et al.* (2005), but these are probably not adaptable to standard planar micromachining techniques. Among the earliest reports of acoustically driven pumping in microfluidics devices without valves made use of Lamb waves in thin SiN plates fabricated through anisotropic etching: flexural plate wave (FPW) fluid pumping devices by Moroney *et al.*
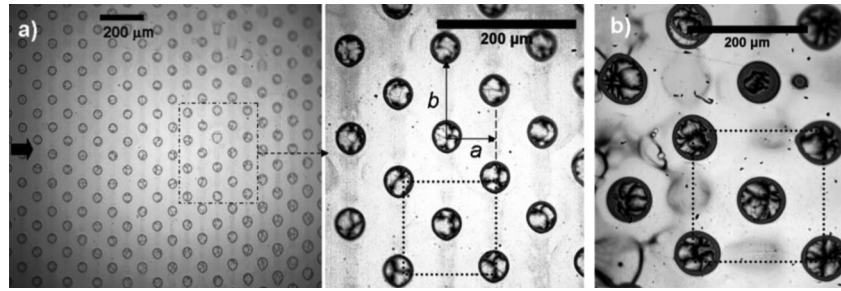
FIG. 9. The patterning of fluid thin films into regularly spaced "dots" using mixed-mode (standing and traveling-wave) Rayleigh SAW. Here $a$ and $b$ are a few tens to a few hundred micrometers, depending on the frequency of the SAW device. From Alvarez, Friend, and Yeo, 2008.

(1991), apparently missed in Laser and Santiago's review. Using a thin ZnO layer as the piezoelectric material and Al interdigital electrodes, the flexural Lamb wave was generated and propagated across the thin structure; this motion was coupled into the fluid set upon the structure in much the same manner as with Rayleigh SAW and caused acoustic streaming. There are a few minor differences between the Rayleigh SAW and the Lamb wave, most notably the latter having a prograde particle motion as the wave passes, in contrast to the former's retrograde motion. But, most importantly, the power available in the FPW device is far less than LN SAW devices, as indicated by the velocities of the fluid that may be induced: The former is measured in only $\mu$m/s, even in cases where the electrode is curved to focus the acoustic energy in the substrate as shown in Fig. 10 from Nguyen and White (2000). Worth noting here is that a thorough theoretical analysis of acoustic evanescent waves
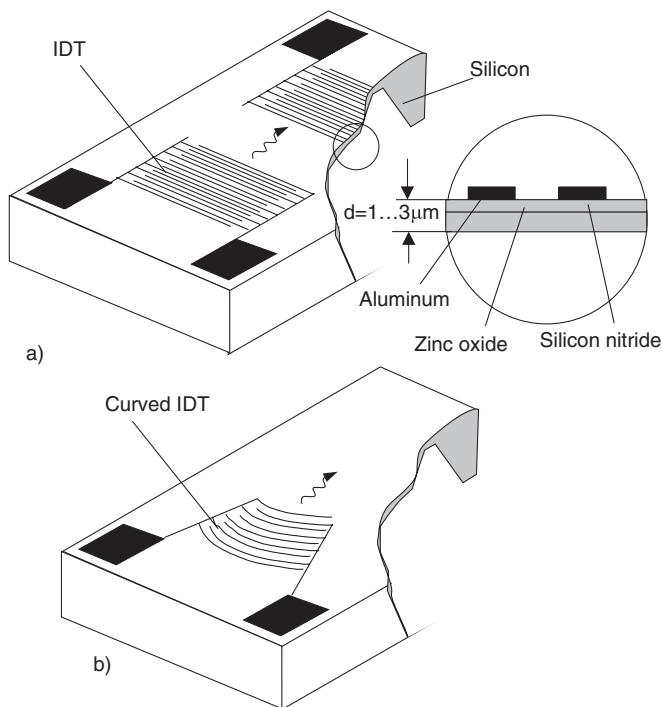


FIG. 10. Illustration of a flexural plate wave micropump structure showing (a) straight and (b) curved interdigital electrodes that are very similar to those used in surface acoustic wave devices. The silicon nitride is the bottom layer in the (a) cross section inset. From Nguyen and White, 2000.

that scatter into a fluid environment in a manner similar to what is used in FPW pumps was presented by Williams and Hill (1987) several years prior to the experimental work. The possible applications for acoustic pumping technology extend into medical applications, for example, the insulin pump reported by Ma *et al.* (2006), where the PZT was used in a Helmholtz cavity arrangement to deliver insulin into a silicon patch with surface machined hollow microneedles designed to painlessly puncture the skin. By applying this idea at far lower frequencies, well into the audible range at around 100 Hz, but in a set of resonance cavities external to the microfluidics device, each holding fluids to be delivered, Langelier *et al.* (2009) were able to selectively pump these fluids through the device as shown in Fig. 11.

Girardo *et al.* (2008) combined SAW in LN with PDMS, the latter a typical material in microfluidics, to form a sort of micropump with a fluid interface still present in the device itself, as shown in Fig. 12. Although the fluid interface is shown to move through the channel, whether the fluid can be *pumped* once it completely fills the channel was not a part of the study. Still, this result is interesting in the context of potential applications where the fluid does not fill the channel due to hydrophobicity, and the ability to perform two-dimensional operations in the same system is a novel feature (Masini *et al.*, 2010).

In this vein, the ability to drive fluids into more complex structures such as tissue engineering scaffolds composed of hydroxyapatite or polymers using SAW is of interest, especially if those fluids carry cells, as described in Sec. IV.C.1. This technique permits the perfusion of cells in seconds for tissue engineering, standing in distinct contrast to the standard practice of perfusing cells into such scaffolds with gravity or suction over several hours, and therefore avoiding problems with culturing the cells due to extended exposure in a drop. Acoustic radiation can also be used to drive fluids and microscale-to-nanoscale objects into tissue by *sonoporation*: Acoustic cavitation adjacent to the cellular membrane that perforates the membrane and allows effective transfection with, surprisingly, high cell viabilities of greater than 80% (Miller *et al.*, 2002). Acoustic cavitation in the context of microfluidics is covered later in this review. Duvshani-Eshet *et al.* (2006) described the use of a contrast agent Optison that greatly enhances the probability of cavitation in tissue using relatively high frequencies beyond 1 MHz and therefore allows *targeted* transfection for cancer treatment, an idea reviewed by Umemura *et al.* (1996) a decade prior and one
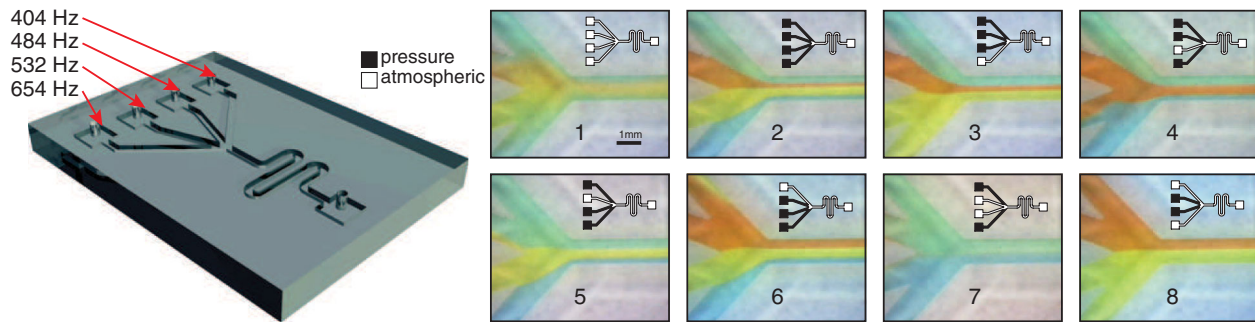
FIG. 11 (color online). By selectively driving the external fluid cavities (not shown) at resonance, Langelier *et al.* (2009) were able to pump fluids at about 100 Pa through their microfluidics device as desired among the four input channels. From Langelier *et al.*, 2009.

studied in some detail by Miller and Song (2002) using a lithotripter. The approach by Duvshani *et al.* improved the transfection of Lipofectamine (Invitrogen, Carlsbad, CA, USA) into prostate cancer cells by about 2 orders of magnitude using sonoporation. The mechanism of sonoporation from cavitation is known to be due to both the shock wave from the collapse of the cavitation bubble and the local Schlichting streaming field about the bubble, microstreaming, that drives the transfection (Pitt *et al.*, 2004). Curiously, researchers are also finding that acoustic streaming induced within cysts from externally applied ultrasound can help identify them. Clarke *et al.* (2005) found acoustic streaming in cystadenomas (potentially cancerous) while streaming was absent in endometriomas (typically harmless); there may be potential ways of using Schlichting (micro)streaming to achieve similar detection strategies.

While the use of sessile drops in microfluidics is treated in a separate part of this study, Guttenberg *et al.* (2004) examined the flow in a trapped drop induced by SAW, calling it a micropump. The flow is reminiscent of the work reported separately by Ito *et al.* (2007) that appears in Sec. IV.D. The mixing behavior within the drop was actually treated by Guttenberg *et al.*, and notably the flow possesses mirror symmetry about two axes giving rise to a vortical flow not common to other studies using sessile drops, with the possible exception of Fu *et al.* (2010), where ZnO was used instead of LN. This is probably due to the high quality of the SAW being induced in the work of Guttenberg *et al.*. Earlier, Lyne (1971) treated mixing in circular cross-sectioned, curved tubes containing fluid as induced by axially delivered pressure waves, and Hall (1974) treated a closely related problem, where the same axial pressure waves were used to induce mixing in a pipe of slowly varying cross section. Jang *et al.* (2005) used truly closed structures in a typical microfluidics device with an inlet and outlet channel from a large cylindrical chamber. By using a PZT element attached across the base of the entire device and driven in piston vibration, they found the fluid in the chamber to move in a recirculatory fashion analogous to the flows reported by Guttenberg *et al.* (2004). Because the PZT element could be driven in several different vibration modes, however, a larger variety of fluid motions were obtained, some suitable for mixing. Sankaranarayanan *et al.* (2008) considered the fluid flow adjacent to LN forced by SAW using the finite element method (ANSYS, Canonsburg, PA, USA), with an aim to mitigate biofouling on LN using the

rapid flow induced in the adjacent boundary layer. They did not consider the effects of the electric field progressing across the surface on the binding of bioproteins, although this effect may also be important. Furthermore, as seen in other studies, the behavior is strongly dependent upon internal reflection from the presence of other interfaces that were omitted in this study. By using bovine serum albumin (BSA) nonspecifically bound to mouse immunoglobulin antibodies IgG bound onto the LN surface, the induced flow was found to strip the BSA
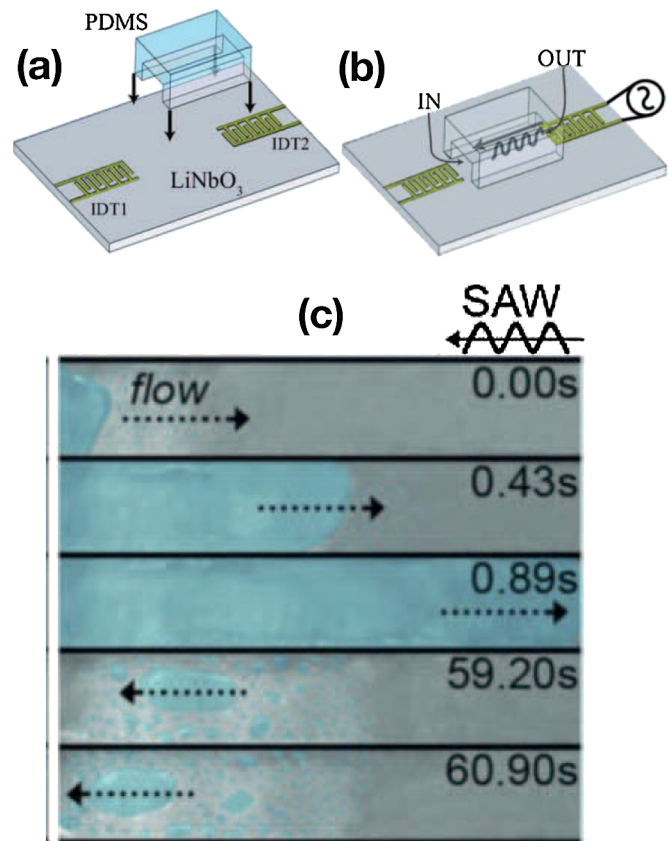


FIG. 12 (color online). The SAW device (a) combined with a PDMS structure that has an open-ended channel. Turning on (b) the Rayleigh SAW gives rise to a fluid flow through the channel; the fluid progresses rapidly through the channel. Since PDMS is hydrophobic minutes after its bonding to a substrate (Friend and Yeo, 2010a), this flow is into a hydrophobic microchannel. From Cecchini *et al.*, 2008.
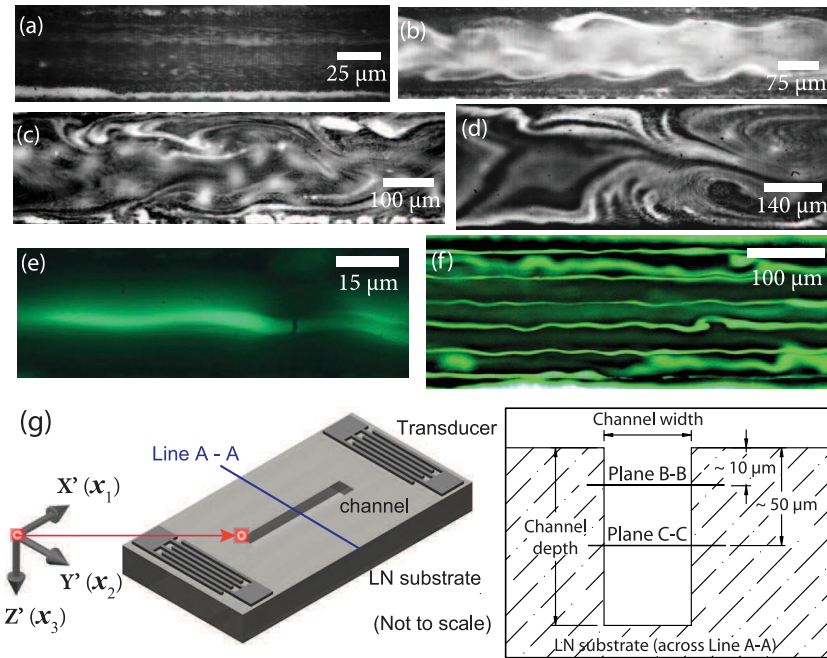
FIG. 13 (color online).   As the width of the 100-$\mu$m deep, 2-cm long laser-cut channel in LN is increased from (a) 25 $\mu$m to (b) 75 $\mu$m, (c) 150 $\mu$m and (d) 280 $\mu$m, the fluid flow within goes from a uniform 2 cm/s flow to a strongly mixing flow. By reducing the input power, particles suspended in the fluid can be made to collect along (e) one or (f) more lines as a consequence of cross-channel standing waves, a topic covered later in this review. The (g) channel cut is parallel to the x axis in the 128YX LN substrate. From Tan, Yeo, and Friend, 2009.

from the IgG surface. The difficulty, however, with the ANSYS simulation they present to model the fluid flow is that it is unable to accommodate the strongly nonlinear phenomena typical of acoustic streaming, described in detail in the previous section, and difficult to use to form a sufficiently fine mesh at the solid-fluid interface to accurately model this interaction due to the very high frequencies used in SAW devices. Much of what might be predicted by ANSYS in these problems should therefore be carefully interpreted. However, because the software is user friendly, it is convenient as a guide to understand complex flow phenomena driven by SAW, as in Raghavan  et al. (2010), for example.

Using a more sophisticated approach incorporating compressibility, viscous effects, and a model of the Stokesian fluid boundary layer, Tan, Yeo, and Friend (2009) found that, in channels physically machined into the LN substrate using exciplex lasers, fluid could be driven to flow in a recirculating fashion along the entire length of the channel if its width was less than one wavelength within the fluid at the SAW excitation frequency. Indeed, Tan, Yeo, and Friend (2010) went further and used the fundamental and several harmonic resonance frequencies of the SAW device together with different power levels to rapidly switch between mixing, particle collection among different numbers of lines parallel to the channel walls, and uniform flow. Mixing across the channel could be obtained if the width of the channel was greater than this distance, as shown in Fig. 13. Tan, Yeo, and Friend (2010) extended this work to describe the use of different power levels and frequency harmonics of the fundamental resonance frequency of the SAW to drive switching between uniform pumping of particle-laden fluids, collection of the particles into one or more lines parallel to the channel, and mixing of the flow. The ability to pump fluids may extend

well beyond these ideas to the nanoscale as discussed in Sec. V.

**4. Jetting and levitation**

As one of the most obvious examples of just how different acoustic excitation of fluids at small scales can be, jetting using SAW is at the same time a simple combination of a Rayleigh SAW device, typically using 128YX LN, a modestly viscous drop atop it, usually water, and a precisely controlled electrical burst of power at the resonance frequency of the IDT. The window for jetting is indeed narrow, between the effects of less power in simply moving the drop and the effects of more power that tend to atomize the drop. Shiokawa  et al. (1990) reported the phenomenon many years ago, and there it remained something of a curiosity until some additional work was done to understand the nature of the jet formation and to consider the behavior of the fluid from a microfluidics perspective, as taken by Tan, Friend, and Yeo (2009) and shown in Fig. 14.

By incorporating the acoustic energy driven into the parent drop through an external body force term in the axisymmetric jet momentum equation of Eggers (1997), a prediction of the jet's velocity $U_j$ can be made as

$$U_j \approx \sqrt{2L_j(\alpha\beta\dot{\xi}^2\text{Re}_{\text{ac}} - g)}, \tag{73}$$

where   $\text{Re}_{\text{ac}} \equiv \rho\dot{\xi}\lambda/[2\pi(4\mu/3 + \mu_B)]$   as   an   acoustic Reynolds number (see the Glossary) but with the velocity defined as approximately equal to the vibration velocity of the substrate $\dot{\xi}$. The jet's length is $L_j$, the fluid's bulk viscosity is $\mu_B$, and $g$ is the gravitational acceleration. This prediction, across a variety of Newtonian fluids, input powers, and drop
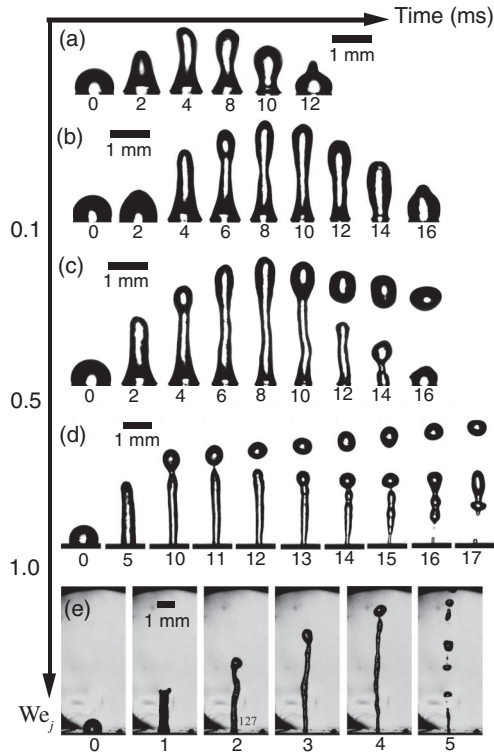
FIG. 14. Experimental images showing the transition from (a) drop vibration to (b) jetting, (c) pinch-off of a single droplet, and (d), (e) jet breakup to form multiple droplets by increasing the jet Weber number $We_j \equiv \rho_f U_j^2 R_j / \sigma$, where $R_j$ and $U_j$ are the radius and velocity of the jet, respectively, and $\sigma$ is the surface tension. From Tan, Friend, and Yeo, 2009.

sizes, appears to correspond well with experimental results as shown in Fig. 15.

Levitating fluid drops is equally challenging and fascinating. Acoustic levitation of fluids is relatively new in comparison to the study of levitation of solid objects, although in recent times the use of acoustics to not only levitate but also transport objects, especially in near-field levitation, has become an interesting field of study (Ide *et al.*, 2007; Koyama
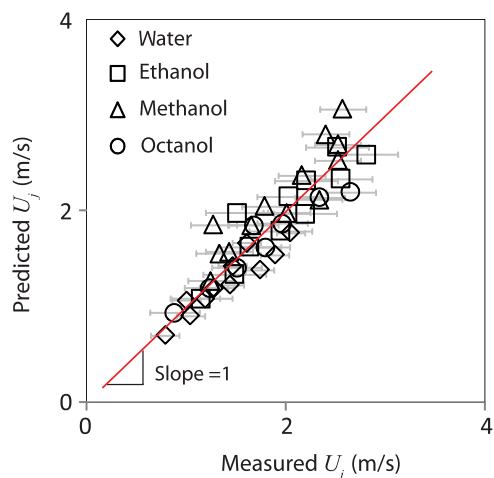


FIG. 15 (color online). Comparison of the predicted jet velocity to the measured jet velocity for various fluids, drop sizes, and power inputs in SAW-induced jetting. From Tan, Friend, and Yeo, 2009.

*et al.*, 2007), mainly because of the noncontact transport phenomena, the ability to rotate objects at very high speeds (Saito *et al.*, 2005), and the interesting complexity of the analysis (Luchini and Charru, 2005). Even SAW is known to be able to levitate objects, although for applications in motors, as reported by Asai and Kurosawa (2005), the gap that forms between the object and the SAW substrate is seen as a problem.

Yarin *et al.* (1998) provided a seminal analysis of the shape of levitated drops. With experimental results at 56 kHz for comparison and verification, they determined both the shape and displacement from the pressure node of 3–5 $\mu\ell$ drops of *n*-hexadecane $C_{49}H_{67}$ while exposed to ultrasound. They did, however, neglect nonlinear acoustic effects, because they were presumed to be insignificant in the far-field levitation arrangement used in their study. But the true value of drop levitation lies in its avoidance of any contact of the drop with a solid surface. Because surface effects strongly dominate volume effects at small scales, this permits the study of small amounts of fluids and how they behave *chemically*. Santesson and Nilsson (2004) provided a comprehensive review of the technique, which uses drops in the 100 $n\ell$–2 $\mu\ell$ range suspended in air, and into which drops as small as $p\ell$ can be inserted by "shooting" them into the levitated drop, accomplished by acoustic ink-jet ejection. They illustrate the many analytical chemistry techniques that are compatible with levitation, from protein crystallization to Raman spectroscopy (Wood *et al.*, 2005), giving some indication of the importance of the technique.

## 5. Atomization

Atomization is integral to a diverse range of engineering systems, from agriculture, medicine, and internal combustion engines to air conditioning and cosmetics (Lefebvre, 1989). Ultrasound has been a popular means to atomize fluids for many years, although the actual mechanism of ultrasonic atomization has been a controversial topic for nearly as long. Taylor (1950) studied the formation of sinusoidal waves on the free surface of a fluid undergoing acceleration perpendicular to the free surface and in the direction of the force of gravity, and almost a century prior Rayleigh (1878) considered the formation of similar waves if the denser fluid was placed above the free surface. Together they illustrated a similar mechanism that has come to be described by the Rayleigh-Taylor instability that also underlies ultrasonic atomization. Alternative theories for explaining vibration-driven atomization have been proposed, most especially cavitation by Mir (1980). While this may be true for phenomena where the Reynolds number is large and the induced pressure wave in the fluid is large, from an explosion, for example, for microfluidics devices and particularly at the very high frequencies typically used, Qi *et al.* (2008) showed that cavitation is not a contributor to atomization. However, the presence of bubbles can be a problem in acoustic microfluidics devices such as ink-jet printers, as described by de Jong *et al.* (2006).

Methods of ultrasonic atomization may be classed into two categories depending on the size of the meniscus relative to the wavelength of the acoustic wave (Friend and Yeo, 2008b). Devices that generate drops sized by the diameter of a

meniscus trapped at a nozzle instead of the acoustic wavelength function through the interaction of a pressure wave induced in the fluid with the meniscus. The fluid is pushed from the nozzle; if the column reaches a sufficient length before being drawn back into the nozzle after passage of the pressure wave [$\pi d_{\mathrm{nozzle}}$ as predicted by Rayleigh (1878), where $d_{\mathrm{nozzle}}$ is the nozzle diameter], the free surface will become unstable and pinch off, forming at least one drop; the drop diameter he predicted as a consequence of this process, $d_{\mathrm{Rayleigh}} = 1.89 d_{\mathrm{nozzle}}$, represents an upper bound for the actual drop diameter. This instability mechanism is the Rayleigh-Plateau instability (Plateau, 1849), not the Rayleigh-Taylor instability, and is covered by Lee and Lal (2004) in their development of an interesting, simple nanodrop generator. This approach has been very effective and commercially successful in ink-jet printing, but the work reported by Maehara et al. (1986) provides a scaling theory for the ejection phenomenon useful for understanding the physics and illustrates an embodiment suitable for generating large numbers of microdrops, a *nebulizer*.

Lang (1962) combined experimental techniques with aerosol drop size estimates from contemporary theories on ultrasonic atomization from about 15 kHz to just less than 1 MHz, and found that the drop size was strongly correlated with the excitation frequency using a version of Kelvin's equation for capillary waves that estimated the drop size as 0.34 times one-half the capillary wavelength,

$$D = 0.34 \sqrt[3]{\frac{8\pi\sigma}{\rho_f f^2}}, \qquad (74)$$

where $D$ is the atomized drop diameter, $f$ is the excitation frequency, and $\sigma$ is the surface tension. Kelvin's equation relies upon a specific assumption of how free surface waves form from vibration: the frequency of the Faraday[4] wave is one-half the excitation frequency. Benjamin and Ursell (1954) developed the basic theory of Faraday waves that rely on a Mathieu equation formulation and which underlies much of the subsequent work in the area, while Douady (1990) is an excellent primer for experimentation in this area, with the work by Bechhoefer et al. (1995) important in ensuring the experiment is arranged properly to avoid the effects of the boundaries.

Zarembo, best known for his contributions to the analysis of finite acoustic wave propagation, also was known for his study of capillary waves on free surfaces (Krasilnikov et al., 1970). Much later, and after the discovery of SAW-based methods for atomization by Shiokawa's group in the 1990s [and only published some 10 years later in Chono et al. (2004)], this result was used to explain the size of drops obtained from SAW atomization by Kurosawa et al. (1995), although they found the 0.34 factor to be inadequate, particularly where Kurosawa et al. (1997) reported 2 years later where the factor had to be increased to 3.8. Their work noted that the mechanism of atomization appeared to be unstable unless the fluid layer was thin and that the atomization process ejected drops in three different size ranges.

Barreras et al. (2002) found a similar phenomenon in a detailed experimental study using a piston ultrasonic atomizer, effectively capturing a number of images that indicated the length scales of each of the instabilities giving rise to the drops. Other means for generating micron-sized drops are described in the literature, and the article by Kripfgans et al. (2004) is especially thorough in describing how atomization produces small drops from a fluid jet that is subsequently exposed to intense ultrasound. Elrod et al. (1989) made use of a piston transducer with a concave cup milled into the irradiating end; when submerged in water by a distance corresponding to the focal length of the concavity, the cup focused the ultrasound to a small region at the fluid surface and allowed the ejection of single drops.

Qi et al. (2010) described a SAW atomizer suitable as a handheld system with applications in drug delivery, mass spectroscopy, and the generation of cell suspensions. Jin et al. (2000) presented an exceptionally useful application of ultrasonic atomization for atomic mass spectroscopy, and although they use a piston atomizer they found superior mist production rates at 1 m$\ell$/ min. Heron et al. (2010) used SAW to achieve the same goal but with more detail on the benefit of such an approach for mass spectroscopy; the SAW may be run in a pulse atomization scheme such as matrix assisted laser desorption ionization or in a continuous mode such as electrospray ionization with excellent quality, and without the need for orifices that can clog, electrodes and the concomitant need for charging which can cause electrochemical oxidation of the sample or dilution of the sample to fit into a reservoir; Ho et al. (2011) substantially extended this contribution in detecting low levels of heavy metals in tap water and the presence of caffeine and 5-Fluorouracil in whole human blood. Introducing a set of high-voltage electrodes in a corona polarization configuration, Kim et al. (2005) were able to print protein chips using charge-directed deposition of protein-laden drops that were formed via SAW atomization. Using the proteins bovine serum albumin and fluorescein isothiocyanate (FITC) conjugated mouse immunoglobulin in separate experiments, they successfully printed spots at different protein concentrations and with an accuracy sufficient to feasibly consider the approach in realistic biological applications.

Ultrasonic atomization is also effective for generating microparticles and nanoparticles, among the many methods reviewed by Biskos et al. (2008), if the nebulized drops are permitted to evaporate to leave dissolved materials behind. Felder et al. (2003) reported on the generation of encapsulating microparticles of polylactic acid, poly(lactic-co-glycolic acid), among other materials for potential use in drug delivery using commercially available ultrasonic atomizers. By working with low concentrations of polymers together with a relatively high-frequency piston atomizer, Forde et al. (2006) used poly-$\varepsilon$-caprolactone (PCL) between 0.1% and 1% weight/volume concentration in acetone to produce a nearly monodisperse distribution of 150–175 nm diameter particles. Using SAW for the same constituents leads to an order of magnitude smaller particles around 15 nm in diameter, mainly due to the rapid nucleation process from the smaller nebulized drops (Friend et al. (2008). Alvarez et al. (2009) used the SAW atomizer to form microparticles

---

[4]Faraday (1831) first observed these waves and the phenomena like so many others has to come to bear his name.
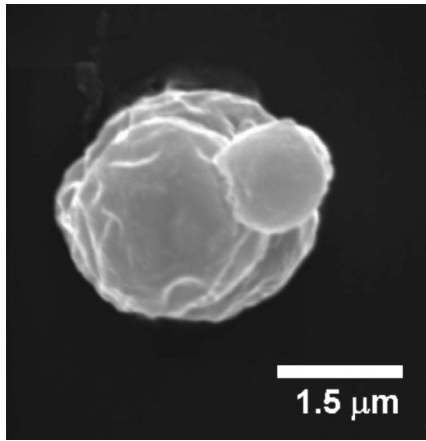
FIG. 16.   A BSA-encapsulated PCL polymer microparticle formed using SAW atomization. From Alvarez  *et al.*, 2009.

of either bovine serum albumin or FITC-bovine albumin encapsulated in PCL, and found that the SAW frequency (either 10 or 20 MHz) and the concentration of the PCL in acetone (either 0.2% or 1% weight/volume) had a strong effect on the final microparticle size, giving over an order of magnitude change in the size alone by changing either of the parameters. Figure 16 shows one such BSA-encapsulated PCL particle generated using this approach about 1.5 $\mu$m in diameter. Using an enzyme-linked immunosorbent assay (ELISA) on the microparticles demonstrated that the BSA survived the atomization, a step absent from previous studies in this area, and showed the collection process gave a yield of ~55%. Omitting the PCL excipient, Alvarez, Yeo, and Friend (2008) showed that nanoparticles of insulin and BSA could be fabricated using SAW atomization of buffered deionized water solutions of these biological proteins at a concentration from 0.5 to 2 mg/m$\ell$. They also showed if the SAW atomized drops were prevented from evaporation, as would happen in inhalation, for example (Groneberg *et al.*, 2003; Yeo, Friend *et al.*, 2010), the nebulized drops would be around 3 $\mu$m in diameter and therefore ideal for drug delivery via the pulmonary system. Because the SAW atomizer is capable of forming nebulized mists of these large molecules without damaging them, it may be a reasonable means to deliver such molecules as a portable device. Qi *et al.* (2010) considered this idea in more depth, focusing instead upon salbutamol, a common drug used in pulmonary delivery though typically as dry particles to treat asthma. They found that the mean aerosol diameter produced by a handheld prototype SAW device, $2.84 \pm 0.14$ $\mu$m, is within the optimum size range for pulmonary delivery. In a two-stage impinger *ex-vivo* model, they demonstrated that ~70%–80% of the drug supplied for atomization would be deposited within the lung, far superior to dry particle inhalers and comparable to large nebulization equipment.

Although the mechanism of atomization was still unclear even 5 to 10 years ago, progress was being made: Goodridge *et al.* (1997) identified a threshold acceleration that, once exceeded, gives rise to ejection of drops from the crests of the capillary wave; the threshold acceleration $a$ is given by

$$a \propto f^{4/3}\left(\frac{\sigma}{\rho}\right)^{4/3}, \tag{75}$$

for a low-viscosity fluid such as water, acetone, and ethanol. As Lang did some years prior, they also connected the robust literature on Faraday waves to the atomization phenomena. James *et al.* (2003), in the formation of a simple mathematical model, explored the nonlinearity of the phenomena at very low frequencies and considered qualitative aspects of the process absent from other papers. A subsequent work by Vukasinovic  *et al.* (2007b) focused specifically on the mechanism of breakup to form single ejected drops and large numbers of drops, which appear under different excitation conditions, and the lengths of jets that form from the capillary wave. Their results are similar to Goodridge  *et al.* (1997) for the transition to atomization, although they also found, for cases where the drop ejection does not directly depend upon the viscosity (i.e., the *capillary* number Ca $\ll$ 1), that the threshold acceleration depends only on a nondimensional drop size that is essentially the same as Eq. (74). They also examined where the breakup of the jet that forms from the capillary wave occurs that produces an ejected drop; for relatively low values of the excitation frequency the breakup occurs very close to the tip, while for large values the breakup location is nearer the base of the jet. Donnelly  *et al.* (2004) was one of the few contributions after Lang to specifically consider ultrasonic atomization in the low MHz range, and notably found that an inviscid scaling law for the drop diameter was superior to a viscous scaling law even to a few MHz in their studies, and in contrast to Goodridge's results. However, they did assume the amplitude of the excitation had no effect on the atomization behavior, an assumption Qi *et al.* (2008) found to be invalid for slightly higher frequencies in the SAW system. Miles (1984, 1993) and Miles and Henderson (1990) considered the formation of Faraday waves from vibration via parametric excitation and made an elegant and mathematically complex effort using weakly nonlinear Hamiltonian mechanics developed from normal mode analysis to determine the configuration and amplitude of the waves over a broad range of viscosities, boundary conditions, and scale, the latter important in the context of what forces are relevant to the wave phenomena. At larger scales, gravity is a significant factor in the formation of the wave, and is especially important for water waves (Dias and Kharif, 1999; Johnson, 2002), while for smaller scales, surface tension dominates (Schwartz and Fenton, 1982); Goodridge  *et al.* (1997) reported the well-known dispersion relationship describing the situation as

$$f^2 = \frac{gk}{4\pi^2} + \frac{\sigma}{4\pi^2\rho}k^3, \tag{76}$$

where $k$ is the wave number of the wave and $g$ is the gravitational constant; the relative contribution of one versus the other depends on the frequency for a particular system. From this, Goodridge showed how a crossover frequency may be determined, $f_c = \sqrt{g\rho/\sigma}/(2\pi) \approx 10^2$ Hz for water. If the frequency of the wave is greater than this value, the surface tension dominates over gravity in the behavior of the wave, which happens to be true for virtually all microfluidics devices and particularly for atomization.

The appearance of the wave at the subharmonic frequency one-half the excitation frequency conveniently matched the analysis framework established around the Mathieu equation,

yet it has been known for some time that the mechanism is not that simple. Indeed, Keolian *et al.* (1981) showed the appearance of capillary waves in shallow water at subharmonic frequencies with other ratios of $f/i$, where $i = 2, 4, 12, 14,$ $16, 18, 20, 22, 24, 28,$ and 35. This, and more complex wave patterns [see, e.g., Binks and van de Water (1997)], is made possible, as shown by Chen and Viñals (1997), by the interaction of triad (three-wave) resonant interactions of the waves on the free surface that does not rely on the quadratic nonlinearity presumed by the weakly nonlinear form that results in the Mathieu equation form. Beyond discrete modes of capillary waves, the appearance of turbulent cascades in the wave interaction for larger systems where gravity is relevant has been shown to exist by Falcon, Laroche, and Fauve (2007). Rather than being made up of waves possessing particular wavelengths, the wave has a broadband distribution of energy with a characteristic dispersion relation between the wave amplitude and frequency of $\xi = f^{-17/6}$.

These phenomena all seem to appear in SAW atomization, shown in Fig. 17. Using laser Doppler vibrometry[5] to measure the vertical velocity of the free surface at a point described by Friend and Yeo (2010), Qi *et al.* (2008) found that excitation of a fluid drop at 20 MHz did not give rise to the Faraday-like capillary wave at 10 MHz, but did generate broadband capillary wave motion as shown in Fig. 18 from about 10 Hz to 100 kHz. The Faraday wave model, relied upon by many researchers over the years (Miles, 1984; Miles, 1993; Li, 2004) and presumes the frequency of the capillary wave will be twice the excitation frequency, fails in this instance.

The combined complexities of nonlinear, two-dimensional wave interaction, capillary wave turbulence [see, e.g., Holt and Trinh (1996)][6], and extended subharmonic cascades across 3 to 6 orders of magnitude all combine to make the description of SAW atomization a fascinating problem. What is the mechanism that allows the capillary wave to appear at a frequency of $10^3$ Hz order from excitation at $10^7$ Hz, and why should the response be broadband, or turbulent as Holt *et al.* described it? Perhaps it is a consequence of turbulence being induced via Reynolds stresses as a converse Lighthill aeroacoustic analogy (Lighthill, 1978), because the appearance of streaming has long been known to be tantamount to the near onset of turbulence in the fluid. Further, if the thickness of the fluid drop is reduced to the depth of the Stokesian boundary-layer thickness discussed in Sec. III.F, the frequency spectrum of the capillary waves changes dramatically from the broadband, relatively low-frequency response to a linear behavior with a large response spike at 20 MHz, matching the excitation frequency. These remain as

---

[5]Laser interferometry is a popular method to measure acoustic wave propagation, even for GHz-order SAW as described by Tachizaki *et al.* (2006); Vanherzeele *et al.* (2007) illustrated how laser Doppler vibrometry can also be used as an alternative to particle image velocimetry in microfluidics, reminiscent of the original use of such technology in laser Doppler anemometry.

[6]The concept of turbulence here is generalized beyond its use in standard fluid dynamics to capillary waves: the length scale of the capillary wave is chaotic to stochastic, and any such terms chosen to describe the capillary wave, deformation, acceleration, or wavelength, possess continuously distributed frequency response spectra.
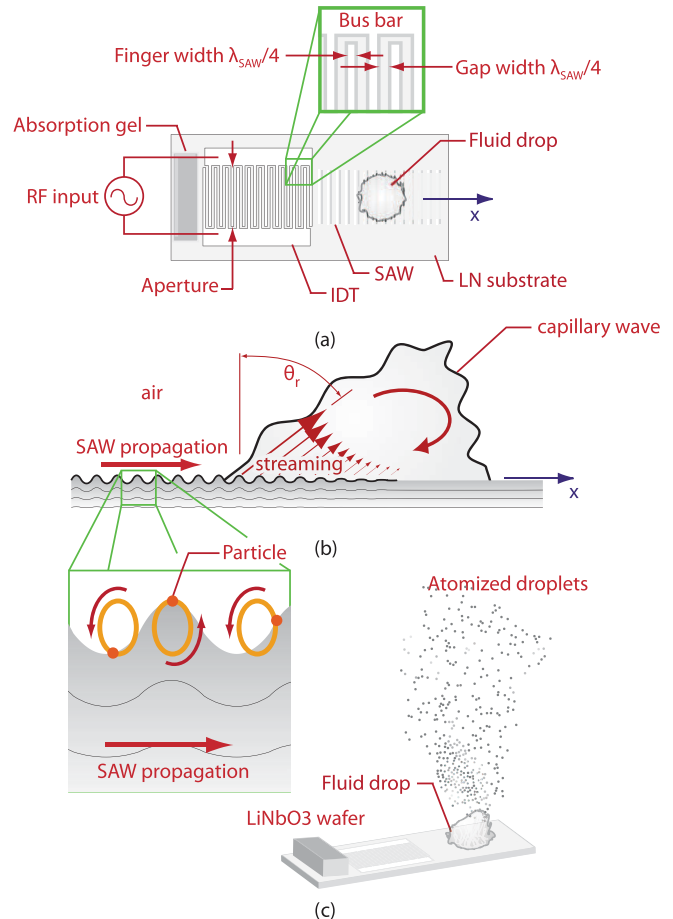
FIG. 17 (color online). (a) The SAW is generated on the substrate and (b) interacts with a fluid drop, causing the drop to deform into an asymmetric conic leaning approximately at the Rayleigh angle, $\theta_r \equiv \sin^{-1}(c_f/c_{SAW})$, where $c_f$ and $c_{SAW}$ are the speed of sound in the fluid and of the SAW in the substrate, respectively. Although indicated here with a simple monofrequency capillary wave, the wave is actually far more complex. The Rayleigh SAW's retrograde particle motion and the exponential decay (c) are indicated, as are the effects of acoustic irradiation which causes drop deformation through first-order effects on the time scale of the acoustic wave and acoustic streaming-driven bulk fluid recirculation on the hydrodynamic time scale. From Qi *et al.*, 2008.

open questions, as do explanations for many of the physical phenomena observed in acoustic microfluidics. Li *et al.* (2008) illustrated other curious phenomena due to capillary waves appearing in sessile drops at relatively low powers due to SAW excitation. By using aqueous suspensions of polystyrene microparticles, they found (see Fig. 19) the particles collected at regions defined by either the SAW wavelength (region A), a combination of the fundamental capillary wave vibration mode and the SAW wavelength (regions B and C), or wholesale vorticial flow of the drop induced by fast streaming (region D). The device operated in a time-dependent *blinking* (Cross and Hohenberg, 1993) fashion in region C, with the particles in the drop collecting at positions defined much as they are in region B, to suddenly be dispersed by rapid rotation of the drop in either the clockwise or counterclockwise direction after a finite but unpredictable amount of time.
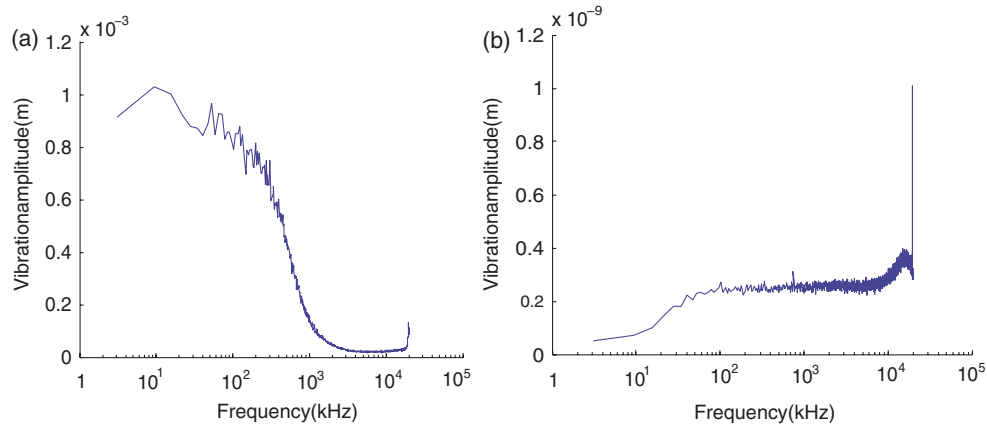
FIG. 18 (color online). Results from a fast Fourier transform frequency sweep using the scanning laser Doppler vibrometer showing the frequency at which the capillary wave on the free surface of the drop is excited. (a) Drop with finite thickness of ∼$10^4$ m: The resonant frequency of the capillary wave is ∼10 kHz. (b) Thin film of thickness $10^6$ m: The resonant frequency of the capillary wave is ∼20 MHz, the exciting frequency. From Qi *et al.*, 2008.

A way to establish the physics of capillary waves generated by ultrasound is to use computational analysis to directly solve the governing equations of motion, similar to what is discussed in determining acoustic streaming in the prior section. The added complexity of having a deformable interface between two fluids (i.e., water and air) makes finding an appropriate method let alone a solution a challenge. While the issue of determining the spatiotemporally evolving interface in two-phase systems is worthy of its own review, and is covered by Yarin (2006) in drop impact and by Craster and Matar (2009) in thin films as examples of the more
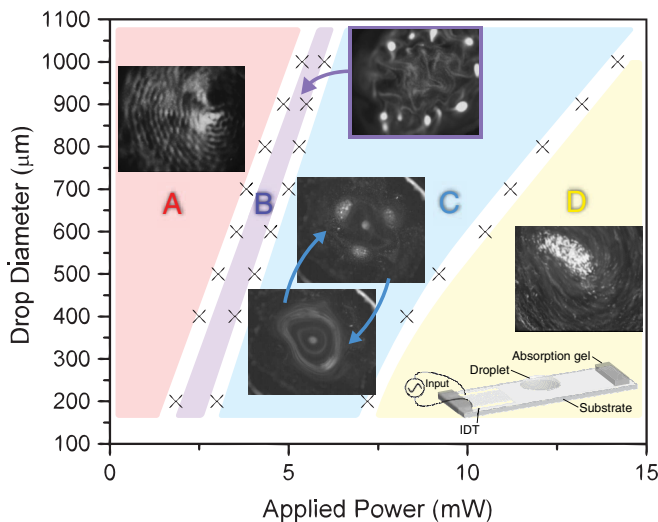


FIG. 19 (color online). The behavior of a sessile drop of a colloidal suspension containing 500 nm fluorescent polystyrene particles atop a Rayleigh SAW device dramatically varies depending on the input power. At relatively low powers (region A) the particles tend to collect in a pattern defined by the wavelength of the SAW in the substrate. As the power is increased there is a narrow region (region B) where the particles collect in distinct spots separated by a distance corresponding to the capillary wavelength on the fluid's surface, followed by a chaotic rotation and collection phenomena in region C and bulk rotation and particle collection in region D reminiscent of Shilton *et al.* (2008). From Li *et al.*, 2008.

general problem, few studies have combined analyses of the piezoelectric material response to electric field excitation, the resulting fluid motion driven by the motion of the piezoelectric material, and the behavior of the free surface all together in a physically relevant system. Schindler *et al.* (2006) provided a solution for the case of SAW interacting with a drop via an intricate technique using a discretized weak formulation of the combined fluid and fluid surface equations, although the assumptions made in finding that solution, incompressibility, steady-state flow, and a fixed body force on the fluid from the SAW, eliminate nearly all of the interesting dynamics of the system. In the model presented by Qi *et al.* (2008), the fluid was treated as a thin, incompressible liquid film to permit the use of lubrication theory. A presumed substrate motion was made using a simple exponential representation that resembled SAW propagation, with decay in its amplitude as the energy leaked into the fluid layer, although it did not take into account the influence of the fluid on the solid substrate and how it might affect the various characteristics of the SAW.

Köster (2007) focused on the flow field within the drop bounded by a free surface and an interface that represents the solid substrate. Köster's approach generally followed the conventional perturbation expansion method up to second order, substituting these variables into the governing equations, followed by selecting terms of the same order to form two sets of equations: Equations of first order govern the propagation of linear acoustic waves [Eqs. (31)] and equations of second order [after time averaging, Eqs. (49)] govern SAW streaming (Morse and Feshbach, 1953; Nyborg, 1965; Zarembo, 1971; Bradley, 1996). The solution technique appears to carry on from the method espoused by Schindler *et al.* (2006), though Köster's model was also unable to capture the formation and evolution of capillary waves. Nonetheless, Köster obtained an asymmetrically shaped drop as actuated by a traveling-wave SAW that is consistent with the experimental results shown by Wixforth *et al.* (2004). In a different numerical study, Dong *et al.* (2006) used commercial software (FLUENT) to solve the complete three-dimensional Navier-Stokes equations with the free

surface of the fluid determined using a volume-of-fluid (VOF) method. Notwithstanding the limitations of the VOF method (Gopala and van Wachem, 2008), especially for the problem at hand, they were able to simulate the bulk deformation of a drop subjected to lateral vibration. We note here that, in the analysis by Dong *et al.*, the equations were solved without perturbation approximations, eliminating the restriction that the deformation should be small. Strangely, Köster's formulation, based on perturbation approximations, showed only bulk deformations without any small-amplitude surface deformations. More recently, Brunet *et al.* (2010) conducted a numerical study of SAW generated fluid motion in a drop with nondeformable free surface and found chaotic behavior of the acoustic field in the drop as a result of the multiple wave reflections from the free surface, perhaps suggesting an explanation for the unusual phenomena seen by Li *et al.* (2008). This result was also observed nearly two decades ago by Thompson *et al.* (1991), where they found period-doubling cascades rife in the fluid due mainly to the nonlinear interaction between the Stokes boundary layer and the Rayleigh streaming vortices in the bulk of the flow: It seems that Rayleigh's law (see Table I) introduced more than a simple linear relationship between the boundary and the bulk, either that or turbulence, closely associated with acous-

tic streaming at large hydrodynamic Reynolds numbers as discussed by Lighthill (1978), could be appearing here. Recently, Li (2004) presented a revision of Miles's equations that admit chaotic behavior in the capillary wave as a consequence of broader knowledge of chaotic behavior of capillary waves as described by Kudrolli and Gollub (1996) than available when Miles (1984) wrote his original equations. The numerical model by Brunet *et al.* assumed both that the acoustic field equations were linear and that the surface of the large (compared to the acoustic wavelength), hemispherical drop was nondeformable and stress free. Because of the assumptions, the surface deformation could not be determined, and the reflections from the surface would be different than what is predicted by their analysis: Not only do the reflections propagate ideally from the undeformed surface but also the reflections are "perfect" under these assumptions; they do not diffract due to interaction with a real free surface possessing surface tension.

Tan, Friend *et al.* (2010) took the analytical approach presented in Sec. III and, to allow for the deformation of the free surface, a coordinate transformation is applied to the fluid equations while incorporating additional equations to define the free surface. With this approach, the bulk deformation of the drop and the unsteady capillary wave are both
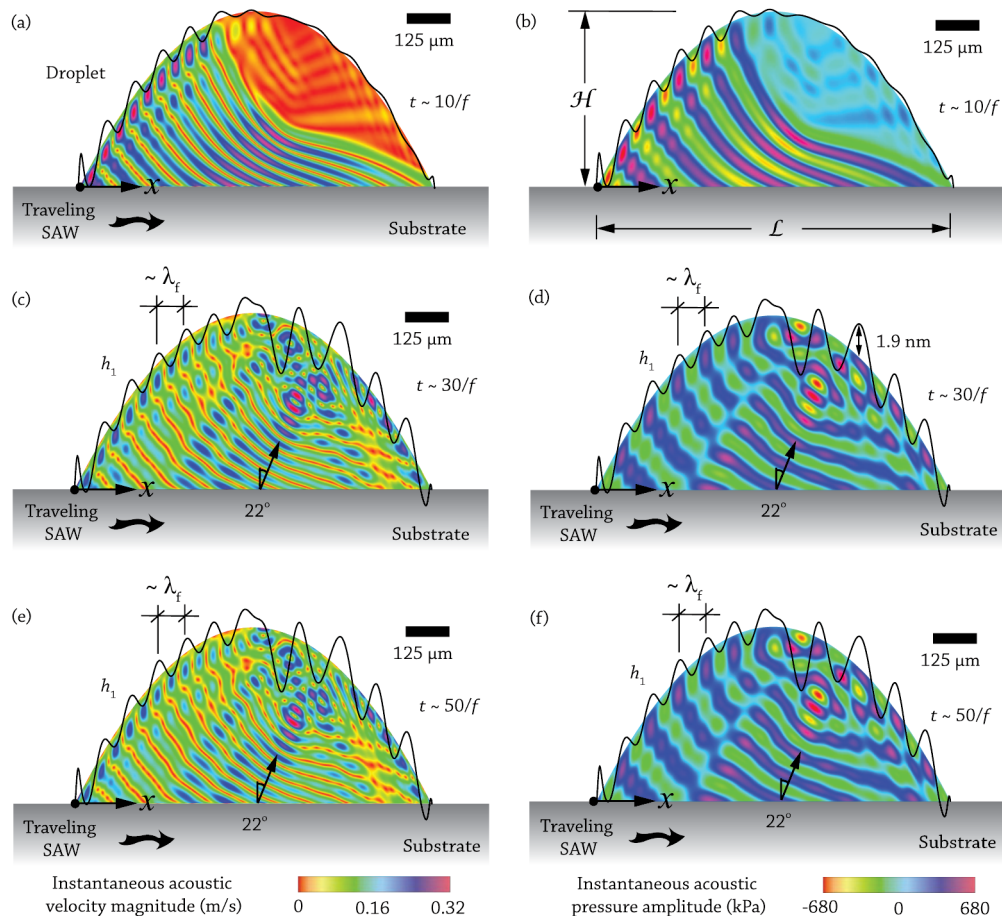


FIG. 20 (color online). Results of the computation of the transmission of acoustic waves into a sessile drop after (a), (b) 10, (c), (d) 30, and (e), (f) 50 periods, using 128YX LN driven by a straight, standard interdigital electrode (IDT) with 30 electrode finger pairs at a resonant frequency of 20 MHz. The amplitude of the electric field input into the IDT was adjusted to deliver a SAW amplitude on the free surface near the drop edge of 1.2 nm. The black lines represent the greatly exaggerated deformation height of the free surface. From Tan, Friend *et al.*, 2010.

determined from first principles via the equations that define the generation and propagation of the SAW, and the consequent formation of the acoustic wave in the fluid and acoustic streaming, incorporating compressibility, viscosity, and full coupling between the piezoelectric substrate and the fluid atop it. Because the capillary wave is predicted, the acoustic wave reflections that occur as a consequence of the large difference in acoustic impedance between—for example, water and air—can be correctly calculated. Further, one can see how the wave propagates into the drop during the initial stages of SAW propagation. Figure 20 shows the fluid velocity and pressure amplitudes from the computation after 10, 30, and 50 periods of time (where a period is $1/f$) for a Rayleigh SAW traveling from left to right in the figure at 20 MHz into a water drop. Notice how the wave front is strongly curved as it passes into the drop after ten periods, apparently due to the changing depth of the fluid at the leading edge of the drop. The Rayleigh angle [$\theta_r \equiv \sin^{-1}(c_f/c_{SAW})$, where $c_f$ and $c_{SAW}$ are the speed of sound in the fluid and of the SAW on the substrate, respectively] as a result of the computation is about 22°. Note the appearance of a pressure boundary in the fluid drops one-third of the distance from the left-hand side; this boundary has been seen experimentally and used by Tan *et al.* (2007b) to collect particles in moving drops. Because of the capillary wave, the reflection of the acoustic wave within the drop is diffused, especially apparent in Fig. 20(e) on the right-hand side of the drop. This analysis technique opens up the possibility for explaining a wide variety of phenomena not only in how the bulk of the fluid and its free surface behave, but also in how particles move about upon and within the fluid as a consequence of the acoustic wave. For some time, the observation of localized patterning of particles suspended in a colloidal solution has been troubling. While Li *et al.* (2008) offered some explanation of the phenomena from particle rafting on the free surface, as will be explained elsewhere in this section, the issue of understanding why the spacing was similar to the SAW's wavelength on the substrate remained unexplained. By making use of the analysis, it becomes more clear what the mechanism is, as shown in the direct comparison in Fig. 21.
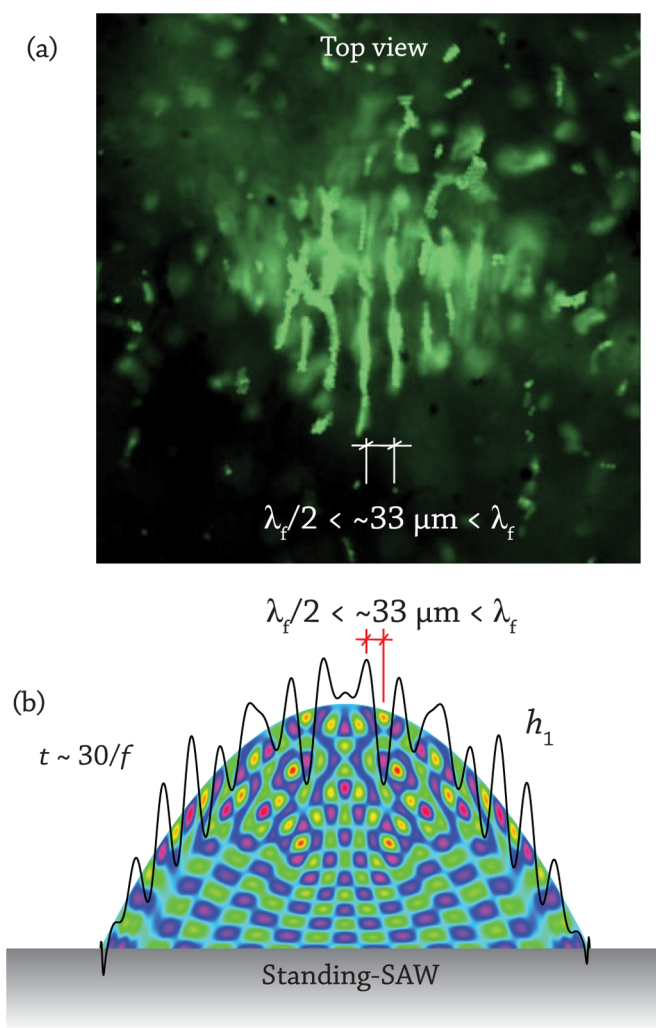
## C. Particles, colloidal suspensions, and bubbles

The manipulation of particles using vibration dates back to at least Chladni's discovery of particles moving to nodes of vibrating plates and membranes in 1787 (Chladni, 1787); curiously, the motion of particles due to vibration has been both controversial, with input from Faraday (1831) to Thomas and Squires (1998), and responsible for a variety of new applications in positioning microparticles to nanoparticles as, for example, considered by Dorrestijn *et al.* (2007). Because the challenge in fabricating nanoscale structures with accuracy and speed over much larger scales is significant, the opportunities presented by acoustic manipulation of particles in this way are also significant. But even Faraday (1831) found that large particles tended to collect at nodes while small particles collected in "heaps" at antinodes, and for reasons that are fascinatingly convoluted. For example, Tan *et al.* (2007a) found that cigarette smoke particles, known to be around 100 nm in size and very adhesive, were actually ejected from the surface of LN by the passage of a Rayleigh SAW; if the wave was allowed to reflect and interfere with itself, a standing wave could be formed with nodes and antinodes, and the smoke particles would collect at the nodes making it possible to visualize the SAW in about 30 s. The mechanism for the cigarette smoke dynamics was due to a combination of boundary-layer (Schlichting) acoustic streaming, acceleration-induced ejection, gravity, and van der Waals forces. Remarkably, despite the insignificant mass of a typical cigarette smoke particle (10 ng), the ejection acceleration imparts a force of 0.1 mN because the surface of the LN was accelerating at about $10^8$ m/s$^2$ while operating at 30 MHz under modest excitation power, strongly ejecting it



FIG. 21 (color online). Particles 6 $\mu$m in diameter collect along lines upon the surface of a 3 $\mu\ell$ sessile drop (height $\sim$ length), using 30 MHz standing-wave Rayleigh SAW generated by two focusing, standing-wave ultrasonic interdigital transducers placed at the left and right of the drop in a configuration reported by Tan, Friend, and Yeo (2009). The distance between two adjacent collection lines is $32 \pm 4$ $\mu$m, roughly the same as one-half the wavelength of the acoustic wave in water; the difference is believed to be due to the curvature of the fluid drop, as illustrated by the (b) computational result showing the free surface profile as a black line and the pressure amplitude in the contour plot. From Tan, Friend *et al.*, 2010.

from the surface except at the nodal locations. But this phenomenon is in air, where most practical applications in microfluidics are in water or a biological fluid with greater density and viscosity.

Haake and Dual (2002) illustrated the typical approach to manipulating particles in fluids with ultrasound: A standing wave formation where the forces on the particles act to drive them to the nodes of the pressure field in the fluid, a phenomenon known since 1866 when Kundt found particles collecting in a pattern in a tube driven by a standing sound wave (Hutchisson and Morgan, 1931). By controlling the distribution of motion in the device, the form of collection can be significantly altered: Vainshtein *et al.* (1996) showed how one could induce particle collection along a continuous line down the central axis of a tube instead of Kundt's discrete collections of particles in cross-sectional planes, each separated from the next by one-half the acoustic wavelength. Adams and Soh (2010) showed a rather sophisticated microfluidics arrangement to achieve band-pass sorting of particles between 1 and 10 $\mu$m in diameter. Audible frequencies are suitable as well; Whitehill *et al.* (2010) showed the ability to collect microparticles in a 10 mm diameter well as shown in Fig. 22 using an audible tone at just 60.59 Hz.

The actual forces on a particle exposed to an acoustic wave are those due to direct irradiation by the acoustic field and indirect irradiation from scattering of the acoustic field from other objects. A simple form of the force due to the direct irradiation on a spherical particle for a *traveling* wave was derived by King (1934):

$$F = 2\pi\rho_{f0}A^2(kD/2)^6\left[\frac{1+\frac{2}{9}(1-\rho_{f0}/\rho_p)}{2+\rho_{f0}/\rho_p}\right], \quad (77)$$
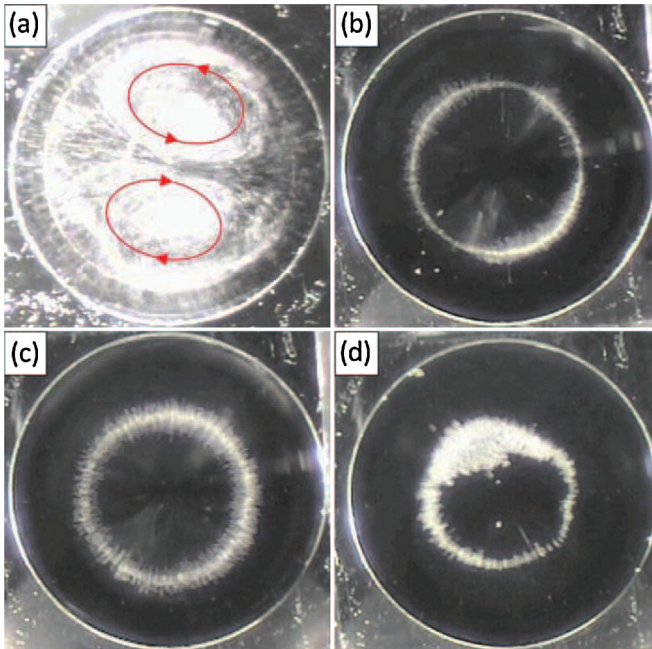


FIG. 22 (color online). The size of the particles affects the ability to collect them via audible acoustic irradiation, as shown by oscillation at 60.59 Hz, for particle diameters of (a) 10–30 $\mu$m, (b) 42 $\mu$m, (c) 60 $\mu$m, and (d) 116 $\mu$m. From Whitehill *et al.*, 2010.

where $A$, $k$, $D$, and $\rho_p$ are the acoustic wave's amplitude and wave number and the particle's diameter and density, respectively. King assumed the fluid was inviscid, the particle was incompressible and small in comparison to the acoustic wavelength, and there were no scattering forces.[7] Most notably, the force $F$ scales with $D^6$, making the transition from significant to insignificant forces on particles from acoustic irradiation very abrupt. Polystyrene particles in water, for example, are strongly driven by such forces using 10 MHz irradiation when their diameter is larger than about 10 $\mu$m, but not at all when they are less than that size, as Rogers *et al.* (2010) reported in using SAW to separate particles in a setup similar to Li, Friend, and Yeo (2007). A small particle contained in a sessile drop such as those in the drops shown in Fig. 23 experiences drag and direct acoustic radiation forces. While the acoustic radiation force scales with $D^6$, the Stokes drag scales with $D$, and this difference offers specific crossover particle diameters as indicated by Fig. 23: At 20 MHz, polystyrene particles larger than about 25 $\mu$m in water will be predominantly affected by direct acoustic forces, while those smaller than about 20 $\mu$m will be affected by acoustic streaming-driven drag forces. For 10 MHz, the crossover diameter is well above 30 $\mu$m, while for 30 MHz, it is about 15 $\mu$m.

In comparison to the forces generated by traveling waves, the forces on particles due to *standing* waves is in most cases stronger; King (1934) determined that

$$F = \pi\rho_{f0}A^2(kD/2)^3\sin 2kx\left[\frac{1+\frac{2}{3}(1-\rho_{f0}/\rho_p)}{2+\rho_{f0}/\rho_p}\right], \quad (78)$$

where the force acts in a direction from the particle to the nearest pressure node for particles with a density greater than the fluid ($\rho_p > \rho_{f0}$); the distance between the particle and the node is $x$. For particles less dense than the fluid, the force upon them is oriented toward the pressure field antinodes.

If we set the forces reported in Eqs. (77) and (78) equal to each other, and if the particle density is similar to the fluid (as is the case with polystyrene in water, melamine in water, and most cells in water), we can state $\rho_{f0} \approx \rho_p$ giving $\sin 2kx = (kD/2)^3$ for the equation describing when the standing and traveling wave-driven acoustic forces would be equal to each other. Notice how the standing wave acoustic force can be any value from zero to the maximum value occurring when $\sin 2kx \rightarrow 1$. For the traveling wave acoustic force to be larger than even this value, $k > 2/D$ or $\lambda < D/2$; in other words, the wavelength would have to be shorter than the radius of the particle for the traveling wave-driven acoustic force to be larger than that of the standing wave. This would not only be difficult in practical microfluidics devices, it is outside the regime where King's equations are even approximately valid. Put another way, for $10^7$ Hz sound in water, the wave number is on the order of $10^4$ m$^{-1}$. For a particle $10^{-5}$ m in size, it would only have to move a distance slightly more than $x \approx \sin^{-1}10^{-3}/10^4$ m $\approx 10^{-8}$ m away from the node of the standing wave before the standing wave force would become larger than the traveling wave force.

_____

[7]Although King (1934) considered a broader set of circumstances in his study, including larger particles, gravity, and particle inertia.
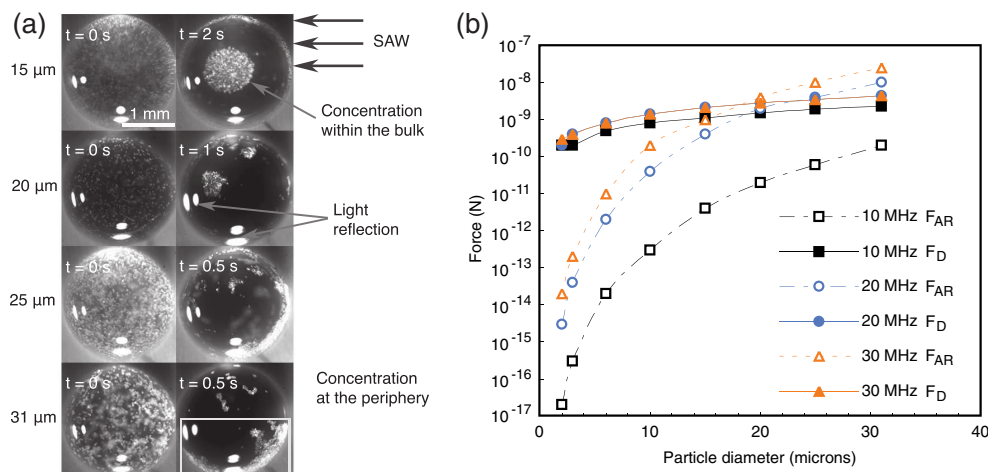
FIG. 23 (color online). Using a setup similar to Li *et al.* (2007a) with a 1.5 $\mu\ell$ water drop set atop a 20 MHz LN SAW device. (a) Polystyrene particles 15 and 20 $\mu$m in diameter concentrate at the center of the drop while 25 and 31 $\mu$m diameter particles concentrate at the periphery. The smaller two sets of particles sit below the crossover diameter of about 22 $\mu$m where (b) the force due to drag $F_D$ is equal to the direct acoustic radiation force $F_{AR}$. Their trajectories are mainly defined by the acoustic streaming-driven Stokes drag forces, and so their behavior is similar to what is seen by Li *et al.*. The larger two sets of particles, on the other hand, are propelled to the side of the droplet and held there by the direct acoustic forces which dominate over the acoustic streaming. From Rogers *et al.*, 2010.

The other aspect to note is the importance of the particle's density compared to the fluid density in these forces; because King did not incorporate particle compressibility, the effect of a difference in the acoustic impedance is absent from the force equations, an assumption eliminated by most subsequent authors including Haake and Dual (2002). An especially cogent review of the area is provided by Qi and Brereton (1995). Doinikov (1996) took into consideration the viscosity and heat conduction of the fluid as well and found that for practical cases the radiation force due to a plane traveling wave should be much larger than predicted by King's theory, with both viscosity and heat conduction significantly contributing to the difference. Though heat conduction is, according to Doinikov, nearly as important as the viscosity, it is routinely ignored [(Spengler *et al.*, 2000; Haake and Dual, 2002; Oberti, Neild *et al.*, 2009), among others], likely because Yosioka and Kawasima (1955) and Gor'kov (1961) chose to ignore it in their widely cited derivations and because the first integral representation by Gor'kov (1961) is especially straightforward to use. Doinikov's versions of the equations are recommended over previous results, especially for traveling wave interactions. Another aspect of the particle interaction with acoustic waves is the interparticle forces that appear from multiple scattering events of the acoustic wave; Doinikov (2001) again presented a thorough study of this aspect. Mitri (2005) separately explored hollow spherical shell particles filled with either air or water, important because of their potential use in drug delivery, localized heating to destroy tumors, and for use in microfluidics in a similar way to bubbles but with more control over the size and shape.

Because bubbles in microfluidics devices have taken on new importance with a flurry of activity in generating them (Cubaud *et al.*, 2005) and using them as valves, mixers (Garstecki *et al.*, 2006; Wang *et al.*, 2009), and transport elements (Marmottant and Hilgenfeldt, 2004), the influence of acoustic radiation on and adjacent to bubbles is also important to consider. The work by Marmottant and Hilgenfeldt (2004), in particular, uses Stokeslet analysis to analyze the flow field, but most interesting in their work is the use of acoustic streaming generated in *doublets* about a bubble in the fluid to homogenize vesicles: The cells are opened, releasing the contents without destroying them. The fact that the bubble participates in the phenomena, and that this can be used to drive flow in a region surrounding it, illustrates the importance of properly treating the interaction of acoustic waves with bubbles. Of course, the fields of sonochemistry and sonoluminescence, collectively reviewed by Brenner *et al.* (2002) and Suslick and Flannigan (2008), rely upon cavitation [see, e.g., Coussios and Roy (2008)] and bubbles in fluids, and the literature in these areas is extensive. But in microfluidics the use of bubbles in fluids is rather different: The bubbles' dimensions and position are controlled in the system and typically have dimensions similar to the characteristic scales of the microfluidics device itself. Although one certainly needs to understand the underlying physics if using acoustic waves with bubbles, controlling the behavior of the bubbles using acoustic forces is also interesting and has many applications in its own right. Doinikov and Dayton (2006) accomplished the former by studying the dynamics of the bubble exposed to ultrasound, in examining the secondary scattering Bjerknes forces appearing between bubbles in an ultrasonic field by Doinikov (1999), and indeed the microstreaming induced about bubbles from the acoustic radiation by Doinikov and Bouakaz (2010). Doinikov and Dayton (2006) also showed that the acoustic force on a free bubble scales with its diameter, squared, if one ignores viscosity; including viscosity, specifically the shear viscosity of the bubble surface, contributes a corrective force that itself scales inversely with respect to the diameter. Compared to the scaling of the force with respect to the diameter to the sixth power for traveling waves in Eq. (77) or the third power for standing waves in Eq. (78) on solid particles, this scaling is weaker and suggests a possible means for particle-bubble

separation in a manner similar to particle-particle separation reported by Rogers *et al.* (2010). Rensen *et al.* (2001) presented an example of how one may control the motion of bubbles in a small fluidic system, where bubbles in a fluid channel are caused to move along a controlled spiral path by the influence of the acoustic radiation passing through the fluid transverse to the fluid's flow in the channel. Tandiono *et al.* (2010) described ultrasonic entrainment of air into closed, filled microfluidic channels through capillary wave generation and air induction through a secondary port, a process unrelated to cavitation which is curiously mentioned in their title. Versluis *et al.* (2010) reported on the acoustic manipulation of the bubble shape itself, generating surface waves on the bubble sufficient to form mode shapes and under certain conditions forcing its breakup. They provided a valuable mathematical model of the phenomena and tied the behavior back to a model derived from the Rayleigh-Plesset equation with good accuracy.

### 1. In sessile drops

Over a decade ago, Woodside *et al.* (1997) made an effort to measure the forces on particles suspended in fluids due to acoustic radiation and viscous drag, not only along the path of acoustic radiation but perpendicular to it, finding that the results corresponded to theory quite well. Although the lateral forces on particles from acoustic irradiation had been known to exist as a weak force, they quantified the force for the purposes of sorting cells. The same year, Yasuda *et al.* (1997) demonstrated the ability to separate (guinea pig) erythrocytes at a hematocrit of 3.3%, about an order of magnitude lower concentration than human blood (with a typical hematocrit of around 35%–50%). Using 500 kHz ultrasound in a thickness-mode, pistonlike vibration for 1–2 min, they were able to concentrate the erythrocytes along a 150-$\mu$m-thick region midway between the transducer faces on the top and bottom of the 800 $\mu$m thick chamber, despite the fact the erythrocytes red blood cell (RBC) have only a slightly larger density than the surrounding fluid ($\rho_{RBC} \approx 1099$ kg/m$^3$). Because they used PZT at high voltages (180 V), the resistive losses

within the PZT would have been excessive, and indeed the erythrocyte sample heated from 20 °C to 35 °C within a few minutes. Despite this, the absence of cavitation allowed the cells to remain whole and damage free based on the standards defined by Yasuda *et al.*, who made this judgement solely on the presence of lysis products in the surrounding fluid.

Spengler *et al.* (2000) observed the rather more general agglomeration of yeast cells in a small 60$\mu\ell$, $15 \times 5 \times 0.8$ mm fluid chamber with thickness sized to accommodate one wavelength of the vibration at 1.9 MHz [with a configuration somewhat similar to Yasuda *et al.* (1997)], and found the yeast cells collected at pressure nodes defined in a way that indicates the presence of Schlichting streaming in their study. Takeuchi and Yamanouchi (1994) reported what is believed to be the earliest use of SAW to collect particles in fluid, using a pair of Rayleigh SAW devices of 128YX LN, each with a floating electrode IDT and dipped as probes into a thin water film. The SAW probes were oriented at the Rayleigh angle so that the propagation of the acoustic wave in the water was parallel to the film. Although the results were modest, they indicated the potential of using SAW to manipulate particles into a pattern defined by the standing wave formed in the thin film. Spengler *et al.* (2003) followed up soon after with a rather comprehensive study of the motion of 1-, 15-, and 25-$\mu$m latex particles in water, incorporating the effects of slow streaming, drag forces, and acoustic radiation forces applied directly on the particles. They did choose to omit, however, the effects of fast streaming and bulk flow that were not relevant at the low intensities of ultrasound in their study.

Oberti, Neild *et al.* (2009) studied the collection phenomenon in sessile drops of aqueous suspensions containing copolymer beads. The drops were set atop a special MEMS vibration structure designed to vibrate ultrasonically up to about 1 MHz, and the particles within moved to apparent nodal positions akin to Chladni figures, as shown in Fig. 24. Li *et al.* (2008), as mentioned, described the appearance of similar patterns using much higher frequencies, although the configuration of the pattern, if it exists, was subject to the input power as shown in Fig. 19.
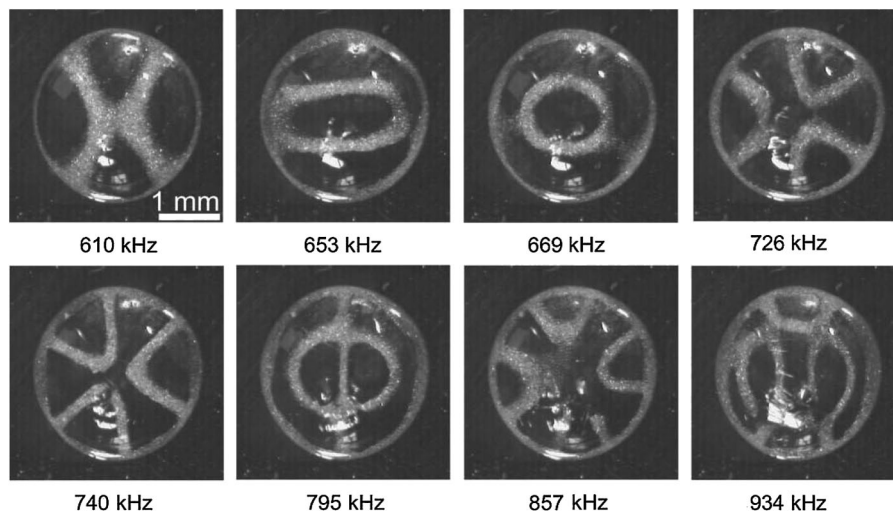


FIG. 24.    As the excitation frequency is raised, distinct patterns appear as defined by the pinning of the particles within a sessile drop; the drop is ~2 mm in diameter and 1 mm in height. From Oberti, Neild *et al.*, 2009.

Wood *et al.* (2008) used a simple interdigital electrode pair to collect particles in a sessile drop along a single axis. The results of their study indicated that the lateral forces on the particles from the acoustic radiation were exceedingly weak, particularly compared with the results seen at lower frequencies by Woodside *et al.* (1997) and Spengler *et al.* (2003): The particles tended to collect along long lines parallel to the fingers of the IDT throughout the interior of the drop. Wood *et al.* (2009) later chose to use two SAW devices in a paired configuration and placed orthogonally to each other to manipulate particles in a sessile drop. By coupling the SAW to a superstrate in a manner first described by Hodgson *et al.* (2009), they were able to group particles together in body-centered cubic configuration [in contrast to the face-centered cubic configuration obtained by Alvarez, Friend, and Yeo (2008) as shown in Fig. 9], regularly spaced with separations between the groups of one-half the wavelength of the SAW. Shi *et al.* (2009) reported an arrangement of IDTs with one perpendicular to the other in a confined microfluidics device. Because the typical substrate used in these studies is LN and anisotropic, the *y*-axis propagation of Rayleigh SAW is very difficult to generate as the electromechanical coupling coefficient is an order of magnitude lower than along the *x* axis (Campbell and Jones, 1968). What the piezoelectric material is or what its cut might be is omitted from their paper. Only PZT and ZnO are isotropic in the plane and are suitable for use in planar devices, but these materials are problematic because PZT is toxic and ZnO is a thin-film material without the power output capabilities of LN.

One of the problems with the approaches to particle collection in drops described to this point is the need to rely on the weak lateral direct acoustic force to aid concentration of particles in two dimensions. Although Wood *et al.* (2009) used two SAW devices to partially get around this problem, their result was still a series of discrete collection points rather than a single point at which most of the particles could be collected, arguably a better outcome for many applications needing particle concentration in sessile drops. By using higher power SAW irradiation of a few hundred milliwatts, Li, Friend, and Yeo (2007) found that the whole drop could be caused to spin at high speeds and induce particle concentration toward the center of the drop due to shear-induced migration (Leighton and Acrivos, 1987), effectively concentrating aqueous suspensions of yeast cells and 3–45 $\mu$m diameter polystyrene particles in a few seconds. They were able to define a critical transition value as a ratio $\chi_c \equiv u_{\mathrm{sm}}/u_{\mathrm{acous}}$, the shear migration velocity $u_{\mathrm{sm}}$ over $u_{\mathrm{acous}}$, the acoustically induced fluid velocity in the drop.[8] When $\chi_c > 2$, microcentrifugation occurs, as shown in Fig. 25. They also demonstrated the separation of red blood cells from plasma in blood samples with starting concentrations of up to 100% whole blood. Because the flow field is especially complex, Raghavan *et al.* (2010) used microparticle image velocimetry and a simplified finite element analysis approach (using ANSYS) to study the flow field generated by the arrangement described by Li *et al.* (2007a), and found
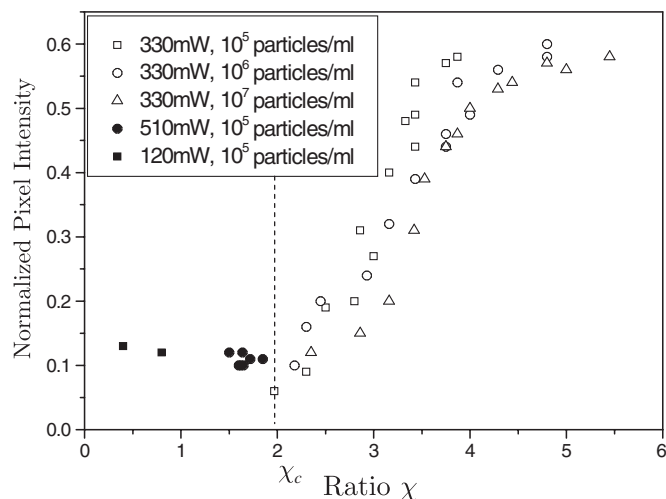


FIG. 25.   An indication of whether particles suspended in a sessile drop will concentrate via the vortex flow phenomenon and shear migration. The filled marks indicate dispersion of the particles, while unfilled marks indicate concentration. The transition to concentration occurs as $\chi$ grows beyond the critical value of $\chi_c = 2$ for 10 $\mu$m polystyrene particles in water. From Li *et al.*, 2007a.

that the flow rotation occurs about a tilted axis, the tilt appearing because of the induced acoustic streaming in the bulk (as fast streaming) at the Rayleigh angle. Shilton *et al.* (2008) extended the work of Li *et al.* (2007a) by exploring other IDT configurations on 128YX LN to determine whether the concentration speed could be improved, from simple straight electrodes to focusing electrodes with either a circular or elliptical focus. They found the speed of concentration to be improved by an order of magnitude by switching from the straight IDT of Li *et al.* (2007a) (and many other researchers) to either the elliptical or circular focusing IDT. Additionally, mixing a solution of glycerin and water was found to be an order of magnitude faster using an elliptically focused IDT rather than the straight IDT, while the circularly focused IDT was actually an order of magnitude slower. This counterintuitive result turns out to be due to the distribution of acoustic energy into the fluid; the circularly focused IDT focuses the acoustic energy into a small region, ineffective for its subsequent delivery into the fluid, while the elliptically focused IDT focuses the acoustic energy along a line parallel to the propagation axis of the SAW, far more effective in coupling into the fluid. The rather different concentration result is due to the shear migration; it requires a gradient in the azimuthal velocity along the radial direction in the drop, which both focusing IDTs are more effective at generating than the straight IDT.

Li *et al.* (2007b) reported the ability to transport particles and cells into hydrophobic, microporous scaffold structures and against large capillary forces as a consequence, modeled by Bok *et al.* (2009). By doing so, the hours-long tedium of gravity-driven perfusion of stem cells into supporting scaffold structures for tissue engineering is reduced to a few seconds. In contrast to the rather direct and simple approach adopted by Yasuda *et al.* (1997) a decade earlier, Li *et al.* (2009) studied the functionality of stem cells exposed to 20 MHz SAW over an extended period to determine whether exposure to intense SAW radiation might leave such cells alive but

---

[8]Note the relation is erroneous in Li, Friend, and Yeo (2007), with $\chi_c$ defined by mistake as the inverse of the relation correctly given here.

dysfunctional. They took fluorescence labeled osteoblast cells, and drove them into polycaprolactone porous scaffolds and found over 80% of the cells to be viable and functional: They were able to generate hydroxyapatite at the same rate as control samples of the cells not exposed to SAW. The survival rates of these cells, at 80%, were statistically similar to the control samples, up to a power sufficient to atomize the sample and cause the loss of cells through their ejection in the atomized mist. In contrast to the conventional wisdom that acoustic radiation damages or kills cells, which is based on experience gained with ultrasonic technology operating at a few tens of kHz, the frequencies used with SAW correspond to time scales smaller than the molecular relaxation time and certainly any relaxation time of cellular structures, and hence there is little shear damage.

Kong *et al.* (2010) demonstrated the ability to align microtubes with the propagation direction of SAW in a two-port device as shown in Fig. 26. They managed to not only move the particles to the nodal lines formed in the pressure field from the SAW, but also managed to cause them to align along the direction of the SAW propagation. With sufficient concentration, the particles actually formed long chains, bridging the nodal lines. Smorodin *et al.* (2005) used gold nanoparticles attached to the ends of carbon nanotubes to accomplish a similar alignment task. Together, they illustrate the ability to align asymmetric particles in addition to moving them about in the fluid. Lopatnikov *et al.* (2009)
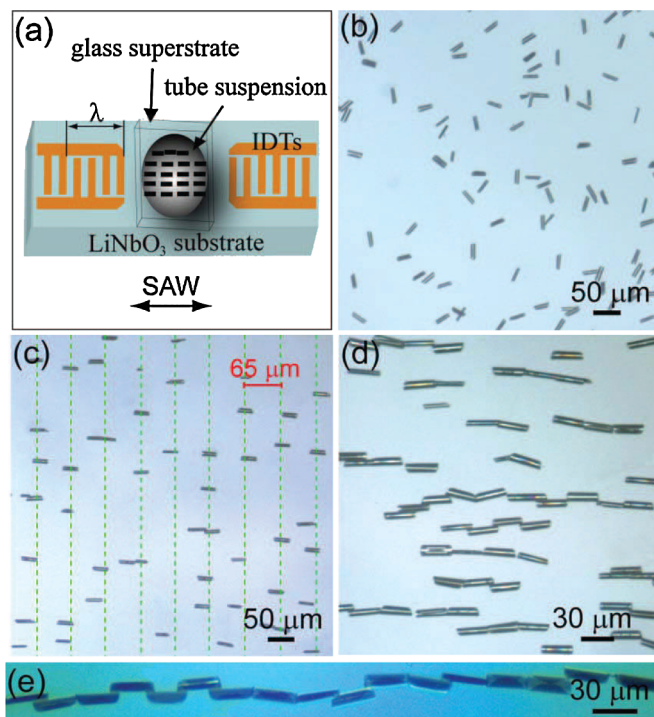


FIG. 26 (color online).   (a) Schematic of the dual-port SAW device from Kong *et al.* (2010), with drop and (b) 7–9 $\mu$m diameter, 30 $\mu$m long Cr tubes in a fluid thin film formed by a glass cover slip, prior to applying the SAW. Applying 13 dBm at 30 MHz to the two IDTs (c) moves the tubes to nodes of the standing SAW in the fluid, and (d) aligns the tubes to the SAW's propagation direction. Increasing the concentration of the tubes in the fluid can (e) cause them to chain together, bridging the nodes. From Kong *et al.*, 2010.

presented an advanced theory, though with a number of questionable assumptions with regard to the acoustic wave propagation, on the forces acting to reorient oblong particles embedded in a liquid crystal due to a shear acoustic wave appearing in the liquid crystal media, finding that the forces due to the acoustic radiation are 2 orders of magnitude greater than gravity if the particles are single-walled carbon nanotubes having a length of 10 $\mu$m, the amplitude of the acoustic wave is defined by a vibration velocity of 1 cm/s, and the liquid crystal has a modulus of 10 pN. Schneider *et al.* (2008) developed a racetrack microfluidics structure in PDMS atop a LN SAW device for the purpose of studying the shear-induced uncoiling of the von Willebrand factor, a glycoprotein that tends to assemble into a multimer that can be stretched up to 100 $\mu$m in length. The factor is crucial to clotting and is one of the reasons for the strongly non-Newtonian characteristics of blood. By placing solutions of the factor into the SAW microfluidics device, they were able to stretch and release multimers of the factor over defined time scales in order to characterize its structure as a microrheometer. In this context, it is worth noting the work of Sarvazyan *et al.* (1990), who considered the effects of amino acids and proteins on the nonlinearity parameter $B/A$ (Beyer, 1960) and found a strong correlation between the concentration of the former on the latter. This is consistent with the expectation of increasingly non-Newtonian behavior of such fluids as the concentration of deformable, charged, and interacting molecules is likewise increased.

### 2. In closed environments

Although the effects of particle collection were known from Kundt's discoveries in the 19th century and as described previously, the effects and potential applications of confining the acoustic radiation in a microfluidics device only became a topic of broad interest in the past couple of decades. Goddard and Kaduchak (2005) demonstrated a method for concentrating particles along a single line through precise control of the acoustic wave in a small cylindrical tube, reminiscent of the work by Vainshtein *et al.* (1996) some 10 years prior, and representative of the many ideas for particle manipulation appearing in the literature in combination with microfluidics. As one of the earliest combinations of acoustic energy and microfluidics for manipulating particles in a closed system known to us, Kaajakari *et al.* (2001) made a broad-based attempt to mix and pump fluids and manipulate suspended particles within. An externally placed bulk PZT disk was used to vibrate, in flexure, a thin silicon disk fabricated into a microfluidics device. By inducing specific modes of vibration within the disk through the use of excitation frequencies from 200 kHz to 10 MHz, and by strategically placing combinations of the disks within the fluidic channels, colloidal suspensions of 2 $\mu$m polystyrene microspheres in water were made to mix and flow through the device. Acoustic streaming, most likely fast coarse-grained streaming, was found to be present and driving the particles about the disks. Nine years later, the same group [Araz and Lal (2010)] reported on a microfluidic particle manipulation system for chromatography that makes use of PZT in vibrating a rather complex microstructure fabricated from polycrystalline Si, SiN, and

$SiO_2$ to effectively separate 3 and 10 $\mu$m particles out of a colloidal suspension.

One of the challenges of using acoustic waves in microfluidics is dealing with the inevitable reflections from interfaces that have a change in the acoustic impedance. Traditionally, the worry has been in effective coupling of acoustic waves into air, and for this particular problem capacitive ultrasonic micromachined arrays are the most widely known solution (Oralkan *et al.*, 2003), if not aerogel materials (Gerlach *et al.*, 1992). But for microfluidics, the problem remains open for the most part, although it is a critical problem for particle manipulations that rely upon traveling-wave acoustic radiation, because the direct acoustic force on typical microparticles in water is an order of magnitude larger for standing waves than for traveling waves. Even if the reflections are relatively weak, as would be expected in a PDMS-water interface with acoustic impedances of 1–1.9 and 1.5 MPa s/m in PDMS and water, respectively (Zhuang *et al.*, 2008), this difference can still cause problems. Choosing another material, similar to mylar (polyester, 1.3 MPa s/m) with a more stable acoustic impedance and near that of water, as Lee *et al.* (2009) did in their study, can help to some extent.

Tan, Yeo, and Friend (2009) used a pair of simple straight IDTs in 128YX LN with a centimeter-long fluid channel cut into the substrate between the IDTs and parallel to the axis of SAW propagation, as shown in Fig. 13. Although the SAW propagates along the length of the channel, and has roughly the same amplitude on either side of the channel, the large difference in acoustic impedance between LN and water guarantees that any acoustic wave formed in the fluid channel will reflect from the LN-water interface. The strong reflections are obvious from the particle collection lines formed in Figs. 13(d) and 13(e) and in the standing-wave analysis results present in Fig. 27. While Shi *et al.* (2008) purposely placed the channel formed in PDMS above the 128YX LN perpendicular to the standing-wave SAW radiation, between a pair of IDTs in a similar configuration, the use of SAW across channels to manipulate particles is unnecessary as can be seen from Fig. 27 because of the presence of a standing wave formed across the channel from SAW propagating along the length of the channel. Furthermore, it does not offer the opportunity to use the SAW to also pump the flow, in contrast to the setup by Tan, Yeo, and Friend (2009). However, the configuration by Shi *et al.* (2008) presented a very attractive result, and as the aperture of the SAW is increased, the ability to drive recalcitrant particles to the nodes is enhanced as they move along the length of the channel. The two-dimensional configuration presented by the same group, Shi *et al.* (2009), is interesting though it is unfortunate that the piezoelectric substrate is not named, because the options available with the ability to effectively drive a SAW along both the *x* and *y* axes with sufficient power output and biocompatibility are nil. To get around the problem of standing-wave formation across the width of the channel, Tan, Tjeung *et al.* (2009) combined a double aperture focusing IDT with a fluid channel cut into 128YX LN with a trapezoidal cross section to suppress the formation of standing waves and managed to show a method for steering particles from side to side of the channel using traveling acoustic waves propagating from one side of the
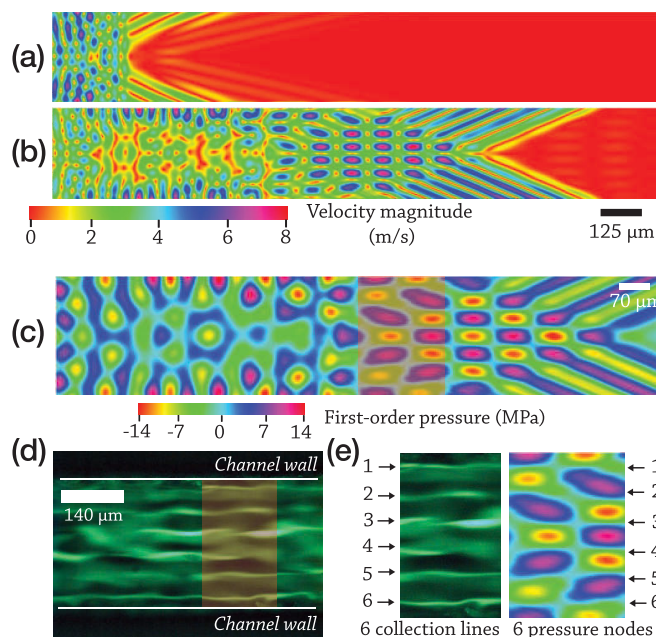


FIG. 27 (color online). The magnitude of the fluid velocity in a 280 $\mu$m wide channel (see Fig. 13) viewed from the top down with $x_1$ from left to right, due to 20 MHz acoustic waves refracting into the water in the channel from the LN after (a) 4 and (b) 10 cycles of the SAW. This model incorporates bidirectional coupling between the piezoelectric LN and the fluid, and (c) the cross-channel standing wave with its pressure nodal lines causes (d) particles to collect along six distinct lines across the width of the channel, directly corresponding (e) to the pressure node lines. From Tan, Yeo, and Friend, 2009.

channel to the other. Simultaneously, the IDT, aligned with the long axis of the fluid channel, pumped the fluid along the channel as an integrated approach. Kapishnikov *et al.* (2006) employed a configuration similar to Shi *et al.* (2008), though with thickness-mode PZT transducers. They tolerated the large difference in acoustic impedance between water (1.5 MPa s/m) and PZT (31.4 MPa s/m) by simply sacrificing the efficiency and included the additional features of converging channels prior to and diverging channels subsequent to the acoustic irradiation section with the intent to continuously separate particles of different sizes from the flow. Using three stages, they were able to separate the cellular material with an efficiency of 99.975% from what they describe as rabbit's blood at a reduced concentration of 25% in phosphate-buffered saline. Using glass-Si-glass for their microfluidics device, Manneberg *et al.* (2009) also used PZT elements to drive particles across microfluidic channels. The PZT elements were attached to the ends of aluminum blocks cut with one end at an angle to convert the thickness-mode vibration of the PZT to what appears to be a Lamb wave that is subsequently propagated in the fluid microchannel to manipulate 10.4 $\mu$m polystyrene and 5 $\mu$m polyamide spheres in suspension in phosphate-buffered saline with 0.05% Tween-20. Although they relied on external syringe pumps to provide the fluid flow, they used specific excitation frequencies for each transducer corresponding to the width of the fluid channel in the path of the channel, between 1.5 and 7 MHz, to obtain a variety of particle collection patterns and merging of particles across tracks.

An obvious application of this ability to segregate and focus particles in channels is flow cytometry, where current approaches that employ sheath flows or dielectrophoresis to hydrodynamically focus cells into a narrow line within the fluidic channel require ample quantities of consumables to generate sheath flow or a planar geometry for all but the latest dielectrophoretic methods (Cheng *et al.*, 2007). A relatively early study by Kumar *et al.* (2005) reported the acoustic separation of hybridoma and lactobacillus using ultrasound irradiation perpendicular to the main axis of flow, with modest efficiency and flow rate. Goddard and Kaduchak (2005) used ultrasound to focus 10 $\mu$m particles and cells in a 190 mm long glass capillary tube with an inner diameter of 1.9 mm along a 14 mm long region exposed to acoustic radiation at 417 kHz from a pair of PZT transducers attached to either side of the tube. They were able to focus the objects to within a 40 $\mu$m region at the center of the flow using this configuration with nearly 100% concentration efficiency. Franke *et al.* (2010) took this idea a step further; although they retained sheath flow for focusing the analyte and the cells within it, they used SAW to aid in focusing the cells and in inducing switching between two outflow channels. The configuration of the IDT is similar to Shi *et al.* (2008), though they do use a tapered IDT to help form a very narrow artificial aperture for the generated SAW that furthermore may be moved along the *width* of the IDT by changing the frequency of the applied electrical signal from about 140 to 150 MHz in their case. The tapered IDT appears again in a recent work by Bourquin *et al.* (2010) to manipulate a drop and particles within.

While a majority of the particle manipulation devices studied so far have made use of either Rayleigh SAW, axially polarized waves from thickness-mode resonators, or Lamb waves, there is some evidence of other forms of acoustic waves being considered for these applications; Yantchev *et al.* (2010) attempted to use Stoneley interface waves to manipulate particles. The variety of interface layers that may be deposited on the piezoelectric substrate and are compatible with microfluidics and the transmission of Stoneley waves, $SiO_2$ on LN, for example, is a clear advantage over Rayleigh SAW devices that use PDMS, where acoustic losses to PDMS are large and pervasive. By bonding $SiO_2$ to lithium tantalate (LT), Yantchev *et al.* propagated a Stoneley wave along their device's $SiO_2$-LT interface bonded together with a thin SU-8 photoresist layer.

Acoustic waves can be used for more than just actuation of particle suspensions. Dukhin and Goetz (2001) described the use of acoustic waves in *characterizing* particle-laden fluids and emulsions, particularly those that are opaque to light, preventing the use of light scattering techniques. Acoustic characterization techniques offered an assessment of the suspended mass (whether for solid objects or bubbles) based on first principles and therefore without a need for calibration, and does so via the inertia of the suspended particles as opposed to light characterization techniques that provided an assessment via the size of the particles, always a challenge when the particles are small, polydisperse, and of unknown morphology. The method can measure particle diameters between 10 nm and 100 $\mu$m. Electroacoustics, an extension of acoustic characterization methods, but with some drawbacks (including sensitivity to double-layer formation and

bubbles), helps provide particle charge information to 1 $\pm$ 0.1 mV, the zeta potential, in addition to the size, and is grouped into two general methods by Dukhin and Goetz: electrokinetic sonic amplitude and colloid vibration current techniques. The former technique measured the sound energy generated by a particle suspension as a consequence of being exposed to an oscillating electric field, while the latter was the converse technique.

Because the objects being manipulated by acoustic forces tend to be much smaller than the acoustic wavelength, suspensions of such particles tend to agglomerate into collections of particles at specific locations in the fluid. Nearly all published experimental work in the area considers only the behavior of small (relative to the acoustic wavelength) particles in the aggregate, not the individual particles by themselves, in notable contrast to the theoretical work that tends to focus upon single particles or perhaps a few in Bjerknes interparticle acoustic scattering forces. For example, Wiklund and Hertz (2006) reported that by focusing 1–10 MHz acoustic radiation, they were able to collect groups of microparticles, beads, for bead-based latex agglomeration, doublet, and singlet assays to enable an inexpensive route to perform fluorescent, electrochemoluminescent, two-photon excitation, and confocal fluorometry of analytes with sensitivities equal to or superior to ELISA and other current techniques. Despite the many applications that exist for a manipulation system able to handle single particles, consider the many publications on optical tweezers, for example (Moffitt *et al.*, 2008), that do this via lasers, very few articles appear in the literature on this topic. Neild *et al.* (2006) used an interesting addition to the typical line-focusing technique seen in a number of other publications: A microgripper that enters the end of an open fluidic channel to fetch individual particles out of the fluid one by one. A slightly different configuration for an invaluable application is provided by Oberti, Moller *et al.* (2009). Combining the acoustic line-focusing technique with a side orifice open to the atmosphere, the tedious process of collecting protein crystals suitable for x-ray crystallography is made simple and permits the crystallographer to continue to use their nylon loop tools as before. Lee *et al.* (2009), on the other hand, sought to directly control individual particles using acoustics as an analogy to optical tweezers. Employing lab-fabricated, focusing ultrasonic transducers from *Y*-cut LN in thickness-mode operation at 23–37 MHz, they were able to trap and retain oleic acid drops of around 125 $\mu$m diameter in water in a region of a few hundred microns in size. Hu *et al.* (2004) presented a simple arrangement to trap individual particles, brine shrimp, thyme, salt crystals, and similar objects with a size of around 50–900 $\mu$m, in the pressure node between vibrating, tapered beams while operating in air or water. This route came about from the group's work in acoustic levitation, and indeed the literature in that area, for example, Hertz (1995), is worth consulting in considering new ideas for trapping particles with acoustics.

### D. Chemistry

Mixing is an important aspect in improving the yield of many chemical reactions, and the ability to deliver sufficient

energy into reactants to thoroughly mix them can be a challenge, especially at the scales of microfluidics where the fluid behavior is laminar. Nguyen and Wu (2005) provided a thorough review of micromixing devices, both passive and active, in closed and open (drop-based) systems. But for a pair of groups using piezoelectric transducers, all the mixing technologies Nguyen and Wu described did not use acoustics. A later work by Frommelt *et al.* (2008), the same group, used tapered IDT structures to drive mixing. One of the groups Nguyen and Wu did cite, Liu *et al.* (2003), actually used near-field, cavitation-driven Schlichting streaming near microcavities machined into a polycarbonate plate, formed of air by capillary forces in immersion in water, and irradiated by thickness-mode vibration of a PZT plate. They found a fivefold enhancement of DNA hybridization in both fluorescence-detection-based and electrochemical-detection-based DNA microarray chips using their approach, compared to conventional diffusion-based biochips. At about the time Nguyen and Wu's review appeared, a number of acoustic micromixing technologies appeared. Lee, well known for his many integrated microfluidics devices using peristaltic pumps (Wang and Lee, 2006), described an ambitious work using Rayleigh SAW to mix fluids passed into a *Y*-shaped microchannel structure formed in PDMS and bonded to the LN substrate carrying the SAW (Tseng *et al.*, 2006). They considered the mixing efficiencies, concentration profiles, increase in temperature of the reactants due to exposure to the SAW (and the associated viscous losses causing the heating), and used the device to drive tryptic digestion of hemoglobin. The trypsin digested product was qualitatively analyzed using mass spectroscopy, indicating that SAW was more effective, the amount of digested peptides increased by 21.1% over the traditional method, and far more rapid than traditional overnight trypsin digestion, requiring only a few minutes to complete. Kulkarni *et al.* (2009) found that SAW irradiation of organic reactants in a sessile drop was very effective for aiding the completion of difficult reactions, such as the Diels-Alder, tetramerization, Kabachnik-Fields, and Baylis-Hillman reactions, without having to resort to microwaves, extraordinary heating (though the drop did reach a temperature of 42 °C for some reactions), catalysts, or large pressures typical of how these reactions are driven in other circumstances. Kulkarni *et al.* (2010) reported in a later work the enhancement of trypsin digestion to produce base peak chromatograms of proteins, reducing the typical time to complete the digestion from overnight to 8 min while simultaneously improving the identification of peptides in the proteins from around 40%–50% with the current process to nearly 80%. They notably duplicated the result of Tseng *et al.* (2006) whose work they were apparently unaware of, though the results were an improvement upon the prior study. Yaralioglu *et al.* (2004) reported a micromixer using thin-film ZnO fabricated on the bottom side of a 545 $\mu$m thick quartz plate, with a 300 $\mu$m wide, 50 $\mu$m thick microchannel fabricated in PDMS atop the plate. By exciting the piezoelectric ZnO together with the quartz as a sort of Langevin transducer at one of the many resonances of the system from 400 to 500 MHz, reasonably good mixing (Re < 1 in the system) was achieved in the channel.

Besides the direct physical manipulation of fluids, solids, and gases with acoustic waves, one can induce or enhance chemical reactions with acoustics. As mentioned, sonochemistry (Suslick and Price, 1999) is among the most widely known combination of these two areas. At the nanoscale, Shchukin *et al.* (2010) described the ability to form metallic nanomaterials in a nonequilibrium state due to cavitation and the consequent extremely large pressure and high temperatures within the fluid near the cavitation bubbles. Nanoalloys and core-shell alloy materials can be formed from sonication of nanoparticle mixtures as well, if appropriate surfactants are used in controlling the zeta potential of the particles and the cavitation bubbles. In the context of microfluidics there has been some additional developments, although the area is in its infancy.

As seen by Kulkarni *et al.*, Ito *et al.* (2007) found that the temperature of fluids exposed to SAW increased rapidly. The temperatures of samples of water, glycerol, and various mixes of these two fluids exposed to SAW dramatically increase, from room temperature to over 40 °C in a little over a minute at modest input voltages. Unfortunately their contribution does not provide any measurements of the power input, power lost as heat to the environment, or power transmitted and lost at the edge of the SAW device, but does note the broad variety of fluid flow behaviors possible in manipulating its viscosity. A related phenomenon, the Ranque-Hilsch (vortex-tube) effect where large and sustained temperature differences can be maintained in fluid flow in a *vortex whistle* configuration that are not directly attributable to the velocity of the flow itself (i.e., such as the high temperature at the stagnation point in transonic flow about an airfoil), was studied by Kurosaka (1982) and found to be due to acoustic streaming. The vortex whistle may be an interesting approach in trying to develop strong temperature variations in microfluidics devices for the future.

## V. FUTURE WORK

Although there has been progress made in the past decade in acoustic microfluidics and related areas, much work remains to be done. Predicting research activity into the future is often folly, but here we note a few possible topics that may lead to significant impact and that have, as yet, seen few researchers consider.

### A. Improvement of analysis techniques

Since the classic analyses of Rayleigh (1884), Westervelt (1953a), Nyborg (1965), and others, the development of computational techniques and equipment sufficiently sophisticated to handle the difficult problem of acoustic streaming in microfluidics, for example, Nguyen and White (2000), Hodgson *et al.* (2009), Tan, Friend, and Yeo (2009), and Tan, Tjeung *et al.* (2009), has enabled an improved understanding of the phenomena in physically relevant settings. The basic equations used in the analysis remain essentially those appearing from classic derivations from 40 years and more ago, and as was noted in this paper, the steps taken in obtaining those derivations were convenient, yet not always strictly justified. A thorough rederivation of the equations based on a sound

mathematical and physical footing, using scaling theory as needed to properly justify the removal of terms and the use of expansion methods, seems an obvious first step in properly treating acoustofluidics. Moreover, there remain tremendous limitations on computation of solutions for nonlinear acoustic streaming problems, especially those with free surfaces. Relatively recent development of lattice Boltzmann algorithms for acoustic streaming by Haydock and Yeomans (2001, 2003) indicates another route to solving such problems that is inherently designed to accommodate complex geometries and free surfaces, and the near future should deliver better analysis techniques via this approach for all acoustic streaming-related problems. As always, the development of improved techniques for direct numerical solution of the Navier-Stokes equations [see, e.g., Martell *et al.* (2009)] should be monitored as this may also lead to new opportunities for analysis and attendant understanding and application.

Further, using methods developed for nonlinear mechanics on the analysis of strongly chaotic phenomena seen in acoustic streaming, suspended particle motion, and free surface deformation may lead to better explanations of the underlying physics. The strange behavior seen by Li *et al.* (2008) in particle collection within sessile droplets, atop fluid free surfaces by Bosch and van de Water (1993), Huepe *et al.* (2006), and Falcon, Fauve, and Laroche (2007) , and the shift of the frequency of response in atomization from the frequency of excitation by 5 orders of magnitude by Qi *et al.* (2008) are but three examples. By using the analysis techniques from other areas, for example, the work by Barashenkov *et al.* (2002) in applying results from random matrix theory and wave-packet dynamics, the work by Huang *et al.* (1999) to use the Hilbert transform instead of the popular Fourier transform because it is far more appropriate for nonlinear systems, better models of the free surface deformation phenomena such as the Camassa-Holm equations (over the older Korteweg–de Vries equations) discussed by Constantin and Lannes (2009), and improving experimental methods such as those used by Snouck *et al.* (2009), a framework is being built to underpin and thoroughly explain Faraday wave mechanics, and these approaches may be useful in related areas across acoustofluidics.

## B. Complex wave propagation, solitons, shock waves, and solid-fluid interaction

A large majority of the phenomena reported in the literature uses only continuously driven acoustic fields. This is both troubling, because of the already complex behaviors seen that require new techniques to analyze, and exciting, because of the variety of discontinuous wave excitation that may be generated and the absence of its use in the microfluidics literature, save for the jetting phenomenon reported by Tan, Friend, and Yeo (2009), and others. Generally, the complexity of the physics and engineering seen in the acoustic microfluidics literature remains focused upon the propagation of the wave in the fluid and its effects on the fluid flow or particles within, without consideration for any additional effects other than nonlinearity.

For other disciplines, the generation of complex waves as they propagate in solids and fluids is a field rich with interesting physical phenomena and engineering applications, from the reverse diffraction and other peculiarities of inhomogeneous waves as reviewed by Declercq *et al.* (2005) to the unusual manner in which sound waves, even *dromions,* propagate and interact in bubbly liquids (Khismatullin and Akhatov, 2001). A crude, old, but still interesting example is the flight actuator (Ota *et al.*, 1985), a piezoelectric device that uses pulse excitation of a multilayer piezoelectric element to drive a mass, a steel ball, into the air. Compared to continuous wave excitation of the piezoelectric material, the impulse excitation that drives a 0.1 mg mass 30 cm into the air by imparting over 0.1 mJ to it is far more dramatic, and indeed it served as the mechanism for high-speed dot-matrix printing for many years. Coupled to fluids, such pulsed strain waves can become shock waves sufficient to destroy calculi in the human body via lithotripsy (Robert *et al.*, 1995). However, for the generation via piezoelectric materials and subsequent propagation of such waves into fluids at the microscale, the literature is nearly silent. Nayanov (1986) described the propagation of large-amplitude Rayleigh waves in $LN/SiO_2$ multilayer structures that become strongly nonlinear cnoidal waves (Korteweg–de Vries solitons) at a generated sound intensity of $I \sim 100$ W/mm$^2$. Because piezoelectric materials typically fail at powers required to generate shock waves, perhaps the absence of many publications in this area comes as little surprise. However, at small scales and with focusing of the acoustic radiation, it may be possible to study such phenomena in detail in the future. Yet the analysis machinery has long been present; Jeffrey and Kakutani (1972) described over three decades ago the analysis of the Korteweg–de Vries–Burgers' equation, among other forms, that can be used as a model equation underlying the nonlinear propagation of finite-amplitude acoustic waves in fluids including dispersion and diffusion.

More physically interesting is the discipline of picosecond laser ultrasonics (Wright and Kawashima, 1992; Hao and Maris, 2001). M. Armstrong *et al.* (2009) described the current state of the art in the femtosecond laser generation and *measurement* of coherent, THz-order, acoustic solitons. They observed the generation of THz electromagnetic radiation as the solitons passed from GaN to AlN and back to GaN, coining the term *nanoseismology* for the propagation of such waves in thin films. Babilotte *et al.* (2010) described the formation of acoustic waves in GaAs with a thin, optically transparent layer of either ZnO or $SiO_2$ propagating from a point where a femtosecond laser irradiates the surface of the GaAs under the thin film, along with a brief review of the field. They viewed the Brillouin mode at 44 GHz and other phonons from 100 to 300 GHz and exercised extraordinary care in the measurement technique which proved to be critical to their findings in the propagation of the waves in the transparent thin layer. But it is interesting that currently the focus remains on the propagation of such waves in solids alone. The contribution by Perez-Arjona *et al.* (2008) in describing stable solitons trapped within a cavity structure containing a viscous media offered a hint of the possibilities in this field if one were to incorporate fluids.

Of course, in piezoelectric media, electric charges accompany the passage of acoustic waves, and for coherent acoustic phonons passing through layered piezoelectric

nanostructures, the charge presents a means to detect the wave (Chen *et al.*, 2007), albeit with limitations on measurement speed due to electronics not present in optical techniques. If one takes the liberal view of charge carriers in semiconductors as a fluid, or, more appropriately, as a gas (Hohenberg *et al.*, 1964), the manipulation and transport of these charge carriers can represent an extension of what is presented in this review. Simple SAW can be used to transport charge carriers in semiconductor quantum well structures fabricated in thin-film GaAs/InGaAs atop LN (Rotter *et al.*, 1999) to even form moving quantum dots as reported by Fletcher *et al.* (2003), naturally leading to the use of such quantum dots in quantum computing by Furuta *et al.* (2004) and even SAW-induced luminescence (Gell *et al.*, 2006) in the quest to obtain a single-photon source. Aside from quantum applications, the ability to transport charge within semiconductors offers interesting applications in UV detectors using epitaxial ZnO thin films (Emanetoglu *et al.*, 2004) and ZnO nanoparticles (Chivukula *et al.*, 2010), and even solar cells (Yakovenko *et al.*, 2009).

### C. Guiding structures in the substrate

A consequence of the massive effort underway in fabricating photonic crystal structures for applications in the communications industry is the concomitant ability to fabricate *phononic* crystal structures with similar methods. By constructing regular defects in one-dimensional, planar, and three-dimensional configurations, the propagation of acoustic waves may be controlled to give extremely narrow *band-gap* responses [as originally reported by Benchabane *et al.* (2006)], tunneling, lensing, negative refraction (Feng *et al.*, 2005), and other acoustically analogous behavior familiar to those working with photonic crystals. Olsson, III and El-Kady (2009) provided a review of the area in illustrating the growing variety of phononic crystal designs for manipulating acoustic waves in the tens to hundreds of megaHertz for microdevices; Fig. 28 shows how one can use flaws in such structures to guide the waves in ways that would be difficult to accomplish via other means. Although the originally proposed use was for acoustic microscopy, little

imagination is required to see how one could use this approach for strategically introducing acoustic energy into microfluidics devices.

For surface acoustic waves, the analysis is slightly different, and fortunately T.-T. Wu *et al.* (2005) analyzed the propagation behavior of such waves in planar photonic crystals of a sort useful for their application in SAW microfluidics. Besides crystalline structures, it is possible to use grooves and ridges to isolate acoustic waves in a single dimension atop a substrate, as reported nearly 40 years ago by Mason *et al.* (1971) for ridges, and only recently by Liu *et al.* (2009) for grooves, as shown in Fig. 29. Over the years these ideas have been used for memory storage and even motors (Tominaga *et al.*, 2005), but they have so far yet to appear in microfluidics. If they eventually do, the results found by Darinskii *et al.* (2009) on the interaction between Rayleigh SAW and steps, depressions, and inclusions on the substrate surface will be useful to keep in mind, as will the work by Newton *et al.* (1999) for sessile drops.

The ability to couple SAW and *photonic* crystals gives one the opportunity to actively manipulate optical radiation with SAW, combining optofluidics and acoustics. de Lima, Jr. and Santos (2005) described how the dielectric properties, dimensions, and geometry of Bragg waveguides and photonic
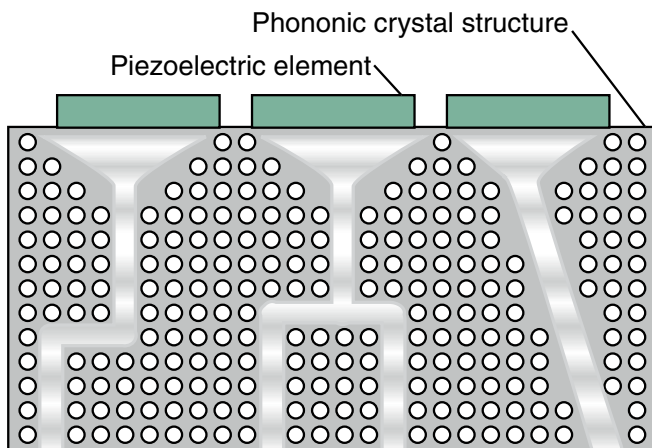
FIG. 28 (color online). Schematic of how one could use phononic crystal structures to steer acoustic waves as desired. From Olsson, III and El-Kady, 2009.
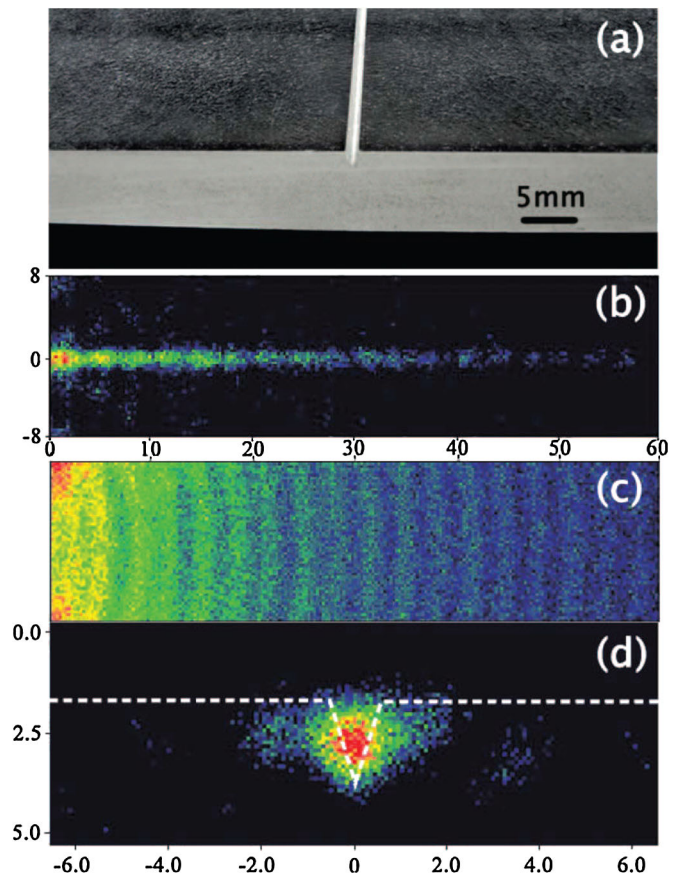
FIG. 29 (color online). (a) The microgroove acts to carry the acoustic wave along its length illustrated by the (b) pressure measurement which clearly shows the isolation of the acoustic wave to the groove compared to a (c) substrate without the groove. Looking (d) end on, the distribution of the acoustic energy is shown to be mainly in the walls of the groove. From Liu *et al.*, 2009.

mirrors, cavities, filters, and waveguides can be changed with the application of SAW in a comprehensive review.

## D. Electret, electroactive polymer, and "artificial muscle" materials

Electrets are designed to transform energy between electrical and mechanical forms, exactly, and confusingly, such as piezoelectric materials, and could become useful for acoustic microfluidics as a convenient alternative to them. The term *electret* was originally defined to mean a (quasi-)permanently polarized dielectric material, an electric counterpart to permanent magnets. Although the meanings overlap, amorphous or inhomogeneous forms of these materials are usually called electrets, sometimes in error.[9] A recent catchphrase for these sorts of materials, artificial muscle, reflects investigators' interest in obtaining a material that matches the extraordinary properties of human muscle tissue (Bar-Cohen, 2004). Unfortunately, the current limitations of most electroactive polymer materials prevent their use in many practical applications, but this situation is bound to change given the broad interest in improving them. With the convenience and near ubiquity of physically soft materials in microfluidics, particularly as of late with biomimicry and tissue engineering (Domachuk *et al.*, 2010) for implants, these materials may prove superior in many applications for acoustically actuating fluids in microfluidics by making acoustic excitation within the castable components such as PDMS possible.

## E. Expansion to nanoscale phenomena

Although much of the potential in microfluidics devices using acoustics has yet to be realized, the use of acoustic waves at the nanoscale cannot be underestimated. Already, the evidence is clear, in Edel *et al.* (2009), for example, that fluidics phenomena at the nanoscale are far different than at larger scales, and that exploiting such phenomena will yield unprecedented technologies just as what has happened in microfluidics. Given the apparently peculiar, non-Fickian nature of fluid flow at the nanoscale (Whitby and Quirke, 2007), it is perhaps no surprise that phonon transport in nanoscale structures with fluids adjacent to them would result in interesting behavior. Insepov *et al.* (2006) reported that if one were to use surface acoustic waves transmitted along carbon nanotubes, the peristaltic motion that occurs along the nanotubes would be sufficient to pump gases beyond 30 km/s along their length, although the frequencies necessary to actually deliver reasonable flow rates of around 10 cm$^3$/min appear to be well into the THz range for their 100-nm-long nanotube. Notwithstanding the many assumptions in their analysis and the inherent problems in using molecular dynamics solutions to interpret the probable behavior of real systems over physically meaningful time scales, their work hinted at the possibilities. The tantalizing

results of other groups, such as that by Nassoy *et al.* (2008) in the experimental vibration of nanotube structures and by Shannon *et al.* (2008) in water purification, indicate the potential of acoustics as a useful means to generate useful fluid motion well into the future. The non-Newtonian behavior of fluids at the nanoscale is yet another intriguing line of possible investigation (Karabacak *et al.*, 2007). The recent work of Lin *et al.* (2007) showed that optically generating acoustic waves within GaN/InGaN in the THz range with spatial control to a few tens of nanometers, less than the diffraction limit, is possible. This and the simplicity of the approach taken by Pezeril *et al.* (2009) in optically generating such waves in glycerol altogether suggests a potential route to acoustic *nanofluidics*.

As always, a key issue in moving to smaller scales is the availability of effective fabrication techniques, and this is certainly true here. In our work, we have chosen two standard tools of nanofabrication, focused ion beam (FIB) milling and electron-beam lithography (EBL), shown in Fig. 30. In contrast to the work of Lacour *et al.* (2005), we found the machining of nanoscale channels in lithium niobate using FIB to be relatively easy, supporting the view expressed by Hashimoto (2000). Such channels may be closed by wafer bonding techniques pioneered roughly 10 years ago (Takagi
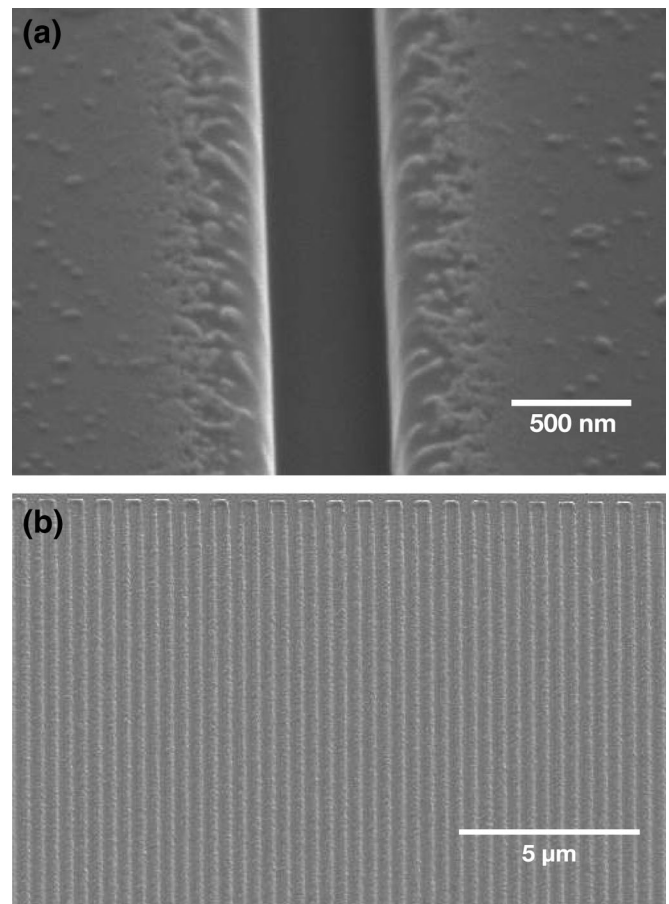
FIG. 30. Channel fabricated directly in LN using (a) a FIB system; the channel is 510 nm wide, 500 nm deep, and runs for 1 cm along the *X* axis of the material. Using EBL, we have been machining IDTs onto the surface for GHz-order SAW using (b) acrylic patterned for use in a liftoff technique.

---

[9]The critical difference among the terms is that electrets retain polarization in thermodynamic nonequilibrium, pyroelectric materials retain polarization in equilibrium, ferroelectrics permit the polarization to be reversed along the polarization axis, and piezoelectric materials may or may not have any polarization at all.

*et al.*, 1999). Another important issue is measurement of the behavior; while there remain many problems in effective measurement of fluid flow at the nanoscale discussed by Mattia and Gogotsi (2008), the acoustic wave itself must be measured. Fortunately, improvements in laser Doppler vibrometry and alternative techniques such as the knife-edge method by Kamizuma *et al.* (2006) make it possible to measure waves in excess of 10 GHz. Using extended ultraviolet light, Siemens *et al.* (2009) were able to measure SAW propagation for waves up to 50 GHz.

# VI. GLOSSARY

The misuse of and confusion surrounding terminology in the acoustic streaming literature have become such a barrier to understanding the underlying phenomena that it is essential to properly identify and define the jargon in this review. We provide descriptions of particular terms with references back to the original usage where possible and what the terms have come to represent in the years since.

*Reynolds number, acoustic:* The orthodox concept of the hydrodynamic Reynolds number as a ratio of the inertial forces to the viscous forces stands apart from the variety of definitions for the *acoustic Reynolds number*. A popular (and some might say *erroneous*, because the number has more to do with the streaming than the acoustics) definition appears to be $\mathrm{Re}_{\mathrm{ac,Crighton}} = \rho_f u_1 \mathcal{L}/\mu$, where $\mathcal{L}$ is a characteristic length of the system (Morse and Ingard, 1968; Crighton, 1979). [Riley (2001) called this the Reynolds number associated with viscosity.] The problem with this definition is that it might work for specific cases but offers little in a more general treatment of acoustic streaming problems. However, there are other definitions; $\mathrm{Re}_{\mathrm{ac,Krylov}} = \rho_f \lambda c_0/\mu$ represents a measure of the effect of viscosity over a wavelength of the acoustic wave and completely omits any measure of the geometry or the wave's amplitude itself (Krylov, 2001). It is a large value for most systems, microfluidic or not: A 10 MHz wave in water gives a value of $\mathrm{Re}_{\mathrm{ac}} = 3.6 \times 10^7$. Zarembo and Krasil'nikov (1959) provided another definition by multiplying Krylov's definition with the acoustic Mach number $\varepsilon_{\mathrm{ac}} = u_1/c_0$, therefore incorporating the amplitude of the wave itself into the definition, $\mathrm{Re}_{\mathrm{ac,Zarembo}} = \rho_f c_0 u_1/\mu\omega$, still a large number in most cases.

Naugolnykh and Ostrovsky (1998) presented a valuable form of the acoustic Reynolds number, Eq. (29), that can help determine whether the propagation of an acoustic wave may be modeled as a linear or nonlinear system, the latter case with either Burgers' equation or the Korteveg–de Vries–Burgers equation. If $\mathrm{Re}_{\mathrm{ac}} \ll 1$, the wave propagates linearly, because either its amplitude is small (infinitesimal) or the dissipation within the fluid is sufficiently strong to dissipate away the energy of the wave before the nonlinear effects cause the wave to overturn and form a shock.

*Reynolds number, hydrodynamic:* The usual Reynolds number $\mathrm{Re}_{\mathrm{hydro}} \equiv \rho_f u_0^2/\omega\mu$ that is typically less than 1 for microfluidics problems, making use of the Eulerian fluid velocity. For microfluidics, it is described by Purcell (1977). In situations incorporating acoustics, the correct fluid velocity must be used for the inertial contribution by including the particle velocity: the *streaming* Reynolds number as

an alternative representation to make this point clear. The hydrodynamic Reynolds number is not as useful as the streaming Reynolds number for problems with significant acoustic wave propagation.

*Reynolds number, streaming:* A Reynolds number where the Lagrangian fluid velocity is used in the expression, for example, $\mathrm{Re}_{\mathrm{st}} = \rho_f u_1^2/\omega\mu$, provided by Riley (2001); some investigators (Morse and Ingard, 1968; Crighton, 1979) confusingly called their streaming Reynolds number an *acoustic* Reynolds number. We define it in Sec. III.D as $\mathrm{Re} = \rho_f U_0 \mathcal{L}/\mu$, where $\mathcal{L}$ is a characteristic length and $U_0 \equiv |\mathbf{U}|$ is the characteristic flow velocity incorporating both the velocity of the fluid itself, $\mathbf{u}_0$, and the effect of the acoustic wave propagation $\mathbf{U} \equiv \mathbf{u}_0 + \langle \mathbf{I} \rangle/\rho_{f0}c_0^2 = \mathbf{u}_0 + \langle \rho_{f1}\mathbf{u}_1 \rangle/\rho_{f0}$; in the presence of an acoustic wave it is better to use than the hydrodynamic Reynolds number.

*Rayleigh (medium-grained) streaming:* Viscous boundary layer [or *Stokes layer*, for example, as defined by Riley (2001)] driven streaming due to a standing-wave acoustic field, lacking compressibility and nonlinear effects (Rayleigh, 1884).[10] Rayleigh streaming has come to mean the vortical streaming present in the fluid bulk, not within the boundary layer itself (Riley, 2001; Boluriaan and Morris, 2003; Hamilton *et al.*, 2003); see Schlichting streaming for the latter. Rayleigh's law of streaming has come to mean the mechanism that drives streaming in the bulk from matching of flow at the edge of the boundary layer (Lighthill, 1978; Riley, 2001). The vortices have dimensions on the order of the acoustic wavelength $\lambda$. Rayleigh also described the flow within the boundary layer, and his paper included a two-dimensional compressible model for streaming in the Kundt tube problem. He took into account the difference between the Lagrangian and Eulerian representation of the fluid flow, a topic Lighthill (1978) colorfully detailed. Note the improved solution by Hamilton *et al.* (2003) applicable to cases of Rayleigh streaming described in the definition for Schlichting streaming below.

*Schlichting (fine-grained) streaming:* Streaming driven within a viscous, incompressible boundary layer, appearing as rotational flow within the boundary, typically as a series of vortices (Schlichting, 1932). The vortices have dimensions on the order of the acoustic wavelength. An improved solution relevant to microfluidics is offered by Hamilton *et al.* (2003), where the true width of the domain defined by a pair of walls along the acoustic wave propagation direction is set and the standing-wave solution is properly treated as having a nonzero divergence in the viscous boundary layer. For cases either where both walls are oscillating or where the system is axisymmetric with an oscillating boundary, Secomb (1978) presented a series of fluid flow solutions assuming *incompressible* viscous fluids; originally the analysis was for vascular flow, but it remains valid for applications in microfluidics.

*Eckart (coarse-grained) streaming:* Some have used this term (Eckart, 1948) to describe a form of streaming appearing in the bulk of the fluid by the action of Reynolds stresses as driven by dissipation of large-amplitude acoustic waves as

---

[10]Some publications refer to this article as published in 1883 in error; it was *read* in 1883 but published in 1884 (MDCCCLXXXIV in footer of article).

they progress through that bulk (Zarembo, 1971; Boluriaan and Morris, 2003; Haydock and Yeomans, 2003; Guttenberg *et al.*, 2005): the viscous boundary layer is ignored. Even so, the viscosity in the bulk is taken into account; indeed it is instrumental to the form of streaming Eckart described in his work. Some notable problems with Eckart's derivation were identified and corrected by Markham (1952), although the results were the same. Heat conduction is ignored. Vortices, if present due to mass conservation, are at least an order larger in size than the acoustic wavelength. Eckart's original analysis offers a one-dimensional solution for the acoustic streaming in the bulk, therefore eliminating the need for the convective acceleration term in the momentum equation, the second term in Eq. (23), but because he relies upon the method of successive approximations, the results remain valid only for slow streaming. Eckart notes that this form of streaming, which he describes as *quartz wind*, appears when the frequency of the acoustic wave is relatively high, 1 MHz and up in water and about 1 kHz and up in air. However, Lighthill (1978) noted that the acoustic intensity must be very low at such high frequencies to avoid invalidating the analysis approach: The transition to fast streaming occurs at very low acoustic radiation intensities. His claim that his results can be used to determine the viscosities of a fluid should be tempered by the observation made by Lighthill (1978) that other forms of dissipation, scattering, thermal, etc., are also likely to be significant and cause an error in this estimate. Later analyses by Kamakura *et al.* (1995) and others have taken into account more realistic acoustic intensity distributions, Gaussian, for example, and nonlinearity of the acoustic wave due to the convective acceleration by relaxing the one-dimensional assumption (Rudenko and Soluîan, 1977).

*Stuart streaming:* Coined by Lighthill (1978) as a form of acoustic streaming including the fluid's inertia in the streaming motion, not just in the modeling of the acoustic wave's propagation, while compressibility is ignored. He stated this idea was first developed by Stuart (1963) 15 years earlier. The *hydrodynamic* Reynolds number must be large, on the order of $10^2$ or more, to have Stuart streaming, implying it is similar in concept to fast streaming, and for this reason it does not explicitly appear in Table I. Stuart noted that with the traditional derivation of boundary-layer theory, no pressure changes were permitted in the boundary layer other than that driven by the external, inviscid flow. Yet in acoustic wave propagation, the pressure is known to be changing through the boundary layer. In his analysis about a cylinder, yet with applicability to more general configurations, he shows that there are two boundary layers, but only if the hydrodynamic Reynolds number for the acoustic streaming is about $10^3$ or greater (Stuart, 1966). Because Stuart uses a perturbation method in his analysis, however, the acoustic Reynolds number must be small, limiting his results to slow streaming just as with Nyborg, Westervelt, and Lighthill.

*Stokes's drift:* The Lagrangian mean of the fluid velocity, also known as the streaming velocity, minus the Eulerian mean of the fluid velocity. The correction to the Eulerian mean of the fluid velocity to give the value of the Lagrangian means of the fluid velocity. In normal fluid dynamics analyses this difference is usually well understood and without controversy, but the trouble it causes in acoustic

streaming problems is substantial. Unfortunately, acoustic streaming phenomena complicate the mean calculations due to the presence of fluid particle oscillation as the acoustic wave passes in addition to the particle's motion from fluid flow. While acoustic streaming is, in part, described by Stokes's drift, in most cases the dominant contributor to streaming is either the appearance of gradients in the Reynolds stress along the propagation path of the acoustic wave or attenuation of the acoustic wave from viscosity that gives rise to a net change in the momentum flux (Lighthill, 1978; Riley, 1998).

*Quartz wind:* Streaming appearing in a fluid from the presence of a very high-frequency (usually MHz order or greater), collimated acoustic wave propagating into the fluid. Named from observations of these phenomena from quartz transducers in the 1920s (Riley, 1998). Some, particularly early investigators, treat quartz wind as being equivalent to acoustic streaming, while others (Haydock and Yeomans, 2003) treat it as equivalent to Eckart streaming, doing so because the acoustic streaming for these cases is perceived to be dominated by viscous dissipation of the acoustic radiation. The association between Eckart streaming and quartz wind is understandable given that Eckart (1948) himself described the acoustic streaming he chose to study as quartz wind. Nowadays the term tends to refer to a specific problem where the high-frequency radiator is enclosed as a piston at one end of a fluid-filled, long pipe with the other end open (Riley, 1998).

*Steady streaming:* A term used especially by Riley (2001) to describe the streaming appearing in a fluid in excess of the Stokes's drift. Riley also offered interesting insights into Eckart streaming (quartz wind) and a unique view of the possibility of generating acoustic streaming in inviscid fluids that possess a free surface.

*Reynolds stress:* The second term in Eq. (23). This term appears especially in work by Lighthill (1978) and Riley (2001) and is defined as the mean value of the acoustic wave's momentum flux. It appears from dissipation of acoustic energy in the fluid, mainly from viscous effects. Gradients in the Reynolds stress give rise to acoustic streaming.

*Stokes boundary layer:* Within this layer the vorticity is nonzero, and the original definition of this layer was from one of the few closed-form solutions of the Navier-Stokes equations (at low Reynolds numbers) describing fluid motion above a flat plate oscillating back and forth in its own plane (Wang, 1991). The thickness of the boundary layer is $\delta_v = \sqrt{2\mu/\rho_f \omega}$, where $\mu$ is the dynamic viscosity, $\rho$ is the density, and $f$ is the oscillation frequency. However, this is not necessarily the length scale over which an acoustic wave is attenuated in a fluid, whether near a boundary or not. The Stokesian boundary-layer solution precludes the motion of the solid boundary perpendicular to its plane, and so while the shear-polarized component of the acoustic wave in the fluid may attenuate within the Stokes boundary layer, the axially polarized component may propagate over far longer distances (see Eckart streaming).

*Lighthill's contribution:* The oft-cited contribution by Sir James Lighthill (1978) revisited acoustic streaming with an emphasis of its effects in air. He aimed to show how classical

analyses from the 1950s by Westervelt (1953a)[11] and Nyborg (1965) were valid only for what we call here slow streaming, $\mathrm{Re_{ac}} \ll 1$, although it should be noted that Westervelt stated his analysis had many limitations, not the least of which was the use of the perturbation method to model the acoustic streaming phenomena. But Lighthill noted that in these previous works the inertial effects on the streaming motion, not on the progression of the acoustic wave, but on the higher-order streaming, were neglected. The justification for doing so was in estimating the relative order of the terms, but the consequences were to again limit the analyses reported by these earlier investigators to cases where $\mathrm{Re} \ll 1$, the same slow streaming limitation as imposed from the use of perturbation analysis. In keeping the inertial effects in the analysis for the higher-order acoustic streaming model, which Lighthill called Stuart streaming, he showed that streaming induced at higher acoustic Reynolds numbers could be more accurately modeled. However, he used the same perturbation approach that Nyborg and Westervelt had used; although Lighthill's analysis was superior to his predecessors, it still prevented one from considering what would happen at large acoustic Reynolds numbers associated with fast streaming. Nevertheless, Lighthill provided many interesting insights into the streaming phenomena worthy of remembering whatever the scale. He clarifies the differences between Eulerian and Lagrangian representations of fluid motion, and points out that there is a distinct difference between the two in acoustic streaming, although the amplitude of fluid motion driven by acoustic streaming is typically far larger than this difference. The actual streaming mechanism for linear motion is the Reynolds stress, the fluid's momentum flux. Following his own and Beyer's work (Beyer, 1960), he noted the problems with measuring and using the acoustic attenuation coefficient because of variability, critically important to acoustic streaming because the large majority of streaming appears from attenuation of the acoustic wave in the fluid. And he noticed the analogy with Einstein's $E = mc^2$ equation, also deftly presented by Bradley (1996), where it is equally valid when expressing the terms as acoustic energy, acoustic mass flux, and the bulk speed of sound, respectively: As acoustic streaming occurs, wherever the acoustic energy appears in the system and propagates away, it is associated with a loss of mass in that part of the system, proportional to that energy divided by the speed of sound, squared. The resulting "squeeze flow," as coined by Bradley, acts to induce fluid flow toward the acoustic energy source. Eckart (1948) noted, in recognition of this equation, that comparing the consequent "inertia of acoustic energy" $m_{\mathrm{acoustic}} = E/c^2_{\mathrm{acoustic}}$ and the similarly defined "inertia of electromagnetic radiation" shows the inertia that may be generated in a fluid upon exposure to an acoustic wave to be far larger than if exposed to an electromagnetic wave. Thus, for example, the motion imparted in a fluid using acoustic means could be estimated to be $c^2_{\mathrm{light}}/c^2_{\mathrm{acoustic}} \approx 10^6$ stronger than via electromagnetism for water. Inherent in this expression, however, is the assumption the velocity of the particle is much less than the velocity of sound, i.e., the hydrodynamic Mach number $M \equiv U_0/c_0 \ll 1$, because the full expression of energy-mass

equivalence is $E^2 = m^2c^4 + p^2c^2$, where $p = mv^2$ is the momentum of the body. As long as $v \ll c$, the momentum of the particle is negligible in this relation. For fluid electrodynamics, the speed of light $c$ is far larger than any fluid phenomena, yet this may not be the case for fluid acoustodynamics with a much lower speed of sound $c_0$.

## REFERENCES

Adams, J. D., and H. T. Soh, 2010, Appl. Phys. Lett. **97**, 064103.

Adler, E., 1994, IEEE Trans. Ultrason. Ferroelectr. Freq. Control **41**, 876.

Ahlers, F. J., N. E. Fletcher, J. Ebbecke, and T. J. B. M. Janssen, 2004, Current Applied Physics **4**, 529.

Alexe, M., C. Harnagea, A. Visinoiu, A. Pignolet, D. Hesse, and U. Gösele, 2001, Scr. Mater. **44**, 1175.

Alvarez, M., J. Friend, and L. Yeo, 2008, Langmuir **24**, 10 629.

Alvarez, M., L. Yeo, and J. Friend, 2008, Nanotechnology **19**, 455103.

Alvarez, M., L. Y. Yeo, J. R. Friend, and M. Jamriska, 2009, Biomicrofluidics **3**, 014102.

Alzuaga, S., J.-F. Manceau, and F. Bastien, 2005, J. Sound Vib. **282**, 151.

Araz, M. K., and A. Lal, 2010, in *Proceedings of the 2010 IEEE 23rd International Conference on Micro Electro Mechanical Systems (MEMS)* (IEEE, New York), pp. 1111–1114.

Armstrong, M., E. Reed, K. Kim, J. Glownia, W. Howard, E. Piner, and J. Roberts, 2009, Nature Phys. **5**, 285.

Asai, K., and M. Kurosawa, 2005, IEEE Trans. Ultrason. Ferroelectr. Freq. Control **52**, 1722.

Asai, K., M. Kurosawa, and T. Higuchi, 1999, in *Proceedings of the 1999 IEEE Ultrasonics Symposium* (IEEE, New York), Vol. 1, pp. 667–670.

Asai, K., M. K. Kurosawa, and T. Higuchi, 2004, Electronics and Communications in Japan (Part III: Fundamental Electronic Science), **87**, 10.

Auld, B., 1973, *Acoustic Fields and Waves in Solids* (Wiley, New York), Vols. 1 and 2.

Babilotte, P., P. Ruello, D. Mounier, T. Pezeril, G. Vaudel, M. Edely, J.-M. Breteau, V. Gusev, and K. Blary, 2010, Phys. Rev. B **81**, 245207.

Barashenkov, I., N. Alexeeva, and E. Zemlyanaya, 2002, Phys. Rev. Lett. **89**, 104101.

Bar-Cohen, Y., 2004, *Electroactive Polymer (EAP) Actuators as Artificial Muscles: Reality, Potential, and Challenges* (SPIE Publications, Bellingham, WA), Vol. PM136, 2nd ed.

Barreras, F., H. Amaveda, and A. Lozano, 2002, Exp. Fluids **33**, 405.

Barth, J., G. Costantini, and K. Kern, 2005, Nature (London) **437**, 671.

Batchelor, G., 1967, *An Introduction to Fluid Mechanics* (Cambridge University Press, London, UK).

---

[11]Also note the errata Westervelt (1953b).

Bechhoefer, J., V. Ego, S. Manneville, and B. Johnson, 1995, J. Fluid Mech. **288**, 325.

Beebe, D., G. Mensing, and G. Walker, 2002, Annu. Rev. Biomed. Eng. **4**, 261.

Benchabane, S., A. Khelif, J.-Y. Rauch, L. Robert, and V. Laude, 2006, Phys. Rev. E **73**, 065601.

Benjamin, T., and F. Ursell, 1954, Proc. R. Soc. A **225**, 505.

Berlincourt, D., D. Curran, and H. Jaffe, 1964, *Piezoelectric and Piezomagnetic Materials and Their Function in Transducers* (Academic Press, New York), Chap. 3, pp. 169–270.

Bertelsen, A., A. Svardal, and S. Tjøtta, 1973, J. Fluid Mech. **59**, 493.

Bertolotti, F., T. Herbert, and P. Spalart, 1992, J. Fluid Mech. **242**, 441.

Bertoni, H., and T. Tamir, 1973, Appl. Phys. A **2**, 157.

Beyer, R., 1978, J. Acoust. Soc. Am. **63**, 1025.

Beyer, R. T., 1960, J. Acoust. Soc. Am. **32**, 719.

Beyer, R. T., 1997, *Nonlinear Acoustics: The Parameter B/A* (Academic Press, New York), Chap. 2, pp. 25–40.

Beyer, R. T., 1998, *Sounds of Our Times, Two Hundred Years of Acoustics* (Springer, New York).

Bhattacharjee, P. K., A. McDonnell, R. Prabhakar, L. Yeo, and J. Friend, 2011, New J. Phys. **13**, 023005.

Binks, D., and W. van de Water, 1997, Phys. Rev. Lett. **78**, 4043.

Biskos, G., V. Vons, C. Yurteri, and A. Schmidt-Ott, 2008, KONA Powder and Particle Journal **26**, 13 [http://www.kona.or.jp/search/26_013.pdf].

Blackstock, D., 1966, J. Acoust. Soc. Am. **39**, 1019.

Blackstock, D. T., 2000, *Fundamentals of Physical Acoustics* (Wiley Interscience, New York).

Blake, T., 1990, Colloids Surf. **47**, 135.

Bok, M., H. Li, L. Yeo, and J. Friend, 2009, Biotechnol. Bioeng. **103**, 387.

Boluriaan, S., and P. Morris, 2003, Int. J. Aeroacoustics **2**, 255.

Bordui, P. F., D. H. Jundt, E. M. Standifer, R. G. Norwood, R. L. Sawin, and J. D. Galipeau, 1999, J. Appl. Phys. **85**, 3766.

Borgnis, F. E., 1953, Rev. Mod. Phys. **25**, 653.

Bosch, E., and W. van de Water, 1993, Phys. Rev. Lett. **70**, 3420.

Bourquin, Y., J. Reboud, R. Wilson, and J. M. Cooper, 2010, Lab Chip **10**, 1898.

Bradley, C., 1996, J. Acoust. Soc. Am. **100**, 1399.

Brenner, M. P., S. Hilgenfeldt, and D. Lohse, 2002, Rev. Mod. Phys. **74**, 425.

Brunet, P., M. Baudoin, O. B. Matar, and F. Zoueshtiagh, 2010, Phys. Rev. E **81**, 036315.

Brunet, P., J. Eggers, and R. Deegan, 2007, Phys. Rev. Lett. **99**, 144501.

Campbell, C., 1998, *Surface Acoustic Wave Devices for Mobile and Wireless Communications* (Academic Press, New York).

Campbell, J., and W. Jones, 1968, IEEE Trans. Sonics Ultrason. **15**, 209.

Cavić, B., M. Thompson, and G. Hayward, 1999, The Analyst **124**, 1405.

Cecchini, M., S. Girardo, D. Pisignano, R. Cingolani, and F. Beltram, 2008, Appl. Phys. Lett. **92**, 104103.

Chagla, F., and P. Smith, 2006, IEEE Trans. Ultrason. Ferroelectr. Freq. Control **53**, 1895.

Chang, H., and L. Yeo, 2010, *Electrokinetically Driven Microfluidics and Nanofluidics* (Cambridge University Press, Cambridge, England).

Chen, C., Y. Wen, H. Chen, T. Liu, C. Pan, J. Chyi, and C. Sun, 2007, Appl. Phys. Lett. **91**, 133101.

Chen, P., and J. Viñals, 1997, Phys. Rev. Lett. **79**, 2670.

Chen, Z., M. Takeuchi, and K. Yamanouchi, 1992, IEEE Trans. Ultrason. Ferroelectr. Freq. Control **39**, 82.

Cheng, I., H. Chang, D. Hou, and H. Chang, 2007, Biomicrofluidics **1**, 021503.

Chilowsky, C., and P. Langevin, 1916, French patent (Brevet français) (502913).

Chivukula, V., D. Ciplys, M. Shur, and P. Dutta, 2010, Appl. Phys. Lett. **96**, 233512.

Chladni, E., 1787, *Entdeckungen uber die Theorie des Klanges* (Weidmanns, Erben und Reich, Leipzig, Germany).

Chono, K., N. Shimizu, Y. Matsui, J. Kondoh, and S. Shiokawa, 2004, Jpn. J. Appl. Phys. **43**, 2987.

Chu, B.-T., and R. E. Apfel, 1982, J. Acoust. Soc. Am. **72**, 1673.

Clarke, L., A. Edwards, and K. Pollard, 2005, J. Ultrasound Med. **24**, 617 [http://www.jultrasoundmed.org/cgi/content/abstract/24/5/617].

Constantin, A., and D. Lannes, 2009, Arch. Ration. Mech. Anal. **192**, 165.

Coussios, C., and R. Roy, 2008, Annu. Rev. Fluid Mech. **40**, 395.

Craighead, H., 2006, Nature (London) **442**, 387.

Craster, R., and O. Matar, 2009, Rev. Mod. Phys. **81**, 1131.

Crighton, D., 1979, Annu. Rev. Fluid Mech. **11**, 11.

Cross, M., and P. Hohenberg, 1993, Rev. Mod. Phys. **65**, 851.

Cubaud, T., M. Tatineni, X. Zhong, and C.-M. Ho, 2005, Phys. Rev. E **72**, 037302.

Curie, J., and P. Curie, 1880, C.R. Hebd. Seances Acad. Sci. **91**, 294.

Darinskii, A., M. Weihnacht, and H. Schmidt, 2009, J. Appl. Phys. **106**, 034914.

Declercq, N., R. Briers, J. Degrieck, and O. Leroy, 2005, IEEE Trans. Ultrason. Ferroelectr. Freq. Control **52**, 776.

de Jong, J., R. Jeurissen, H. Borel, M. van den Berg, H. Wijshoff, H. Reinten, M. Versluis, A. Prosperetti, and D. Lohse, 2006, Phys. Fluids **18**, 121511.

de Lima, Jr., M. M., and P. V. Santos, 2005, Rep. Prog. Phys. **68**, 1639.

Demirci, U., 2005, Rev. Sci. Instrum. **76**, 065103.

Deng, Y., L. Liu, Y. Cheng, C.-W. Nan, and S.-J. Zhao, 2003, Mater. Lett. **57**, 1675.

Dias, F., and C. Kharif, 1999, Annu. Rev. Fluid Mech. **31**, 301.

Doinikov, A., 1999, J. Acoust. Soc. Am. **106**, 3305.

Doinikov, A., 2001, J. Fluid Mech. **444**, 1.

Doinikov, A., and P. Dayton, 2006, J. Acoust. Soc. Am. **120**, 661.

Doinikov, A. A., 1996, Phys. Rev. E **54**, 6297.

Doinikov, A. A., and A. Bouakaz, 2010, J. Acoust. Soc. Am. **127**, 703.

Domachuk, P., K. Tsioris, F. Omenetto, and D. Kaplan, 2010, Adv. Mater. **22**, 249.

Dong, L., A. Chaudhury, and M. K. Chaudhury, 2006, Eur. Phys. J. E **21**, 231.

Donnelly, T., J. Hogan, A. Mugler, N. Schommer, M. Schubmehl, A. Bernoff, and B. Forrest, 2004, Phys. Fluids **16**, 2843.

Dorrestijn, M., A. Bietsch, T. Açıkalın, A. Raman, M. Hegner, E. Meyer, and C. Gerber, 2007, Phys. Rev. Lett. **98**, 026102.

Douady, S., 1990, J. Fluid Mech. **221**, 383.

Dukhin, A., and P. Goetz, 2001, Adv. Colloid Interface Sci. **92**, 73.

Duvshani-Eshet, M., L. Baruch, E. Kesselman, E. Shimoni, and M. Machluf, 2006, Gene Therapy **13**, 163.

Dyke, M. V., 1975, *Perturbation Methods in Fluid Mechanics* (The Parabolic Press, Stanford, CA).

Eckart, C., 1948, Phys. Rev. **73**, 68.

Edel, J. B., and A. deMello, 2009, *Nanofluidics: Nanoscience and Nanotechnology* (Royal Society of Chemistry, Cambridge, UK).

Eggers, J., 1997, Rev. Mod. Phys. **69**, 865.

Eguíluz, V. M., M. Ospeck, Y. Choe, A. J. Hudspeth, and M. O. Magnasco, 2000, Phys. Rev. Lett. **84**, 5232.

Ellis, J., G. McHale, G. Hayward, and M. Thompson, 2003, J. Appl. Phys. **94**, 6201.

Elrod, S., B. Hadimioglu, B. Khuri-Yakub, E. Rawson, E. Richley, C. Quate, N. Mansour, and T. Lundgren, 1989, J. Appl. Phys. **65**, 3441.

Emanetoglu, N. W., J. Zhu, Y. Chen, J. Zhong, Y. Chen, and Y. Lu, 2004, Appl. Phys. Lett. **85**, 3702.

Falcon, E., S. Fauve, and C. Laroche, 2007, Phys. Rev. Lett. **98**, 154501.

Falcon, E., C. Laroche, and S. Fauve, 2007, Phys. Rev. Lett. **98**, 094503.

Falkovich, G., A. Weinberg, P. Denissenko, and S. Lukaschuk, 2005, Nature (London) **435**, 1045.

Fantner, G., et al., 2006, Ultramicroscopy **106**, 881.

Faraday, M., 1831, Phil. Trans. R. Soc. London **121**, 299.

Felder, C., M. Blanco-Prieto, J. Heizmann, H. Merkle, and B. Gander, 2003, Journal of Microencapsulation **20**, 553.

Feng, L., X. Liu, Y. Chen, Z. Huang, Y. Mao, Y. Chen, J. Zi, and Y. Zhu, 2005, Phys. Rev. B **72**, 033108.

Fletcher, N. E., J. Ebbecke, T. J. B. M. Janssen, F. J. Ahlers, M. Pepper, H. E. Beere, and D. A. Ritchie, 2003, Phys. Rev. B **68**, 245310.

Forde, G., J. Friend, and T. Williamson, 2006, Appl. Phys. Lett. **89**, 064105.

Frampton, K., S. Martin, and K. Minor, 2003, Appl. Acoust. **64**, 681.

Franke, T., S. Braunmuller, L. Schmid, A. Wixforth, and D. A. Weitz, 2010, Lab Chip **10**, 789.

Friend, J., K. Nakamura, and S. Ueha, 2004, IEEE Trans. Ultrason. Ferroelectr. Freq. Control **51**, 871.

Friend, J., and L. Yeo, 2008a, *Encyclopedia of Micro- and Nanofluidics*, Chap. Piezoelectric Materials for Microfluidics (Springer, New York), pp. 1654–1662.

Friend, J., and L. Yeo, 2008b, *Encyclopedia of Micro- and Nanofluidics*, Chap. Piezoelectric Microdispensers (Springer, New York), pp. 1662–1672.

Friend, J., and L. Yeo, 2010a, Biomicrofluidics **4**, 026502.

Friend, J., and L. Yeo, 2010b, Biomicrofluidics **4**, 026501.

Friend, J., L. Yeo, D. Arifin, and A. Mechler, 2008, Nanotechnology **19**, 145301.

Frommelt, T., M. Kostur, M. Schäfer, P. Talkner, P. Hänggi, and A. Wixforth, 2008, Phys. Rev. Lett. **100**, 034502.

Fu, Y., J. Luo, X. Du, A. Flewitt, Y. Li, G. Markx, A. Walton, and W. Milne, 2010, Sens. Actuators. B Chem. **143**, 606.

Furuta, A., and K. Uchino, 1993, J. Am. Ceram. Soc. **76**, 1615.

Furuta, S., C. H. W. Barnes, and C. J. L. Doran, 2004, Phys. Rev. B **70**, 205320.

Gallego-Juarez, J., 1989, J. Phys. E **22**, 804.

Gantner, A., R. H. W. Hoppe, D. Köster, K. Siebert, and A. Wixforth, 2007, Comput. Visual Sci. **10**, 145.

Garrett, S., and D. Stat, 1977, J. Acoust. Soc. Am. **62**, 449.

Garstecki, P., M. Fuerstman, M. Fischbach, S. Sia, and G. Whitesides, 2006, Lab Chip **6**, 207.

Gelfand, S., 1998, *Hearing: An Introduction to Psychological and Physiological Acoustics* (Marcel Dekker, New York).

Gell, J., et al., 2006, Appl. Phys. Lett. **89**, 243505.

Gerlach, R., O. Kraus, J. Fricke, P. Eccardt, N. Kroemer, and V. Magori, 1992, J. Non-Cryst. Solids **145**, 227.

Gerszten, R., and T. Wang, 2008, Nature (London) **451**, 949.

Girardo, S., M. Cecchini, F. Beltram, R. Cingolani, and D. Pisignano, 2008, Lab Chip **8**, 1557.

Glorieux, C., K. Van de Rostyne, V. Gusev, W. Gao, W. Lauriks, and J. Thoen, 2002, J. Acoust. Soc. Am. **111**, 95.

Goddard, G., and G. Kaduchak, 2005, J. Acoust. Soc. Am. **117**, 3440.

Goddard, G., C. Sanders, J. Martin, G. Kaduchak, and S. Graves, 2007, Anal. Chem. **79**, 8740.

Goodridge, C., W. Shi, H. Hentschel, and D. Lathrop, 1997, Phys. Rev. E **56**, 472.

Gopala, V. R., and B. G. van Wachem, 2008, Chem. Eng. J. **141**, 204.

Gor'kov, L., 1961, Dokl. Akad. Nauk SSSR **140**, 88 [http://adsabs-s.harvard.edu/abs/1962SPhD....6..773G ].

Grate, J., S. Martin, and R. White, 1993, Anal. Chem. **65**, 940A.

Groneberg, D. A., C. Witt, U. Wagner, K. Chung, and A. Fischer, 2003, Respiratory Medicine **97**, 382.

Guttenberg, Z., H. Müller, H. Habermüller, A. Geisbauer, J. Pipper, J. Felbel, M. Kielpinski, J. Scriba, and A. Wixforth, 2005, Lab Chip **5**, 308.

Guttenberg, Z., A. Rathgeber, S. Keller, J. Radler, A. Wixforth, M. Kostur, M. Schindler, and P. Talkner, 2004, Phys. Rev. E **70**, 056311.

Haake, A., and J. Dual, 2002, Ultrasonics **40**, 317.

Hall, D., 2001, J. Mater. Sci. **36**, 4575.

Hall, D. E., 2002, *Musical Acoustics* (Brooks-Cole, Belmont, MA), 3rd ed.

Hall, P., 1974, J. Fluid Mech. **64**, 209.

Hamilton, M., J. Tjøtta, and S. Tjøtta, 1985, J. Acoust. Soc. Am. **78**, 202.

Hamilton, M. F., Y. A. Ilinskii, and E. A. Zabolotskaya, 2003, J. Acoust. Soc. Am. **113**, 153.

Hamilton, M. F., and C. L. Morfey, 1998, *Nonlinear Acoustics* (Academic Press, New York), Chap. 3, pp. 41–62.

Hanma, K., and B. Hunsinger, 1976, in *Proceedings of the 1976 Ultrasonics Symposium*, edited by J. de Klerk and B. R. McAvoy (IEEE, New York), pp. 328–331.

Hao, H., and H. Maris, 2001, Phys. Rev. B **64**, 064302.

Hartmann, C., and B. Abbott, 1989, Proc. IEEE **1**, 79.

Hasegawa, T., J. Friend, K. Nakamura, and S. Ueha, 2005, Jpn. J. Appl. Phys. **44**, 4658.

Hasegawa, T., T. Kido, T. Iizuka, and C. Matsuoka, 2000, Acoust. Sci. Tech. **21**, 145.

Hashimoto, K., 2000, *Surface Acoustic Wave Devices in Telecommunications: Modelling and Simulation* (Springer-Verlag, Berlin) and also personal communication in March 2006.

Hashimoto, K., and M. Yamaguchi, 2001, IEEE Trans. Ultrason. Ferroelectr. Freq. Control **48**, 1181.

Haydock, D., and J. Yeomans, 2001, J. Phys. A **34**, 5201.

Haydock, D., and J. Yeomans, 2003, J. Phys. A **36**, 5683.

Hemsel, T., and J. Wallaschek, 2000, Ultrasonics **38**, 37.

Heron, S., R. Wilson, S. Shaffer, D. Goodlett, and J. Cooper, 2010, Anal. Chem. **82**, 3985.

Hertz, H., 1995, J. Appl. Phys. **78**, 4845.

Hill, C. R., J. C. Bamber, and G. Haar, 2004, Eds., *Physical Principles of Medical Ultrasonics* (Wiley, New York), 2nd ed.

Ho, J., M. K. Tan, D. Go, L. Yeo, J. Friend, and H.-C. Chang, 2011, Anal. Chem. **83**, 3260.

Hode, J., J. Desbois, P. Dufilie, M. Solal, and P. Ventura, 1995, in *Proceedings of the IEEE Ultrasonics Symposium* (IEEE, New York), pp. 39–50.

Hodgson, R. P., M. Tan, L. Yeo, and J. Friend, 2009, Appl. Phys. Lett. **94**, 024102.

Hohenberg, P., et al., 1964, Phys. Rev. **136**, B864.

Holt, R., and E. Trinh, 1996, Phys. Rev. Lett. **77**, 1274.

Howe, M., 2007, *Hydrodynamics and Sound* (Cambridge University Press, Cambridge, England).

Hu, J., J. Yang, and J. Xu, 2004, Appl. Phys. Lett. **85**, 6042.

Huang, F., C. Liao, and G. Lee, 2006, Electrophoresis **27**, 3297.

Huang, N., Z. Shen, and S. Long, 1999, Annu. Rev. Fluid Mech. **31**, 417.

Huang, S.-B., M.-H. Wu, Z. Cui, Z. Cui, and G.-B. Lee, 2008, J. Micromech. Microeng. **18**, 045008.

Huepe, C., Y. Ding, P. Umbanhowar, and M. Silber, 2006, Phys. Rev. E **73**, 016310.

Hughes, D. R., A. H. Nuttall, R. A. Katz, and G. C. Carter, 2009, J. Acoust. Soc. Am. **125**, 958.

Hunt, F. V., 1955, J. Acoust. Soc. Am. **27**, 1019.

Hunt, F. V., 1978, *Origins in Acoustics: The Science of Sound from Antiquity to the Age of Newton* (Yale University Press, New Haven, CT).

Hutchisson, E., and F. B. Morgan, 1931, Phys. Rev. **37**, 1155.

Ide, T., J. Friend, K. Nakamura, and S. Ueha, 2007, Sens. Actuators. A Phys. **135**, 740.

Insepov, Z., D. Wolf, and A. Hassanein, 2006, Nano Lett. **6**, 1893.

Irschik, H., 2002, Engineering Structures **24**, 5.

Issenmann, B., A. Nicolas, R. Wunenburger, S. Manneville, and J.-P. Delville, 2008, Europhys. Lett. **83**, 34 002.

Ito, S., M. Sugimoto, Y. Matsui, and J. Kondoh, 2007, Jpn. J. Appl. Phys. **46**, 4718.

Jackson, F., and W. Nyborg, 1958, J. Acoust. Soc. Am. **30**, 614.

James, A., B. Vukasinovic, M. Smith, and A. Glezer, 2003, J. Fluid Mech. **476**, 1.

Jang, L.-S., S.-H. Chao, M. R. Holl, and D. R. Meldrum, 2005, Sens. Actuators. A Phys. **122**, 141.

Jeffrey, A., and T. Kakutani, 1972, SIAM Rev. **14**, 582.

Jia, Q., T. McCleskey, A. Burrell, Y. Lin, G. Collis, H. Wang, A. Li, and S. Foltyn, 2004, Nature Mater. **3**, 529.

Jin, Q., F. Liang, Y. Huan, Y. Cao, J. Zhou, H. Zhang, and W. Yang, 2000, Laboratory Robotics and Automation **12**, 76.

Johnson, R., 2002, J. Fluid Mech. **455**, 63.

Jullian, C., J. F. Li, and D. Viehland, 2004, J. Appl. Phys. **95**, 4316.

Jung, H., 2005, Opt. Eng. (Bellingham, Wash.) **44**, 024601.

Kaajakari, V., A. Sathaye, and A. Lal, 2001, in *Digest of Technical Publications, The 11th International Conference on Solid State Sensors and Actuators: Transducers 2001 and Eurosensors XV* (IEEE, Munich, Germany), Vol. 1, pp. 958–961.

Kadota, M., 2005, Jpn. J. Appl. Phys. **44**, 4285.

Kamakura, T., K. Matsuda, Y. Kumamoto, and M. A. Breazeale, 1995, J. Acoust. Soc. Am. **97**, 2740.

Kamizuma, H., T. Omori, K. Hamishoto, and M. Yamaguchi, 2006, IEEE Trans. Ultrason. Ferroelectr. Freq. Control **53**, 1186; their capabilities to 10 GHz were discussed in a personal communication in October 2009.

Kapishnikov, S., V. Kantsler, and V. Steinberg, 2006, J. Stat. Mech., P01012.

Karabacak, D. M., V. Yakhot, and K. L. Ekinci, 2007, Phys. Rev. Lett. **98**, 254505.

Keisuke, A., N. Kentaro, U. Sadayuki, and T. Shinobu, 2004, Jpn. J. Appl. Phys. **43**, 2857.

Keolian, R., L. A. Turkevich, S. J. Putterman, I. Rudnick, and J. A. Rudnick, 1981, Phys. Rev. Lett. **47**, 1133.

Khismatullin, D., and I. Akhatov, 2001, Phys. Fluids **13**, 3582.

Kim, J., Y. Yamagata, M. Takasaki, B. Lee, H. Ohmori, and T. Higuchi, 2005, Sens. Actuators. B Chem. **107**, 535.

Kim, K.-P., and C.-H. Lee, 2007, Integr. Ferroelectr. **88**, 103.

King, L., 1934, Proc. R. Soc. A **147**, 212.

Kobayashi, D., H. Matsumoto, and C. Kuroda, 2008, Chem. Eng. J. **135**, 43.

Kondoh, J., Y. Okiyama, S. Mikuni, Y. Matsui, H. Yatsuda, and M. Nara, 2007, in *Proceedings of the 2007 IEEE International Frequency Control Symposium* (IEEE, New York), pp. 20–24.

Kong, X. H., C. Deneke, H. Schmidt, D. J. Thurmer, H. X. Ji, M. Bauer, and O. G. Schmidt, 2010, Appl. Phys. Lett. **96**, 134105.

König, F., E. Mason, F. Wong, and M. Albota, 2005, Phys. Rev. A **71**, 033805.

Köster, D., 2007, SIAM J. Sci. Comput. **29**, 2352.

Koyama, D., T. Ide, J. Friend, K. Nakamura, and S. Ueha, 2007, IEEE Trans. Ultrason. Ferroelectr. Freq. Control **54**, 597.

Krasilnikov, V. A., T. T. Long, and L. K. Zarembo, 1970, Nature (London) **227**, 1128.

Kripfgans, O. D., M. L. Fabiilli, P. L. Carson, and J. B. Fowlkes, 2004, J. Acoust. Soc. Am. **116**, 272.

Krylov, V., 2001, *Noise and Vibration from High-speed Trains* (Thomas Telford, London).

Kudrolli, A., and J. P. Gollub, 1996, Phys. Rev. E **54**, R1052.

Kulkarni, K., J. Friend, L. Yeo, and P. Perlmutter, 2009, Lab Chip **9**, 754.

Kulkarni, K., S. H. Ramarathinam, J. Friend, L. Yeo, A. Purcell, and P. Perlmutter, 2010, Lab Chip **10**, 1518.

Kumar, M., D. Feke, and J. Belovich, 2005, Biotechnol. Bioeng. **89**, 129.

Kuo, S., and D. Morgan, 1999, Proc. IEEE **87**, 943.

Kurosaka, M., 1982, J. Fluid Mech. **124**, 139.

Kurosawa, M., A. Futami, and T. Higuchi, 1997, in *International Conference on Solid State Sensors and Actuators (TRANSDUCERS '97)* (IEEE, New York), Vol. 2, pp. 801–804.

Kurosawa, M., T. Watanabe, A. Futami, and T. Higuchi, 1995, Sens. Actuators. A Phys. **50**, 69.

Kushibiki, J., T. Ishikawa, and N. Chubachi, 1990, Appl. Phys. Lett. **57**, 1967.

Kutty, T., and R. Balachandran, 1984, Mater. Res. Bull. **19**, 1479.

Lacour, F., N. Courjal, M. Bernal, A. Sabac, C. Bainier, and M. Spajer, 2005, Opt. Mater. **27**, 1421.

Lal, A., R. Duggirala, and H. Li, 2005, IEEE Pervasive Computing, **4**, 53.

Lang, R., 1962, J. Acoust. Soc. Am. **34**, 6.

Länge, K., B. Rapp, and M. Rapp, 2008, Anal. Bioanal. Chem. **391**, 1509.

Langelier, S., D. Chang, R. Zeitoun, and M. Burns, 2009, Proc. Natl. Acad. Sci. U.S.A. **106**, 12 617.

Laser, D., and J. Santiago, 2004, J. Micromech. Microeng. **14**, R35.

Laude, V., D. Gérard, N. Khelfaoui, C. Jerez-Hanckes, S. Benchabane, and A. Khelif, 2008, Appl. Phys. Lett. **92**, 094104.

Lauterborn, W., T. Kurz, R. Geisler, D. Schanz, and O. Lindau, 2007, Ultrason. Sonochem. **14**, 484.

Lee, A. P., M. V. Patel, A. R. Tovar, and Y. Okabe, 2010, Journal of the Association for Laboratory Automation **15**, 449.

Lee, C., and A. Lal, 2004, IEEE Trans. Ultrason. Ferroelectr. Freq. Control **51**, 1514.

Lee, J., S. Teh, A. Lee, H. Kim, C. Lee, and K. Shung, 2009, Appl. Phys. Lett. **95**, 073701.

Lefebvre, A., 1989, *Atomization and Sprays* (CRC Press, New York).

Leighton, D., and A. Acrivos, 1987, J. Fluid Mech. **181**, 415.

Lewis, M., 1977, *Proceedings of the IEEE Ultrasonics Symposium* (IEEE, New York), pp. 744–752.

Li, C., P.-M. Wu, A. Browne, S. Lee, and C. Ahn, 2007, in *Proceedings of the 2007 IEEE Sensors Symposium* (IEEE, New York), pp. 462–465.

Li, H., A. Dasvarma, L. Yeo, J. Friend, and K. Traianedes, 2009, Biomicrofluidics **3**, 034102.

Li, H., J. Friend, and L. Yeo, 2007a, Biomedical Microdevices 9, 647.

Li, H., J. R. Friend, and L. Y. Yeo, 2007b, Biomaterials 28, 4098.

Li, H., J. Friend, and L. Yeo, 2008, Phys. Rev. Lett. 101, 084502.

Li, Y., 2004, Chaos Solitons Fractals 22, 965.

Lighthill, J., 1978, J. Sound Vib. 61, 391.

Lighthill, M., 1952, Proc. R. Soc. A 211, 564.

Lin, K., C. Lai, C. Pan, J. Chyi, J. Shi, S. Sun, C. Chang, and C. Sun, 2007, Nature Nanotech. 2, 704.

Liu, K.-C., J. Friend, and L. Yeo, 2008, J. Sound Vib. 321, 115.

Liu, F., S. Peng, H. Jia, M. Ke, and Z. Liu, 2009, Appl. Phys. Lett. 94, 023505.

Liu, R., R. Lenigk, R. Druyor-Sanchez, J. Yang, and P. Grodzinski, 2003, Anal. Chem. 75, 1911.

Long, M., 2006, Architectural Acoustics (Elsevier Academic Press, Burlington, MA).

Lopatnikov, S., J. Deitzel, and J. Gillespie, Jr., 2009, Mol. Cryst. Liq. Cryst. 506, 87.

Love, A., 1944, A Treatise on the Mathematical Theory of Elasticity (Dover, New York), 4th ed.

Lu, J., et al., 2005, Nature (London) 435, 834.

Luchini, P., and F. Charru, 2005, Phys. Fluids 17, 122106.

Lucklum, R., and P. Hauptmann, 2006, Anal. Bioanal. Chem. 384, 667.

Lurton, X., and D. Jackson, 2004, J. Acoust. Soc. Am. 115, 443.

Lyne, W. H., 1971, J. Fluid Mech. 45, 13.

Ma, B., S. Liu, Z. Gan, G. Liu, X. Cai, H. Zhang, and Z. Yang, 2006, Microfluid. Nanofluid. 2, 417.

Maehara, N., S. Ueha, and E. Mori, 1986, Rev. Sci. Instrum. 57, 2870.

Maezawa, M., R. Kamada, T. Kamakura, and K. Matsuda, 2008, Jpn. J. Appl. Phys. 47, 4076.

Manneberg, O., S. Melker Hagsäter, J. Svennebring, H. Hertz, J. Kutter, H. Bruus, and M. Wiklund, 2009, Ultrasonics 49, 112.

Manz, A., Y. Miyahara, J. Miura, Y. Watanabe, and H. Miyagi, 1990, Sens. Actuators. B Chem. 1, 249.

Marchiano, R., and J.-L. Thomas, 2008, Phys. Rev. Lett. 101, 064301.

Markham, J. J., 1952, Phys. Rev. 86, 497.

Marmottant, P., and S. Hilgenfeldt, 2004, Proc. Natl. Acad. Sci. U.S.A. 101, 9523.

Martell, M., J. Perot, and J. Rothstein, 2009, J. Fluid Mech. 620, 31.

Martin, G., H. Schmidt, and B. Wall, 2004, IEEE Trans. Ultrason. Ferroelectr. Freq. Control 51, 858.

Martinez, A. W., S. T. Phillips, M. J. Butte, and G. M. Whitesides, 2007, Angewante Chemie 46, 1318.

Marx, K., 2003, Biomacromolecules 4, 1099.

Masini, L., S. G. Marco Cecchini, R. Cingolani, D. Pisignano, and F. Beltram, 2010, Lab Chip 10, 1997.

Mason, I., R. de la Rue, R. Schmidt, E. Ash, and P. Lagasse, 1971, Electron. Lett. 7, 395.

Mattia, D., and Y. Gogotsi, 2008, Microfluid. Nanofluid. 5, 289.

Maynard, J., E. Williams, and Y. Lee, 1985, J. Acoust. Soc. Am. 78, 1395.

McHale, G., M. Banerjee, and M. Newton, 1999, Phys. Rev. B 59, 8262.

McHale, G., M. I. Newton, and F. Martin, 2003, J. Appl. Phys. 93, 675.

Mcintyre, M. E., 1981, J. Fluid Mech. Digital Archive 106, 331.

Meacham, J., M. Varady, F. Degertekin, and A. Fedorov, 2005, Phys. Fluids 17, 100605.

Medwin, H., C. Clay, and T. Stanton, 1999, J. Acoust. Soc. Am. 105, 2065.

Meyvantsson, I., and D. Beebe, 2008, Anal. Chem. 1, 423.

Miles, J., 1984, J. Fluid Mech. 146, 285.

Miles, J., 1992, J. Fluid Mech. 244, 645.

Miles, J., 1993, J. Fluid Mech. 248, 671.

Miles, J., and D. Henderson, 1990, Annu. Rev. Fluid Mech. 22, 143.

Miller, D., S. Pislaru, and J. Greenleaf, 2002, Somatic Cell and Molecular Genetics 27, 115.

Miller, D., and J. Song, 2002, Ultrasound Med. Biol. 28, 1343.

Milsom, R., N. Reilly, and M. Redwood, 1977, IEEE Trans. Sonics Ultrason. 24, 147.

Mir, J., 1980, J. Acoust. Soc. Am. 67, 201.

Mitragotri, S., 2005, Nat. Rev. Drug Discov. 4, 255.

Mitri, F., 2005, Ultrasonics 43, 681.

Moffitt, J., Y. Chemla, S. Smith, and C. Bustamante, 2008, Annu. Rev. Biochem. 77, 205.

Monat, C., P. Domachuk, and B. Eggleton, 2007, Nat. Photon. 1, 106.

Moroney, R., R. White, and R. Howe, 1991, Appl. Phys. Lett. 59, 774.

Morse, P., and H. Feshbach, 1953, Methods of Theoretical Physics (McGraw-Hill, New York).

Morse, P., and K. Ingard, 1968, Theoretical Acoustics (McGraw-Hill, New York).

Muralt, P., 2000, J. Micromech. Microeng. 10, 136.

Nachef, S., D. Cathignol, J. N. Tjøtta, A. M. Berg, and S. Tjøtta, 1995, J. Acoust. Soc. Am. 98, 2303.

Nassau, K., H. Levinstein, and G. Loiacono, 1966, J. Phys. Chem. Solids 27, 983.

Nassoy, P., D. Cuvelier, R. Bruinsma, and F. Brochard-Wyart, 2008, Europhys. Lett. 84, 18 004.

Naugolnykh, K., 2009, Acoust. Phys. 55, 338.

Naugolnykh, K., and L. Ostrovsky, 1998, Nonlinear Wave Processes in Acoustics, Cambridge Texts in Applied Mathematics (Cambridge University Press, Cambridge, England).

Nayanov, V., 1986, Pis'ma Zh. Eksp. Teor. Fiz. 44, 245 [http://jetpletters.ac.ru/ps/1387/article_21037.pdf].

Neild, A., S. Oberti, F. Beyeler, J. Dual, and B. Nelson, 2006, J. Micromech. Microeng. 16, 1562.

Nelson, D., 1996, Phys. Rev. Lett. 76, 4713.

Newton, M., M. Banerjee, T. Starke, S. Rowan, and G. McHale, 1999, Sens. Actuators. A Phys. 76, 89.

Nguyen, N., and R. White, 2000, IEEE Trans. Ultrason. Ferroelectr. Freq. Control 47, 1463.

Nguyen, N., and Z. Wu, 2005, J. Micromech. Microeng. 15, R1.

Nobel Foundation, 1967, Nobel Lectures, Physics 1901–1921 (Elsevier, New York), pp. 88–94.

Noblin, X., A. Buguin, and F. Brochard-Wyart, 2004, Eur. Phys. J. E 14, 395.

Nyborg, W. L., 1965, Acoustic Streaming, edited by W. P. Mason and R. N. Thurston (Academic Press, New York), Chap. 11, pp. 265–329.

Oberti, S., D. Moller, S. Gutmann, A. Neild, and J. Dual, 2009, J. Appl. Crystallogr. 42, 636.

Oberti, S., A. Neild, R. Quach, and J. Dual, 2009, Ultrasonics 49, 47.

Ohba, Y., K. Arita, T. Tsurumi, and M. Daimon, 1994, Jpn. J. Appl. Phys. 33, 5305.

Ohno, K., K. Tachikawa, and A. Manz, 2008, Electrophoresis 29, 4443.

Olsson, III, R., and I. El-Kady, 2009, Meas. Sci. Technol. 20, 012002.

Oralkan, O., A. Ergun, C. Cheng, J. Johnson, M. Karaman, T. Lee, and B. Khuri-Yakub, 2003, IEEE Trans. Ultrason. Ferroelectr. Freq. Control 50, 1581.

Ota, T., T. Uchikawa, and T. Mizutani, 1985, Jpn. J. Appl. Phys. 24, 193, Supplement 24-3 [http://jjap.jsap.jp/link?JJAPS/24S3/193/].

Park, G.-T., J.-J. Choi, C.-S. Park, J.-W. Lee, and H.-E. Kim, 2004, Appl. Phys. Lett. **85**, 2322.

Perez-Arjona, I., V. Sánchez-Morcillo, and G. Valcárcel, 2008, Europhys. Lett. **82**, 10002.

Pezeril, T., C. Klieber, S. Andrieu, and K. Nelson, 2009, Phys. Rev. Lett. **102**, 107402.

Pipkin, A., and R. Rivlin, 1959, Arch. Ration. Mech. Anal. **4**, 129.

Pitt, W., G. Husseini, and B. Staples, 2004, Expert Opinion on Drug Delivery **1**, 37.

Plateau, J., 1849, Acad. Sci. Bruxelles Mém. **23**, 5.

Polla, D., and L. Francis, 1998, Annu. Rev. Mater. Sci. **28**, 563.

Priya, S., 2007, J. Electroceram. **19**, 167.

Purcell, E., 1977, Am. J. Phys. **45**, 3.

Qi, A., L. Yeo, and J. Friend, 2008, Phys. Fluids **20**, 074103.

Qi, A., L. Yeo, J. Friend, and J. Ho, 2010, Lab Chip **10**, 470.

Qi, Q., 1993, J. Acoust. Soc. Am. **94**, 1090.

Qi, Q., and G. Brereton, 1995, IEEE Trans. Ultrason. Ferroelectr. Freq. Control **42**, 619.

Raghavan, R., J. Friend, and L. Yeo, 2010, Microfluid. Nanofluid. **8**, 73.

Ramos, E., S. Cuevas, and G. Huelsz, 2001, Phys. Fluids **13**, 3709.

Randall, C., N. Kim, J. Kucera, W. Cao, and T. Shrout, 1998, J. Am. Ceram. Soc. **81**, 677.

Rayleigh, J. W. S., and R. B. Lindsay, 1945, *The Theory of Sound* (Courier Dover Publications, North Chelmsford, MA), 2nd ed.

Rayleigh, L., 1878, Proc. London Math. Soc. **1**, 4.

Rayleigh, L., 1884, Phil. Trans. R. Soc. London **175**, 1.

Reed, E., M. Armstrong, K. Kim, and J. Glownia, 2008, Phys. Rev. Lett. **101**, 014302.

Rensen, J., D. Bosman, J. Magnaudet, C. Ohl, A. Prosperetti, R. Tögel, M. Versluis, and D. Lohse, 2001, Phys. Rev. Lett. **86**, 4819.

Rife, J., M. Bell, J. Horwitz, Y. Kabler, and R. C. Auyeung, and W. Kim, 2000, Sens. Actuators A, Phys. **86**, 135.

Riley, N., 1998, Theor. Comput. Fluid Dyn. **10**, 349.

Riley, N., 2001, Annu. Rev. Fluid Mech. **33**, 43.

Robert, M., O. Delbos, J. Guiter, and D. Grasset, 1995, British Journal of Urology **76**, 435.

Rogers, P., J. Friend, and L. Yeo, 2010, Lab Chip **10**, 2979.

Romanowicz, B., R. Allen, V. Cormier, J. Gomberg, J. Hole, G. Masters, D. Schutt, A. Sheehan, J. Tromp, and M. Wysession, 2009, "*Seismological Grand Challenges in Understanding Earth's Dynamic Systems*," Report of the National Science Foundation, Denver, CO, p. 76.

Rotter, M., A. Kalameitsev, A. Govorov, W. Ruile, and A. Wixforth, 1999, Phys. Rev. Lett. **82**, 2171.

Royer, D., and E. Dieulesaint, 2000, *Elastic Waves in Solids I: Free and Guided Propagation*, Advanced Texts in Physics (Springer-Verlag, Berlin).

Rozenberg, L. D., 1971, *High-Intensity Ultrasonic Fields, Ultrasonic Technology*, Monographs in Geoscience, edited by Lewis Balamuth (Plenum Press, New York) (translated from Russian by J. S. Wood).

Rudenko, O., and S. Soluîân, 1977, *Theoretical Foundations of Nonlinear Acoustics*, Studies in Soviet Science: Physical Sciences (Consultants Bureau, a division of Plenum Publishing Corporation, New York) (translated from Russian by Robert T. Beyer).

Ryu, Y. R., S. Zhu, J. D. Budai, H. R. Chandrasekhar, P. F. Miceli, and H. W. White, 2000, J. Appl. Phys. **88**, 201.

Saito, J., J. Friend, K. Nakamura, and S. Ueha, 2005, Jpn. J. Appl. Phys. **44**, 4666.

Saito, Y., H. Takao, T. Tani, T. Nonoyama, K. Takatori, T. Homma, T. Nagaya, and M. Nakamura, 2004, Nature (London) **432**, 84.

Salieb-Beugelaar, G. B., G. Simone, A. Arora, A. Philippi, and A. Manz, 2010, Anal. Chem. **82**, 4848.

Sankaranarayanan, S., S. Cular, V. Bhethanabotla, and B. Joseph, 2008, Phys. Rev. E **77**, 066308.

Santesson, S., and S. Nilsson, 2004, Anal. Bioanal. Chem. **378**, 1704.

Sarvazyan, A., T. Chalikian, and F. Dunn, 1990, J. Acoust. Soc. Am. **88**, 1555.

Schindler, M., P. Talkner, and P. Hänggi, 2006, Phys. Fluids **18**, 103303.

Schlichting, H., 1932, Z. Phys. **33**, 327.

Schneider, S., S. Nuschele, A. Wixforth, C. Gorzelanny, A. Alexander-Katz, R. R. Netz, and M. Schneider, 2008, Proc. Natl. Acad. Sci. U.S.A. **104**, 7899.

Schröder, C. T., and W. R. Scott, Jr., 2001, J. Acoust. Soc. Am. **110**, 2867.

Schufle, J. A., 1981, Isis **72**, 86.

Schwartz, L., and J. Fenton, 1982, Annu. Rev. Fluid Mech. **14**, 39.

Schwarzer, S., and A. Roosen, 1999, J. Eur. Ceram. Soc. **19**, 1007.

Secomb, T. W., 1978, J. Fluid Mech. **88**, 273.

Setter, N., 2008, *Trends in Ferroelectric/Piezoelectric Ceramics* (Springer, Berlin), Chap. 25, p. 553.

Setter, N., *et al.*, 2006, J. Appl. Phys. **100**, 051606.

Shannon, M., P. Bohn, M. Elimelech, J. Georgiadis, B. Mariñas, and A. Mayes, 2008, Nature (London) **452**, 301.

Shchukin, D. G., D. Radziuk, and H. Möhwald, 2010, Annu. Rev. Mater. Res. **40**, 1.

Shi, J., D. Ahmed, X. Mao, S. Lin, A. Lawit, and T. Huang, 2009, Lab Chip **9**, 2890.

Shi, J., X. Mao, D. Ahmed, A. Colletti, and T. Huang, 2008, Lab Chip **8**, 221.

Shilton, R., M. K. Tan, L. Y. Yeo, and J. R. Friend, 2008, J. Appl. Phys. **104**, 014910.

Shiokawa, S., Y. Matsui, and T. Ueda, 1990, Jpn. J. Appl. Phys. **29**, 137.

Shutilov, V., 1988, *Fundamental Physics of Ultrasound* (Gordon and Breach Science Publishers, New York) (translated from Russian by M. E. Alferieff).

Siemens, M., Q. Li, M. Murnane, H. Kapteyn, R. Yang, E. Anderson, and K. Nelson, 2009, Appl. Phys. Lett. **94**, 093103.

Singh, M., and A. C. Pipkin, 1966, Arch. Ration. Mech. Anal. **21**, 169.

Smith, R., and F. Welsh, 1971, J. Appl. Phys. **42**, 2219.

Smorodin, T., U. Beierlein, J. Ebbecke, and A. Wixforth, 2005, Small **1**, 1188.

Snouck, D., M.-T. Westra, and W. van de Water, 2009, Phys. Fluids **21**, 025102.

Sobanski, M., C. Robert Tucker, N. Thomas, and W. Terence Coakley, 2000, Bioseparation **9**, 351.

Sodano, H., D. Inman, and G. Park, 2004, Shock and Vibration Digest **36**, 197 [http://www.me.mtu.edu/~hsodano/Publications/SVD%202004%20Power%20Harvesting%20Review.pdf].

Spengler, J., W. Coakley, and K. Christensen, 2003, AIChE J. **49**, 2773.

Spengler, J., M. Jekel, K. Christensen, R. Adrian, J. Hawkes, and W. Coakley, 2000, Bioseparation **9**, 329.

Squires, T., and S. Quake, 2005, Rev. Mod. Phys. **77**, 977.

Sritharan, K., C. Strobl, M. Schneider, A. Wixforth, and Z. Guttenberg, 2006, Appl. Phys. Lett. **88**, 054102.

Starritt, H. C., F. A. Duck, and V. F. Humphrey, 1991, Phys. Med. Biol. **36**, 1465.

Stone, H., A. Stroock, and A. Ajdari, 2004, Annu. Rev. Fluid Mech. **36**, 381.

Stuart, J., 1966, J. Fluid Mech. **24**, 673.

Stuart, J. T., 1963, in *Laminar Boundary Layers*, edited by L.
Rosenhead (Oxford: Clarendon Press, London, UK), Chap. 7,
1st ed., pp. 347–408.

Suslick, K., and G. Price, 1999, Annu. Rev. Mater. Sci. **29**, 295.

Suslick, K. S., and D. J. Flannigan, 2008, Annu. Rev. Phys. Chem.
**59**, 659.

Tachizaki, T., T. Muroya, O. Matsuda, Y. Sugawara, D. H. Hurley,
and O. B. Wright, 2006, Rev. Sci. Instrum. **77**, 043713.

Takagi, H., R. Maeda, N. Hosoda, and T. Suga, 1999, Appl. Phys.
Lett. **74**, 2387.

Takeuchi, M., H. Shimizu, R. Kajitani, K. Kawasaki, Y. Kumagai,
A. Koukitu, and Y. Aoyagi, 2007, J. Cryst. Growth **298**, 336.

Takeuchi, M., and K. Yamanouchi, 1994, Jpn. J. Appl. Phys. **33**,
3045.

Tan, M., 2010, Ph.D. thesis (Monash University).

Tan, M., J. Friend, and L. Yeo, 2007a, Appl. Phys. Lett. **91**, 224101.

Tan, M., J. Friend, and L. Yeo, 2007b, Lab Chip **7**, 618.

Tan, M., L. Yeo, and J. Friend, 2009, Europhys. Lett. **87**,
47 003.

Tan, M. K., J. Friend, and L. Y. Yeo, 2009, Phys. Rev. Lett. **103**,
024501.

Tan, M. K., J. R. Friend, O. K. Matar, and L. Y. Yeo, 2010, Phys.
Fluids **22**, 112112.

Tan, M. K., R. Tjeung, H. Ervin, L. Y. Yeo, and J. Friend, 2009,
Appl. Phys. Lett. **95**, 134101.

Tan, M. K., L. Y. Yeo, and J. Friend, 2010, Appl. Phys. Lett. **97**,
234106.

Tandiono, S.-W. Ohl, D. S.-W. Ow, E. Klaseboer, V. V. T. Wong, A.
Camattari, and C.-D. Ohl, 2010, Lab Chip **10**, 1848.

Taylor, G., 1950, Proc. R. Soc. A **201**, 192.

Teh, S., R. Lin, L. Hung, and A. Lee, 2008, Lab Chip **8**, 198.

Thomas, B., and A. Squires, 1998, Phys. Rev. Lett. **81**, 574.

Thompson, C., A. Mulpur, V. Mehta, and K. Chandra, 1991, J.
Acoust. Soc. Am. **90**, 2097.

Tiersten, H., 1963, J. Acoust. Soc. Am. **35**, 234.

Tjøtta, J., and S. Tjøtta, 1994, in *Proceedings of the 1994
Ultrasonics Symposium* (IEEE, New York), Vol. 2, pp. 709–714.

Tominaga, M., R. Kaminaga, J. Friend, K. Nakamura, and S. Ueha,
2005, IEEE Trans. Ultrason. Ferroelectr. Freq. Control **52**,
1735.

Tseng, W.-K., J.-L. Lin, W.-C. Sung, S.-H. Chen, and G.-B. Lee,
2006, J. Micromech. Microeng. **16**, 539.

Ueha, S., Y. Tomikawa, M. Kurosawa, and K. Nakamura, 1993,
*Ultrasonic Motors: Theory and Applications*, Monographs in
Electrical and Electronic Engineering Vol. 29 (Clarendon Press,
Oxford).

Umeda, M., K. Nakamura, and S. Ueha, 1996, Jpn. J. Appl. Phys.
**35**, 3267.

Umemura, S., K. Kawabata, K. Sasaki, N. Yumita, K. Umemura,
and R. Nishigaki, 1996, Ultrason. Sonochem. **3**, S187.

Vainshtein, P., M. Fichman, K. Shuster, and C. Gutfinger, 1996, J.
Fluid Mech. **306**, 31.

Vanherzeele, J., M. Brouns, P. Castellini, P. Guillaume, M.
Martarelli, D. Ragni, E. Primotomasini, and S. Vanlanduit,
2007, Optics and Lasers in Engineering **45**, 19.

Vega, J. M., S. Rüdiger, and J. Viñals, 2004, Phys. Rev. E **70**,
046306.

Versluis, M., D. E. Goertz, P. Palanchon, I. L. Heitman, S. M. van
der Meer, B. Dollet, N. de Jong, and D. Lohse, 2010, Phys. Rev. E
**82**, 026321.

Vukasinovic, B., M. Smith, and A. Glezer, 2007a, J. Fluid Mech.
**587**, 395.

Vukasinovic, B., M. K. Smith, and A. Glezer, 2007b, Phys. Fluids
**19**, 012104.

Wang, C., and G. Lee, 2006, J. Micromech. Microeng. **16**, 341.

Wang, C. Y., 1991, Annu. Rev. Fluid Mech. **23**, 159.

Wang, D., D. Lin, K. Wong, K. Kwok, J. Dai, and H. Chan, 2008,
Appl. Phys. Lett. **92**, 222909.

Wang, S., Z. Jiao, X. Huang, C. Yang, and N. Nguyen, 2009,
Microfluid. Nanofluid. **6**, 847.

Wang, T., and C. Lee, 1998, *Nonlinear Acoustics*, edited by
M. F. Hamilton and D. T. Blackstock (Academic, New York),
p. 177.

Wang, Y., *et al.*, 2002, Appl. Phys. Lett. **80**, 97.

Watanabe, S., T. Fujiu, and T. Fujii, 1995, Appl. Phys. Lett. **66**,
1481.

Watson, B., J. Friend, and L. Yeo, 2009, Sens. Actuators. A Phys.
**152**, 219.

Watson, B., L. Yeo, and J. Friend, 2010, Rev. Sci. Instrum. **81**,
063901.

Wautelet, M., 2001, Eur. J. Phys. **22**, 601.

Weibel, D., W. DiLuzio, and G. Whitesides, 2007, Nat. Rev.
Microbiol. **5**, 209.

Weis, R., and T. Gaylord, 1985, Appl. Phys. A **37**, 191.

West, M., 1994, Music and Letters **75**, 161.

Westervelt, P., 1953a, J. Acoust. Soc. Am. **25**, 60.

Westervelt, P. J., 1953b, J. Acoust. Soc. Am. **25**, 799.

Whitby, M., and N. Quirke, 2007, Nature Nanotech. **2**, 87.

White, R., 1997, Faraday Discuss. **107**, 1.

White, R., and F. Voltmer, 1965, Appl. Phys. Lett. **7**, 314.

Whitehill, J., A. Neild, T. W. Ng, and M. Stokes, 2010, Appl. Phys.
Lett. **96**, 053501.

Whitesides, G., 2006, Nature (London) **442**, 368.

Whitley, D., R. Dorn, J. Simon, R. Rechtman, and T. Whitley, 1999,
Cambridge Archaeological Journal **9**, 221.

Wiklund, M., and H. Hertz, 2006, Lab Chip **6**, 1279.

Williams, J., 1976, in *Ceramic Fabrication Processes*, edited by
F. Y. Wang, Treatise on Materials Science and Technology Vol. 9
(Academic Press, New York), pp. 173–198

Williams, J. E. F., and D. C. Hill, 1987, J. Fluid Mech. **184**, 101.

Wilson, S., *et al.*, 2007, Materials Science and Engineering. R,
Reports **56**, 1.

Wixforth, A., 2003, Superlattices Microstruct. **33**, 389.

Wixforth, A., C. Strobl, C. Gauer, A. Toegl, J. Scriba, and Z. v.
Guttenberg, 2004, Anal. Bioanal. Chem. **379**, 982.

Wood, B., P. Heraud, S. Stojkovic, D. Morrison, J. Beardall, and D.
McNaughton, 2005, Anal. Chem. **77**, 4955.

Wood, C., S. Evans, J. Cunningham, R. O'Rorke, C. Wälti, and A.
Davies, 2008, Appl. Phys. Lett. **92**, 044104.

Wood, C. D., J. E. Cunningham, R. O'Rorke, C. Wälti, E. H.
Linfield, A. G. Davies, and S. D. Evans, 2009, Appl. Phys. Lett.
**94**, 054101.

Woodside, S., B. Bowen, and J. Piret, 1997, AIChE J. **43**, 1727.

Wright, M., 2006, J. Acoust. Soc. Am. **120**, 1807.

Wright, O., and K. Kawashima, 1992, Phys. Rev. Lett. **69**, 1668.

Wu, T., H. Tang, Y. Chen, and P. Liu, 2005, IEEE Trans. Ultrason.
Ferroelectr. Freq. Control **52**, 1384.

Wu, Y., D. Zhou, G. Spinks, P. Innis, W. Megill, and G. Wallace,
2005, Smart Materials and Structures **14**, 1511.

Wu, T.-T., Z.-C. Hsu, and Z.-G. Huang, 2005, Phys. Rev. B **71**,
064303.

Xiao, Y., and K. Bhattacharya, 2008, Arch. Ration. Mech. Anal.
**189**, 59.

Yakovenko, V., M. Grayson, and H. Drew, 2009, arXiv:0912.5390.

Yantchev, V., J. Enlund, I. Katardjiev, and L. Johansson, 2010, J.
Micromech. Microeng. **20**, 035031.

Yao, K., X. He, Y. Xu, and M. Chen, 2005, Sens. Actuators. A Phys.
**118**, 342.

Yaralioglu, G., I. Wygant, T. Marentis, and B. Khuri-Yakub, 2004, Anal. Chem. **76**, 3694.

Yarin, A., 2006, Annu. Rev. Fluid Mech. **38**, 159.

Yarin, A., M. Pfaffenlehner, and C. Tropea, 1998, J. Fluid Mech. **356**, 65.

Yasuda, K., S. Haupt, S. Umemura, T. Yagi, M. Nishida, and Y. Shibata, 1997, J. Acoust. Soc. Am. **102**, 642.

Yeo, L. Y., J. R. Friend, M. P. McIntosh, E. N. Meeusen, and D. A. Morton, 2010, Expert Opinion on Drug Delivery **7**, 663.

Yoo, J., and T. Rossing, 2006, J. Acoust. Soc. Am. **120**, EL78.

Yoshino, Y., T. Makino, Y. Katayama, and T. Hata, 2000, Vacuum **59**, 538.

Yosioka, K., and Y. Kawasima, 1955, Acustica **5**, 167.

Zarembo, L., 1971, in *Acoustic Streaming* (Plenum Press, New York), Pt. III, pp. 138–199.

Zarembo, L., and V. Krasil'nikov, 1959, Phys. Usp. **2**, 580.

Zarembo, L., and V. Krasil'nikov, 1960, Sov. Phys. Usp. **2**, 1004.

Zhuang, X., D. Lin, O. Oralkan, and B. Khuri-Yakub, 2008, J. Microelectromech. Syst. **17**, 446.